5-8-2004

Fluorescence Resonance Energy Transfer (FRET) Based Sensors for Bioanalysis

Gabriela Blagoi
University of New Orleans

FLUORESCENCE RESONANCE ENERGY TRANSFER (FRET) BASED SENSORS FOR BIOANALYSIS

A Dissertation

Submitted to the Graduate Faculty of the
University of New Orleans
in partial fulfillment of the
requirements for the degree of

Doctor of Philosophy
in
The Department of Chemistry

by

Gabriela Blagoi

B.S., Politehnica University, Bucharest, Romania, 1994
M.S, Politehnica University, Bucharest, Romania, 1995
M.S., University of New Orleans, New Orleans, 2002

August 2004

ACKNOWLEDGMENTS

The research and writing of this dissertation would have never been completed without the direction, encouragement and continuous support of my advisor, Prof. Zeev Rosenzweig.

I would also like to express my gratitude to:
- Prof. Ronald Evilia, Prof. Bruce Gibb, Prof. Paul Hanson, Prof. Mathew Tarr and Prof Guijun Wang for their advice and discussion on my research work.
- Prof. Nitsa Rosenzweig of Xavier University for providing cell cultures and assisting with biological aspects of these studies.
- Prof. Constantin Luca and Prof. Mircea Badea from Politehnica University of Bucharest “infecting me” with their love of Chemistry.
- All my past and present group members for the exceptionally friendly atmosphere in our lab.
- My close friends: Thuvan Nguyen, Jin Ji, Li Chen, Harry Rees, Edith Bauer, Liliana Viciu, Mihai Viciu, Doinita Neiner, Gabriela Grasa, Maria Tanase, Anca Bleotu, Mihaela Ilie, Mirela Ionita-Manzatu, Laura Lucan, Simona Elena Draganoiu for their love and support.
- My aunt and my uncle, Dr. Maria and Dr. Dumitru Manoiu, who are responsible for my early inclination towards Chemistry.

Lastly, I would like to dedicate this thesis to my wonderful parents Ana and Ion Blagoi.

TABLE OF CONTENTS

List of Figures vi

List of Tables xiii

Abstract xiv

Chapter 1: Background of FRET Based Sensors 1
1.1. Fluorescence and Fluorophores 2
1.1.1. Jablonski Diagram 8
1.1.2. Characteristics of Fluorescence Emission 10
1.2. Fluorescence Sensors 12
1.2.1 Mechanism of Sensing 15
1.2.1.1 Fluorescence Quenching 15
1.2.1.2. Fluorescence Resonance Energy Transfer (FRET) and Inner Filter Effects (IFE) 17
1.2.1.2.1. Energy Transfer. Fluorescence Resonance Energy Transfer (FRET) 17
1.2.1.2.2. Inner Filter Effects (IFE) 24
1.3. Measurements of FRET Efficiency Using Fluorescence Microscopy 26
1.4. Carbohydrate Binding Proteins. Lectins 28

Chapter 2: Experimental 31
2.1. Materials and Reagents 31
2.2. Instrumental Methods 32
2.2.1. Spectrofluorometry Measurements 32
2.2.1.1. Light Source 33
2.2.2.2. Monochromator 34
2.2.2.3. Photomultiplier Tube (PMT) Detector 34
2.2.2. Digital Fluorescence Imaging Microscopy System 35
2.2.2.1. Microscope Objective 36
2.2.2.2. Dichroic Mirror 38
2.2.2.3. Excitation and Emission Filters 38

2.2.2.4. The Filter Cube....39
2.2.2.5. Light Sources....39
2.2.2.6. CCD Camera....40
2.2.2.7. Gratings....45
2.3. Protocols and Procedures....45
2.3.1. Loading of Donor or Acceptor Dyes into Macrophage Cells....45
2.3.2. Preparation of pH Sensitive Sulforhodamine Encapsulating Liposomes....46
2.3.2.1. Injection Method....46
2.3.2.2. Freeze-Thaw Method for pH Sensitive Liposomes....46
2.3.2.3. Sephadex Column Preparation....47
2.3.2.4. Liposome Separation by Sephadex Column....47
2.3.3. Delivery of Labeled Liposomes into Murine Macrophage Cells....48
2.3.4 Maintenance and Preparation of J 774 Murine Macrophage Culture....48
2.3.5. Phospholipid Cocktail for Lipobead Coating....49
2.3.6. Preparation of Lipobeads....49
2.3.7. HEPES Buffer for Lectin Work....50
2.3.8. Preparation of FITC –Con A Coated Beads....50
2.3.9. Preparation of poly-L-Lysine Adhesive Slides....51
2.4. Digital Fluorescence Imaging Analysis....51
2.5. Error Analysis....52
2.6. Methods for Evaluating FRET Efficiency....55
2.6.1. Donor Quenching....55
2.6.2. Acceptor Enhancement....55
2.6.3. Ratio Imaging....56
2.6.4. Choice of Excitation, Emission and Dichroic Mirrors Used in FRET Microscopy....57

Chapter 3: Energy Transfer- A New Analytical Method to Monitor Drug Delivery....58
3.1. Introduction....58
3.2. Specific experimental and technical details....61
3.3. Results and Discussion....63
3.3.1 Choice of Donor - Acceptor Pair....63
3.3.2 Photostability of the Donor and Acceptor Dyes Loaded into Murine Macrophage Cells....63
3.3.3. Delivery of Donor Fluorophores into Acceptor Labeled Macrophages into Cells....64
3.3.4. Delivery of Acceptor Fluorophores into Donor Labeled Macrophages Cells....66

3.4. Summary and Conclusions 73

Chapter 4: Fluorescence Resonance Transfer (FRET) Sensing Lipobeads for Bioanalysis 75
4.1. Introduction 75
4.2. Specific Experimental and Technical Details.....78
4.3. Results and Discussion 80
4.3.1. Choice of Fluorescent Indicators 80
4.3.2. Characterization of Donor Labeled FRET Sensing Lipobeads 81
4.3.2.1. Photostability of Lipobeads.....82
4.3.2.2. Influence of the Phospholipid Composition on the Donor Absorption into the Lipobead Membrane 83
4.3.2.3. Energy Transfer Efficiency in FRET Sensing Lipobeads.....84
4.4. Summary and Conclusions… 86

Chapter 5: Design, Synthesis and Application of Particle-Based FRET Sensors for Screening Carbohydrates and Glycoproteins.....88
5.1. Introduction 88
5.2. Specific Experimental and Technical Details.....92
5.3. Results and Discussion 96
5.3.1. Choice of Fluorescent Indicators 96
5.3.2. Characterization and Properties of the FRET Sensing Particles 97
5.3.3. Photostability and Leaking Stability of the FRET Sensing Particles 98
5.3.4. Dextran-TR Binding Studies 99
5.3.5. Determination of Binding Constant of Dextran-TR 104
5.3.6. FRET Inhibition Assays….....105
5.4. Discussion.....108

Chapter 6: Discussion 110

References.....115

Vita.....123

LIST OF FIGURES

Chapter 1

Figure 1.1.Stuctures of a) Fluorescein, b) Sulforhodamine B and c) Texas Red structure 5

Figure 1.2. Structures of a) Fluorescein Diacetate, b) Cell Tracker Orange and c) Calcein Acetoxymethyl (Calcein AM) 7

Figure1.3. Jablonski diagram describing radiative and nonradiative transitions in molecular systems.....9

Figure 1.4. Modified Jablonski diagram for dynamic quenching and FRET.....17

Figure 1.5. A spectral overlap (marked in diagonal lines) between the donor emission and the acceptor absorption is required for fluorescence resonance energy transfer (FRET) between donor and acceptor fluorophores 18

Chapter 2

Figure 2.1. Illustration of a typical light path in an inverted fluorescence microscope 37

Figure 2.2. Schematic diagram of a CCD pixel. Each pixel in a CCD is a tiny capacitor that is formed by growing a layer of silicon dioxide on top of a polysilicon substrate. A metal electrode, called gate, is deposited on this structure 41

Figure 2.3. The geometry of a front and back-illuminated CCD chip 42

Figure 2.4. Schematic diagram of charged coupled devices (CCD) cameras: (a) conventional full frame CCD with a single parallel register, (b) frame transfer and (c) inter-line transfer 43

Figure 2.5. Digital fluorescence images of FRET sensing beads and their data processing: a) initial fluorescence image b) the same image after the selection of the desired beads c) and following the selection of the image background 53

Chapter 3

Figure 3.1. Fluorescence images of Sulforhodamine (5μM) labeled murine macrophages prior (a) and following incubation with 25nM Calcein AM for 30 minutes (b). Fluorescence images were taken through the FRET channel (λ_{ex}=480 nm, λ_{em}> 590nm) 64

Figure 3.2 FRET efficiency between Sulforhodamine (5 μM) labeled macrophages and increased concentrations of the donor, Calcein AM. The FRET magnitude was determined by recording the increase in the ratio between the sensitized acceptor signal, Fa, and the donor fluorescence, Fd in the presence (a) and absence (b) of Sulforhodamine 66

Figure 3.3. Delivery of Sulforhodamine (500 μM) into Calcein AM (5 μM) labeled macrophages. The FRET magnitude was determined by recording the decrease in the ratio between the donor signals: (a) prior (F_{d0}) and (b) following the delivery of Sulforhodamine (F_d). Fluorescence images were taken through the donor channel (λ_{ex}=480 nm, 520 nm > λ_{em}> 550nm) 68

Figure 3.4. Fluorescence images of the Calcein AM(5 μM) labeled murine macrophages prior (a) and following incubation with 500 μM Cell Tracker Orange for 30 minutes (b). Fluorescence images were taken through the donor channel (λ_{ex}=480 nm, 520 nm > λ_{em}> 550nm).....69

Figure 3.5. Delivery of CellTracker Orange into Calcein AM labeled macrophages monitored by FRET. Donor channel fluorescence was recorded in the absence (square dots), the presence of 250μM (filled circle dots) and 500μM (triangle dots) CellTracker Orange 71

Figure 3.6. Fluorescence image of J774 murine macrophages loaded with liposomes containing Sulforhodamine. The liposomes were prepared a phospholipid cocktail containing a mixture of DOPE: N-succinyl DOPE (7:3) liposomes containing Sulforhodamine using freeze-thaw method. The fluorescence image was taken through the acceptor channel (λ_{ex}=546 nm, λ_{em}> 580nm) 72

Chapter 4

Figure 4.1. A schematic diagram illustrating the principle of FRET sensing lipobeads. Adsorption or biding of fluorescent acceptor molecules to lipobeads containing a fluorescent donor results in FRET signal enhancement.....77

Figure 4.2. Structure of the donor labeled phospholipid used to prepare the FRET sensing lipobeads, *N*-(fluorescein-5-thiocarbamoyl)-1,2-dihexadecanoyl-*sn*-glycero-3-phosphoethanolamine triethylammonium salt (Fluorescein-DHPE) 81

Figure 4.3. Digital fluorescence image of 1.6 μm FRET sensing lipobeads. The image was taken through an excitation filter: λ_{ex}=480 nm, a dichroic mirror: 505nm; an emission filter: λ_{em}>515 nm; objective: 40X with N.A= 0.7and a neutral density filter: 1.0 for 0.5 seconds.....82

Figure 4.4. Effect the composition of phospholipid cocktail on the fluorescence intensity of FRET sensing lipobeads 84

Figure 4.5. Fluorescence spectra of FRET sensing lipobeads in the presence of increasing Sulforhodamine concentrations: a) 0 μM, b) 10.0 μM, c) 20.0 μM, d) 40 μM. The spectra were not corrected for inner filter effects 85

Figure 4.6. The variation of energy transfer efficiency (Fa/Fd) against increasing acceptor concentrations a) FRET sensing lipobeads and b) Carboxyfluorescein solution(500nM) 86

Chapter 5

Figure 5.1. Illustration of the Particle-Based FRET Sensors for Screening Carbohydrates and Glycoproteins. FRET sensing particles in the absence (top) and presence (bottom) of glycoprotein or carbohydrate inhibitors. The FRET efficiency decreases with increasing inhibitor concentrations 92

Figure 5.2. Absorption and fluorescence spectra of Fluorescein and Texas Red. The area marked with diagonal lines represents the overlap integral between the donor emission and acceptor absorption.....97

Figure 5.3. Digital fluorescence images of FRET sensing particles through the donor+acceptor channel (λex=470nm, λem>520nm) in a) the absence of dextran-TR, and b) when dextran-TR is bound to the FITC-ConA labeled particles. c) A digital fluorescence image of the particles through the FRET channel (λex=470nm, λem>590nm) when dextran-TR molecules are bound to the FRET sensing particles. 100

Figure 5.4. Fluorescence spectra of the FRET sensing particles: a) in the absence of dextran-TR, b) immediately following the addition of 1.2 μg/ml dextran-TR and c) when the FRET between dextran-TR and the FITC-ConA labeled particles reached equilibrium (15 min).....102

Figure 5.5. The FRET signal between dextran-TR and FITC-ConA coated particles as a function of dextran-TR concentration. The FRET magnitude was determined by following the decrease in the donor fluorescence. The fluorescence intensity of the particles (F_d) was measured through the donor cube (λex=470nm, 520nm<λem<560nm) and was normalized to the initial donor fluorescence (F_{d0}). 103

Figure 5.6. Determination of the apparent association constant between dextran-TR and FRET sensing particles based on the equation [5.1] 105

Figure 5.7 The inhibition of dextran-TR binding to FITC-ConA labeled particles by galactose, mannose, avidin, ovalbumin and glucoseoxidase. The error bars were obtained from three analyses of fields containing about 100 particles 108

LIST OF TABLES

Table 2.1. Optimal filter combinations for fluorescence imaging used in FRET microscopy 57

ABSTRACT

The objective of my PhD study was to develop and characterize new methods and sensors based on fluorescence resonance energy transfer (FRET) for bioanalysis.

Chapter 3 describes the use of FRET between donor fluorophores and acceptor labeled murine macrophage cells. FRET microscopy was used to determine whether the donor molecules truly permeate through the cell membrane or only adsorb to the cell surface. This method was found to be partially successful since the donor red tail fluorescence overlapped with the sensitized acceptor fluorescence and led to false reading of FRET. We found that is easier to monitor delivery of acceptor molecules into donor-labeled cells. Using donor labeled cells it was possible to determine whether the acceptor molecules were actually delivered into cells. However, a relatively high acceptor concentration in the hundreds of micromolar level was needed to obtain measurable FRET signals in the 3-D cellular system. The results underscored the need to reduce the dimensionality of FRET systems in order to increase the FRET efficiency between donor and acceptor molecules.

Chapter 4 describes the development of FRET sensing lipobeads labeled with donors and their use to evaluate the interactions of acceptor molecules with the phospholipid membrane of FRET sensing lipobeads. The change in the dimensionality of the system in which FRET occurs, improved the sensitivity of our measurements by 3-folds compared to FRET measurements in solution. We concluded that a molecular recognition component had to be added to the sensing particles to further increase their selectivity and sensitivity.

Chapter 5 describes the development of FRET trap sensing beads and their use for screening nonfluorescent carbohydrates and glycoproteins. The FRET sensing technique was based on binding between dextran molecules labeled with Texas Red (Dextran-TR) and polystyrene microparticles labeled with Fluorescein tagged Concanavalin A (FITC-ConA). It was found that carbohydrates and glycoproteins inhibit the binding between dextran-TR and FITC-ConA labeled particles. The inhibition effect was concentration dependent thus enabled screening carbohydrates and glycoproteins based on their inhibition potency. The dissertation critically evaluates the performance of FRET microscopy and FRET based sensors in delivery and screening applications.

CHAPTER 1

BACKGROUND OF FRET BASED SENSORS

Fluorescence based sensors and biosensors have been valuable analytical tools since fluorescence is a highly sensitive and selective phenomenon [1, 2]. Recent developments in the field of biosensors enabled their employment in new applications primarily focusing on real time monitoring of biomolecular interactions. For example, biosensors were used to monitor processes like ligand fishing [3], signal transduction in cells [4, 5], cell adhesion [6], enzymatic reactions [7], and protein conformation changes and aggregation [8, 9]. Fluorescence based biosensors have also been employed in the drug discovery in studies involving primary screening of drug candidates as well as clinical trials [10-13]. Fluorescence biosensors demonstrate significant advantages over commonly used electrochemical sensing techniques since they do not consume their targeted analyte. Several problems of current fluorescence sensors include instabilities due to high photobleaching rates of sensing fluorophores and leakage of fluorophores from the sensing support. Other environmental parameters such as pH, polarity and temperature also affect the analytical properties of fluorescence sensors. Most currently used fluorescence sensors are based on a direct interaction of the sensing fluorophores with their targeted analyte. Unfortunately there is a limited number of analytes (pH, oxygen, calcium) that interact directly with fluorophores. Therefore there is a clear need for the development of new sensing techniques to expand the scope of analytes that

coud be detected with sensors. Fluorescence resonance energy transfer (FRET) could be used to detect analytes previously inaccessible to fluorescence sensing technology. Since FRET depends highly on the distance between donor and acceptor molecules, FRET based sensors could also provide valuable information about systems involving ligand-receptor binding or interactions between fluorescent drugs and acceptor labeled cells. Furthermore, FRET based sensors are less affected by environmental and illumination factors and therefore offer improvement in analytical performance compared to fluorescence intensity-based sensors. Several sections are presented in this chapter to explain fluorescence and fluorescence sensing techniques. These include fluorescence microscopy, the principles of fluorescence energy transfer (FRET) and the parameters affecting the energy transfer efficiency.

1.1. Fluorescence and Fluorophores

Luminescence is the emission of light from electronically excited states of materials. Luminescence is divided formally into fluorescence and phosphorescence, based upon the nature of the excited state. Fluorescence is the emission of light from a singlet state, when the electrons are paired. The lifetime of fluorescence is generally in the range of 10^{-8} sec. Phosphorescence is the emission of light from a triplet-excited state, when the electrons are unpaired. Phosphorescence lifetimes are longer than fluorescence lifetimes and range between 10^{-3} and 1sec. The phosphorescence transition from the triplet excited state to the ground state is forbidden since the electrons in the ground and excited states have different spin orientations [14-15].

Fluorescence occurs typically in aromatic substances that show molecular planarity and orbitals with delocalizated electrons over multiple conjugated double bounds. Recently, hundreds of fluorescent molecules (fluorophores) have been discovered and used in different applications [16-19]. Fluorophores are categorized as intensity-based sensing probes and wavelength-ratiometric probes. Intensity-based probes are fluorophores that display changes in emission intensity but do not display spectral shifts. The changes in the fluorescence intensity are typically due to different quantum yields of the free and complexed forms, rather than differences in the absorption spectrum. Considering a fluorescent probe, F, which reacts with an analyte, A:

$$A + F \rightarrow AF \quad (1.1)$$

The analyte concentration [A] is expressed as:

$$[A] = K_D (F-F_i) / (F_F - F) \quad (1.2)$$

where F_i is the fluorescence intensity when the fluorophore is in the free form, F_F is the fluorescence intensity when the fluorophore is completely reacted with the analyte. F is the fluorescence intensity when the indicator is incompletely complexed by the analyte A. K_D is the dissociation constant of the complex formed between the analyte and the fluorescent probe.

The relation (1.2) shows the major limitation of the intensity-based probes. The range of analyte concentrations that could be detected by these probes is limited to $0.1\ K_D<[A]<10K_D$. Concentrations lower than $0.1\ K_D$ or higher than $10K_D$ will produce little change in the observed signal. Wavelength-ratiometric probes have spectral shifts in their excitation or emission spectra when binding analytes. The analyte concentrations

are determined from the ratio of emission or excitation intensities, independent of the overall probe concentration. Using wavelength-radiometric probes the fluorescence measurements are independent of the fluorophore concentration, in contrast to intensity-based measurements.

Fluorescein, Sulforhodamine B and Texas Red are commonly used green and red fluorophores. Their inherent emission properties make them suitable for a broad spectrum of applications [20-25]. The structures of these fluorophores are shown in figure 1.1 [26]. These fluorescent dyes and their derivatives were frequently used in our experiments since they are characterized by large emission quantum yields and spectral Stoke shifts. Fluorescein is a pH sensitive dye, presenting several ionic forms [14, 26]. The changes in the absorption and emission spectra represent shifts in the equilibrium between the two fluorescent anions, the mono and dianion forms. These changes in the emission and excitation spectra could be used for wavelength-ratiometric pH measurements. However, due to its anionic charges at physiological pH, Fluorescein does not permeate with high yield into living cells. In order to overcome this limitation and to minimize the background fluorescence of fluorophores located outside the cells, nonfluorescent cell permeable derivatives of Fluorescein were recently developed. Fluorescein Diacetate and Calcein Acetoxymethyl (Calcein AM) (figure 1.2) are two examples of nonfluorescent molecules that permeate freely through cell membranes. These molecules become fluorescent after the cleavage of the ester bonds by nonspecific cellular esterases. Calcein AM is less prone to leakage outside the cellular cytoplasm since it bears more charged residues than Fluorescein Diacetate.

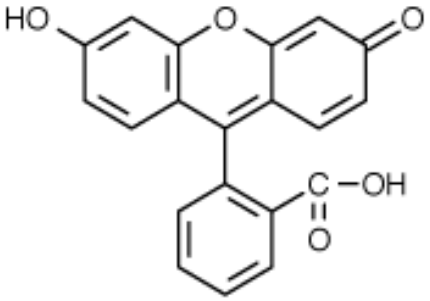

a)

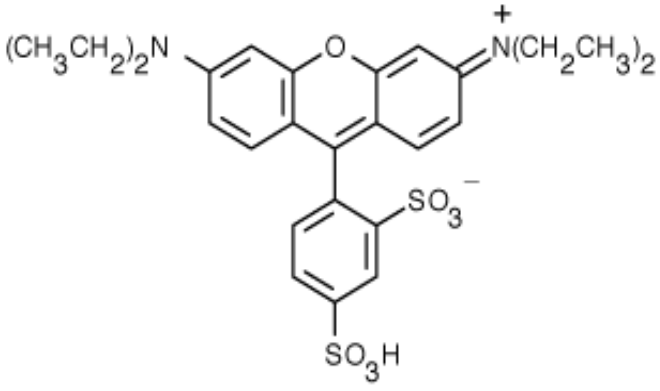

b)

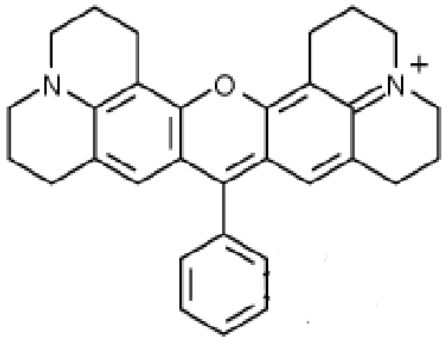

c)

Figure 1.1. Structures of a) Fluorescein, b) Sulforhodamine B and c)Texas Red.

Sulforhodamine and Texas Red (figure 1.1) are long wavelength excitable dyes with excitation wavelengths: 565 nm and 610 nm respectively. These red dyes are insensitive to pH changes and less prone to bleaching compared to Fluorescein dyes, making them more suitable for a broader range of applications. Cell Tracker Orange, a derivative of Tetramethylrhodamine is used mainly as a probe for long-term cell labeling since it undergoes glutathione S-transferase mediated reactions in the cellular milieu [26]. Rhodamine and Texas Red cell permeable derivatives were used for long term cellular studies such as quantifying cellular thiol levels [27], cell viability, cell fusion [28,29] and transplantation [30]. The use of these red dyes minimizes the effect of cell autofluorescence on the measurements.

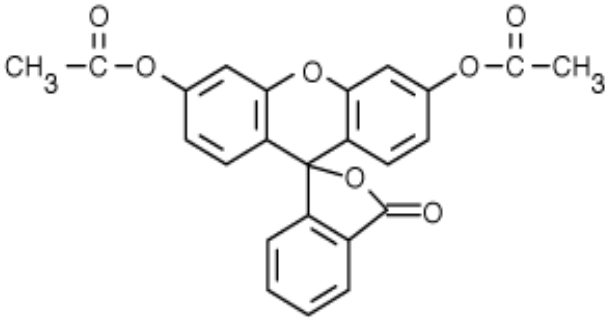

a)

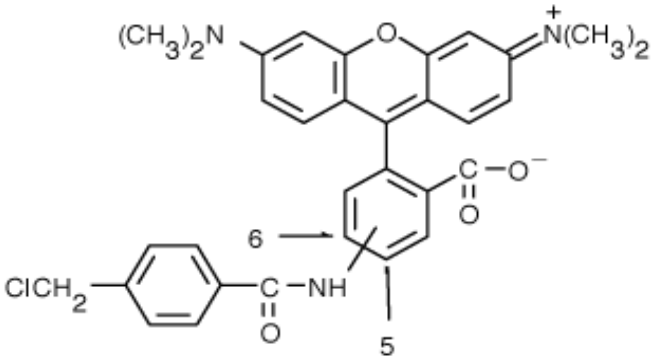

b)

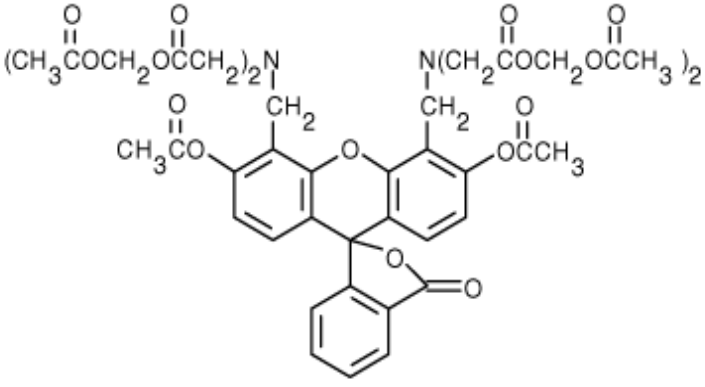

c)

Figure 1.2. Structures of a) Fluorescein Diacetate, b) Cell Tracker Orange and c) Calcein Acetoxymethyl (Calcein AM).

1.1. 1. Jablonski Diagram

The process of fluorescence, especially for organic molecules, is explained by the Jablonski diagram [14]. A typical Jablonski diagram is illustrated in figure 1.3. The singlet ground state, S_0, the first, S_1 and the second, S_2, electronic excited states are depicted. The vibrational energy levels are denoted by 0,1,2, etc. The absorption of photons typically occurs from the lowest vibrational level of S_0 to a vibrational state of S_1 or S_2. After the light was absorbed by the fluorophore several processes take place. Molecules rapidly relax to the lowest vibrational level of S_1 through a process called internal conversion. This process occurs within 10^{-12} sec. Fluorescence emission starts from a thermally equilibrated state, the lowest vibrational level of the excited state, S_1, and ends at a higher vibrational state of the ground-state level, S_0, which subsequently reaches quickly thermal equilibrium. The fluorescence lifetime of S_1 is generally in the range of 10^{-8} sec. The consequence of the emission to the high vibrational level of S_0 is that the fluorescence emission is the mirror image of the absorption spectrum of the $S_0 \rightarrow S_1$. In fact, the similarity of the emission and absorption spectra of a molecule proves that the electronic excitation required for a molecule to fluoresce does not alter the nuclear geometry (Frank-Condon principle). Due to the energy loss within the excited state, the energy of the emitted photons is lower than the absorption energy. Consequently, the wavelength of the emitted photons is longer than the wavelength of the excitation photons. The difference between the fluorescence wavelength and the absorption wavelength is defined as the Stokes shift. A larger Stokes shift increases the sensitivity of fluorescence measurements as it allows emission photons to be detected against a lower background, better spectrally separated from the excitation photons.

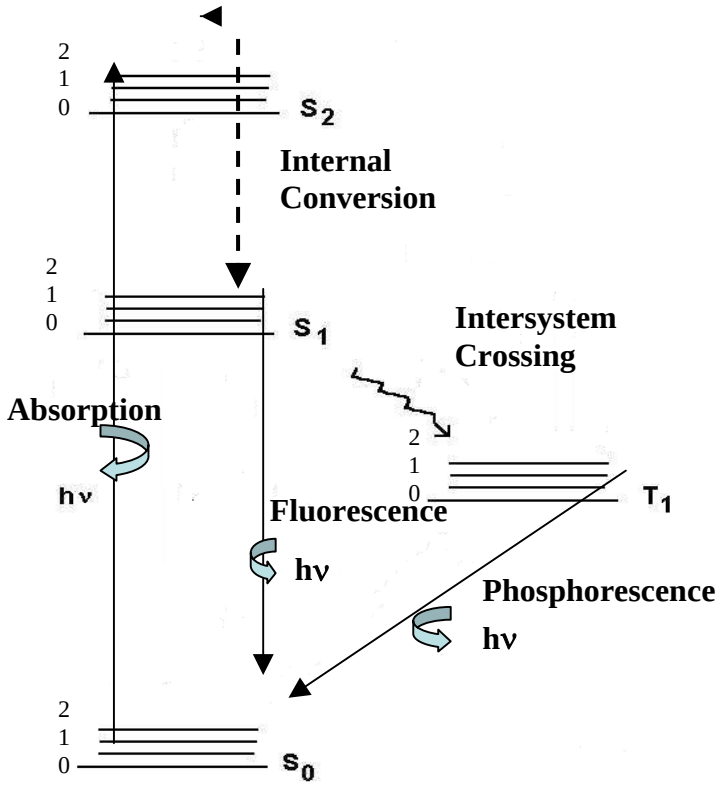

Figure1.3. Jablonski diagram describing radiative and nonradiative transitions in molecular systems.

In some special cases, molecules in S_1 could undergo another transition to a triplet state, T_1. Emission of photons from the triplet state, T_1, is named phosphorescence and is shifted to lower energies (longer wavelengths) compared to fluorescence. The transition from the excited triplet state, T_1, to the ground level, S_0, is forbidden, thus the phosphorescence lifetimes are several orders of magnitude longer than fluorescence lifetimes. Heavy atoms, like bromine and iodine increase the rate of intercrossing system from S_1 to T_1, thus increase the phosphorescence quantum yield. Three significant nonradiative deactivation processes are associated with fluorescence: internal conversion, intersystem crossing and vibrational relaxation. Internal conversion is the radiationless transition between energy states of the same spin state. Intersystem crossing is a radiationless transition between different spin states. Vibrational relaxation of the fluorophores takes place very quickly ($<1 \times 10^{-12}$ sec) and quenches the fluorescence emission. Vibrational relaxation occurs due to collisions between excited molecules and quenchers, while the fluorophore is in the ground or excited states.

1.1.2. Characteristics of Fluorescence Emission

Fluorescence is a cyclical process; a fluorescent molecule can be repetitively excited and detected. Since a single fluorophore generates thousands of photons the sensitivity of fluorescence-based methods is higher than the sensitivity of absorption methods. Recently, fluorescence techniques made possible the detection of single molecules and single molecule events. Unfortunately, fluorescent molecules are characterized by high rate of photobleaching. Photobleaching results in a loss of fluorescence due to the destruction of the fluorophore by irradiation. The mechanism of photobleaching is not

well understood. It often involves a reaction of excited fluorophores with singlet oxygen that leads to decomposition of fluorophores [14].

Generally, fluorescence molecules display a number of common characteristics that enable differentiation between fluorescence and scattering phenomena (Raman, Raleigh):

- Emission occurs at longer wavelengths than the absorption wavelength (Stokes' Shift).
- Emission spectra are independent of the excitation wavelength.
- Quantum yields are generally independent of the excitation wavelength.

Fluorescence Lifetime and Quantum Yield

The most important characteristics of fluorophores are their quantum yield (Q) and fluorescence lifetime (τ). The quantum yield, Q, is defined as the ratio between the number of emitted photons and the number of absorbed photons [14]. Emission quantum yields approache unity for substances with the brightest emission. For example, Fluorescein derivatives have quantum yield close to unity. Emission quantum yields are expressed as:

$$Q = \frac{\Gamma}{\Gamma + k_{nr}} \qquad (1.3)$$

where: Γ - emissive rate of the fluorophore

k_{nr} - rate of nonradiative decay to S_0.

The fluorophore excited lifetime (τ) determines the extent in which the excited molecules could interact with their environment. In general, fluorescence lifetimes range

between 10 nsec and 10μsec. The fluorescence lifetime is given by the following equation.

$$\tau = \frac{1}{\Gamma + k_{nr}} \qquad (1.4)$$

In fact only a few molecules would emit exactly at t =τ. Thus, the fluorescence lifetime is only an average value representing the average lifetime of an ensamble of fluorophores. The quantum yield of fluorophores affects the sensitivity of the fluorescence measurement. A bright fluorophore, with a large quantum yield would increase the sensitivity of the measurement while minimizing the required probe amount.

1.2. Fluorescence Sensors

A chemical sensor is a device or instrument that determines the detectable presence or concentration of a given analyte. The chemical interaction between the analyte and the sensor occurs at the solid interface. A transducer transforms the analyte-sensor interaction into a continuous optical or electrical signal, which is proportional to the analyte concentration. If the sensor contains a biological sensing element that interacts specifically with the analyte, the sensor is called a biosensor. The choice of an appropriate transducer for a given analyte depends on the desirable analytical properties such as the detection limit, precision, reproducibility and cost of the sensor. The sensitivity and selectivity of biosensors depend not only on the analyte binding affinity and specificity towards the biological recognition element but also on the transducer performance [31, 32]. Traditionally, biological sensing elements are based on catalytic properties of enzymes, microorganisms, and tissues or on the molecular

recognition reactions of antibodies, nucleic acids, lectins and receptor proteins. Recently G-protein-coupled receptor ligands (GPCRs) were extensively used in combination with fluorescence based sensors to screen potential drugs. These receptors mediate the cellular response to hormones and neurotransmitters. Numerous diseases are related to mutations in GPCRs structure [33].

A fluorescence based bio/chemical sensor designed for intracellular analysis must be highly compatible with the cellular environment, have low cytotoxicity, and high chemical stability and photostability. In order to prevent cytotoxicity upon insertion of the sensor into the cell, the fluorophore should be isolated from the cellular milieu by a compatible matrix. In our laboratory we improved the compatibility of miniaturized fluorescence sensors by using a phospholipid layer to coat the surface of the sensor [34, 35].

Fluorescence analogs of drugs have been used to investigate the delivery properties of various drug formulations into single cells [36, 37]. There are several problems associated with this technique. These include toxicity associated with the excessive fluorescent probe loading, possible interference reactions and lack of site specific information. In addition, when using classical fluorescence microscopy techniques it is difficult to distinguish between molecules absorbed on the surface of cells and molecules located inside the cytoplasm. Fluorescence resonance energy transfer (FRET) is a fluorescence phenomenon that has the advantage of being largely dependent on the distance between the donor and acceptor molecules [38]. This technique could be used to determine whether molecules are actually delivered into

cells. The proximity between donor labeled cell and an acceptor tagged drug, for example, could be evaluated by FRET.

Lately, submicrometric fiber optic sensors were used for site-specific cellular analysis as an alternative to free fluorophores [39-41]. Fiber optic sensors are limited to measurements in one cell at a time. Recently fabricated fiber sensors arrays improve the throughput of fiber optic sensors [42, 43]. However, they are not suitable for single cell measurements because of their large size. Even the insertion of a single fiber optic sensor into cells may damage the cellular membrane. Fiber optic sensing arrays could be used effectively to measure extracellular events. Particle based fluorescence sensors have been used as an alternative to fiber optic sensors in cellular analysis [34, 35]. Advantages of particle based fluorescence sensors compared to microelectrodes and fiber optic sensor include better protection against interferences, increased simplicity and sensitivity. The sensing fluorescent probe can be immobilized to the particle surface through chemical bonding or physical absorption [34, 35] or embedded within the particles during polymerization [44]. Polymer particle based sensors proved to be an excellent tool for single cell analysis [45, 46]. Particle-based fluorescence sensors and biosensors were also used for in vitro screening of potential drugs and provided detailed information on drug binding activity to receptors and on binding kinetics (on/off reaction rates) [47,48]. Nevertheless, there is a limited number of analytes that can be identified and quantified by fluorescence sensors since they are mainly based on direct interactions between fluorophores and their targeted analytes. Therefore, there is a need to develop new sensors with the capability to detect a wider range of analytes.

The development of particle-based FRET sensors in this study provided a novel way to overcome the lack of site specific information and to expand the range of analytes that could be quantified by fluorescence techniques. For example, the FRET based sensors described in chapter 5 were used for carbohydrate and glycoprotein screening, previously inaccessible to fluorescence sensors.

1.2.1 Mechanism of Sensing

Fluorescence based sensors exhibit changes in fluorescence intensity, wavelength, anisotropy and lifetime in the presence of targeted analytes (figure 1.4). Intensity based sensors are very practical since the necessary instrumentation is simple, sensitive and easily adaptable to various sensor configurations.

1.2.1.1 Fluorescence Quenching

Fluorescence quenching is a process that reduces the intensity of the fluorescence without changing the fluorophore emission spectrum. The decrease in the fluorescence intensity is proportional to the quencher concentration. The quenchers are molecules that interact with the fluorescent probe. There are several types of fluorescence quenching phenomena: collisional, dynamic and self quenching. Collisional quenching is often used in fluorescence sensing. The collisions between the analyte-quencher and the sensing fluorophore result in a decrease of the sensor fluorescence. When quenching occurs by a dynamic mechanism, the excited state is depopulated without allowing normal fluorescence emission. A decrease in the fluorescence lifetime

accompanies the decrease in the fluorescence intensity of the fluorophore. The dependence of the fluorescence of the sensors, F, on the quencher concentration, [Q], is given by the Stern-Volmer equation:

$$\frac{F_0}{F} = \frac{\tau_0}{\tau} = 1 + k_q \tau_0 [Q] = 1 + K[Q] \qquad (1.5)$$

Where, F_0, F and τ_0, τ are the intensities and lifetimes of the fluorophore in the absence and the presence of the quencher, K is the Sterner–Volmer quenching constant and k_q is the bimolecular quenching constant.

Self-quenching or “concentration quenching” occurs when a fluorophore acts as its own quencher. This phenomenon occurs at high concentration of fluorescence dyes. A variety of phenomena could contribute to the magnitude of self quenching: radiationless transfer of energy between identical molecules (when the Stokes shift is small), formation of larger aggregates of dyes or through a Stern-Volmer mechanism in solution. Common fluorescent dyes like Fluorescein, Rhodamine and Texas Red and their derivatives have a distinct upper concentration limit where self -quenching occurs. Fluorescence quenching based sensors were used to determine various analytes like oxygen and chloride [14, 34]. It should be noted that a fluorescent probe could be quenched not only by the targeted analyte but also by other species like solvent molecules or other substances in the sample. The sensor’s response should be corrected for these possible interferences.

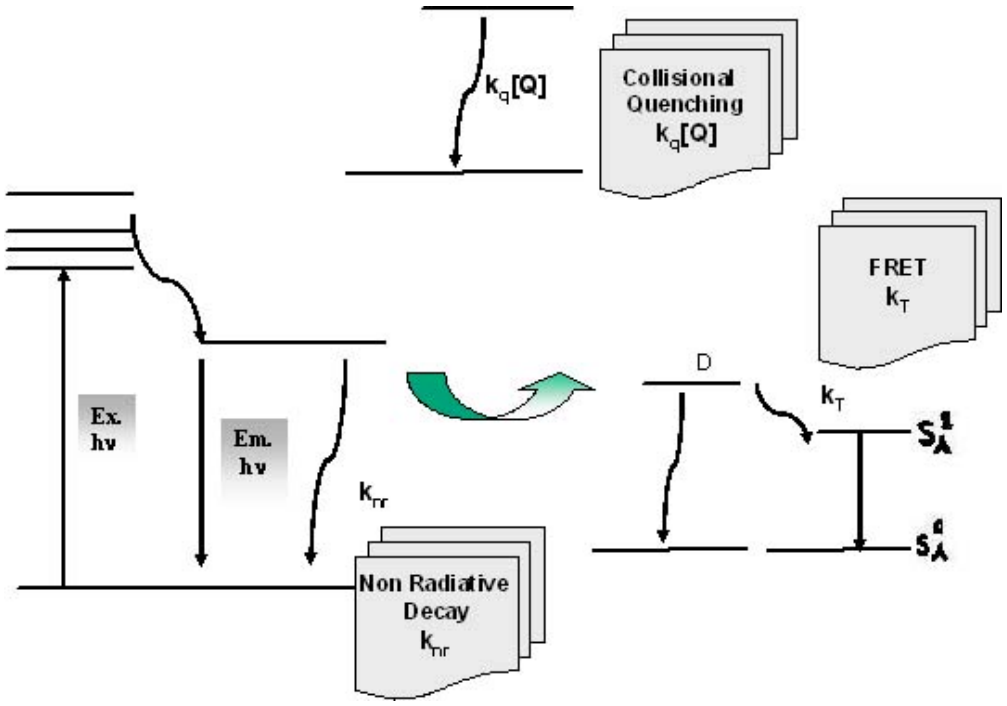

Figure 1.4. Modified Jablonski diagram for dynamic quenching and FRET.
Legend: hν- energy of the absorbed/emitted photons, k_{nr}-non radiative decay rate, k_q-bimolecular quenching constant, k_T-transfer rate in fluorescence resonance energy transfer (FRET) and S_A^0, S_A^2 - ground and excited singlet states of the acceptor molecule.

1.2.1.2. Fluorescence Resonance Energy Transfer (FRET) and Inner Filter Effects(IFE)

1.2.1.2.1. Fluorescence Resonance Energy Transfer (FRET)

Fluorescence resonance energy transfer (FRET) is a non-radiative energy transfer from the excited state of a donor (D) to an acceptor (A). FRET occurs when the emission spectrum of a fluorescent donor overlaps the absorption spectrum of an acceptor (figure 1.5). As a result, the donor lifetime is shortened and the acceptor fluorescence is

sensitized [14, 49-51]. The distance between the donor and acceptor has to be in the range of 1-10 nm for FRET to occur.

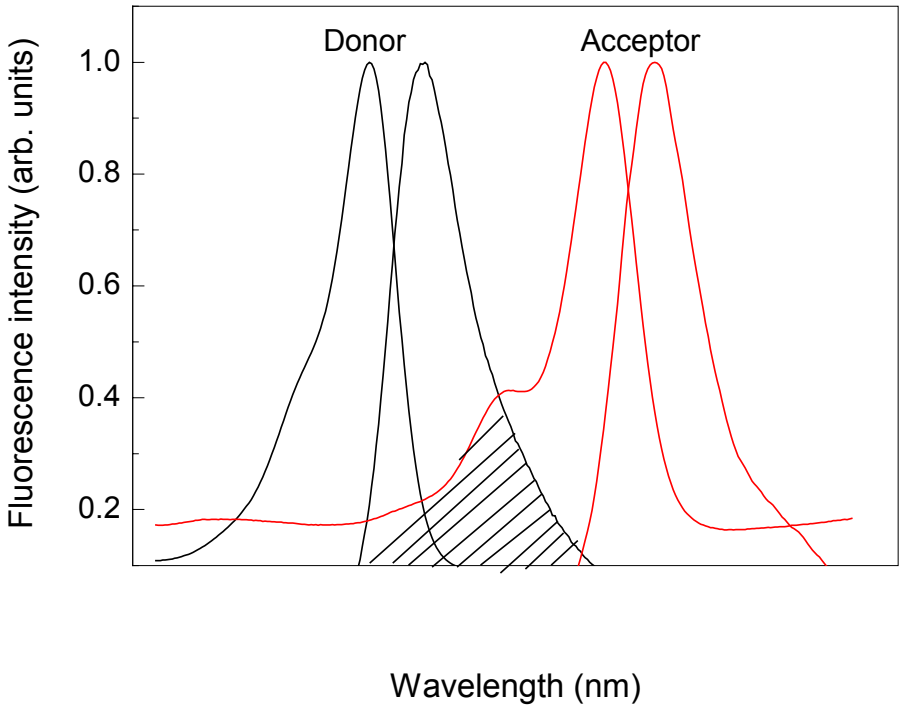

Figure 1.5. A spectral overlap (marked in diagonal lines) between the donor emission and the acceptor absorption is required for fluorescence resonance energy transfer (FRET) between donor and acceptor fluorophores.

Mechanism of FRET

The idea of a nonradiative transfer of electronic excited energy was first proposed by J. Perrin in 1920. The model proposed by F. Perrin showed that energy could be transferred over hundreds or even thousands of angstroms. It was Th. Forester [52, 53]

in 1946 that concluded that FRET could occur over distances up to 100Å. Galanin advanced the possibility of “inductive resonance” between molecules spaced at such a distance [54]. Forster and Galanin observed a nontrivial fluorescence quenching in solutions containing millimolar levels of acceptor molecules [52-54]. This nontrivial energy transfer could not be explained as occurring due to a trivial reabsorption of donor emission by acceptors. At these large concentrations the intermolecular distances are about 100Å or less, therefore the results proved that nonradiative transfer is possible when the donor and acceptors are within this distance range.

Two mechanisms could account for nonradiative energy transfer inductive resonance and exchange interaction. The inductive resonance mechanism is based on contributions from Coulomb interactions while the second is based on exchange interactions [49]. The exchange interactions are significant only for distances between donor and acceptor molecules that are smaller than 10Å. The inductive-resonance mechanism is used to describe energy transfer over larger distances. Several phenomenological theories were developed to explain FRET. These theories consider donor-acceptor relations such as their spatial arrangement and their diffusion kinetics providing descriptive models of FRET. These theories also allow comparisons with experimental data [55]. For a more detailed consideration, reference [49] should be consulted. The dipole-dipole approximation applied by Th. Forster in his inductive-resonance theory is used exclusively to explain FRET. The essence of this approximation is explained below.

Inductive-Resonance Theory

The theory assumes that the donor and the acceptor are placed at a sufficient large distance so that their electronic clouds do not interact. Consequently, the electronic spectra of the donor and acceptor are not deformed. In order for FRET to occur the acceptor must have an absorption band overlapping the donor emission band and a set of equal or similar levels of energy. In this case a flow of energy from the donor to the acceptor is possible. The phenomenon is equivalent to resonance between two mechanical pendulums.

Forster calculated the energy transfer probability as:

$$P = (2\pi/\hbar)|\langle H\rangle|^2 \delta \qquad (1.6)$$

where P is the probability of the nonradiative energy transfer from the donor to the acceptor, <H>, is the matrix element of the Hamiltonian for their interaction, and δ is the density of states. Assuming that <H> is a sum of Coulomb interactions of external electrons of the donor and acceptor, expanded in Taylor series, the Hamiltonian of the dipole-dipole interaction can be written as:

$$H = \frac{e^2}{R^3 \varepsilon}[r_D r_A - \frac{3}{R^2}(r_D R)(r_A R)] \qquad (1.7)$$

where R is a vector connecting the donor and acceptor oscillators, r_D and r_A are the vectors connecting the centers of molecules with the optical electrons, e is the electron charge, ε is the dielectric permeability of the medium to the optical frequencies. The rate constant of the energy transfer considering the wave function as a product of the

electron wavefunction and the vibrational function and normalizing the spectrum of the donor can be expressed as:

$$k_t = \frac{9000(\ln 10)K^2\varphi}{128\pi^5 n^4 N\tau_0 R^6}\int_0^\infty F_D(\nu)\varepsilon_a(\nu)\frac{d\nu}{\nu^4} \qquad (1.8)$$

where K^2 is the orientation factor, $F_D(\nu)$ is the spectral distribution of the donor fluorescence (normalized to the wavenumbers), $\varepsilon_a(\nu)$ is the molar coefficient of the acceptor extinction, N is Avogadro's number, n is the refractive index of the solvent, τ_0 is the intrinsic lifetime of the donor in the absence of the acceptor, and R is the distance between the donor and the acceptor.

The expression (1.8) was written by Forster in the following reduced form:

$$k_t = \tau^{-1}\left(\frac{R_0}{R}\right)^6 \qquad (1.9)$$

where τ is the measured lifetime of the donor in the absence of the acceptor. It is related to τ_0 via the quantum yield of the fluorescence:

$$\tau = \varphi\tau_0 \qquad (1.10)$$

The parameter R_0 from equation (1.9) is called the Forster distance, the distance at which the energy transfer efficiency is 50%.

$$R_0 = \sqrt[6]{\frac{9000(\ln 10)K^2\varphi}{128\pi^5 n^4 N}\int_0^\infty F_D(\nu)\varepsilon_A(\nu)\frac{d\nu}{\nu^4}} \qquad (1.11)$$

The value of Forster distance, R_0, can be calculated by substituting in equation (1.11) the values of the spectral parameters obtained from the donor and acceptor. Typically the values of the Forester distance range between 20 and 70 Å [14, 50].

The decay of the donor intensity and the quantum yield were described by Forester for a completely homogeneous solution. Forester showed that the efficiency of this process (E) is dependent on the sixth power of the distance between the donor and acceptor, hence highly sensitive and specific phenomenon to any change that might affect the donor or the acceptor.

$$E = \frac{R_0^6}{R_0^6 + R^6} \tag{1.12}$$

For a randomly distributed solution, R_0 is expressed as:

$$R_0 = \left(\frac{3000}{2\pi^{3/2} N A_0} \right)^{1/3} \tag{1.13}$$

where N is Avogadro number and A_0 is the concentration of the acceptor at which the energy transfer is 76%. Relation (1.13) reveals important feature of energy transfer between donors and acceptors. For a system of randomly distributed donors and acceptors, the concentration of the acceptor required for efficient FRET is in the milimolar range. The high acceptor concentration complicates the FRET measurements since inner filter effects (IFE) interfere significantly with FRET.

Effect of Orientation Factors

The orientation factor K^2, which defines the relationship between the donor and acceptor dipole moments can range between 0 for perpendicular dipole moments and 4 for parallel dipole moments. For example K^2 is assumed equal to 2/3 for random orientations. There are a number of extensive discussions in the literature about the effect of different donor and acceptor orientation geometries on the efficiency of the energy transfer [56-61]. The orientation factor, K^2, is important only when the geometry between interacting donor and acceptor molecules is well defined. In most applications of FRET, in which the labeling procedure introduce considerable heterogeneity the orientation factors are less important [62].

Effect of System Dimensionality on FRET

For randomly distributed acceptors, the donor fluorescence decrease depends on the dimensionality of the acceptor distribution. Different distribution functions are used when the acceptor molecules are dispersed in a volume (three-dimensional or 3D), in a plane or along a line. For example, planar distribution is possible when the donor and acceptor absorbed into a membrane (two-dimensional or 2D), linear distribution (uni-dimensional or 1D) could be realized when dyes intercalate into a DNA helix. For a random distribution of acceptors and donors (like in solution), assuming no diffusion and no excluded volume, the intensity decays of the donors, in the presence of acceptors, can be calculated using the following analytical form [63-66]:

$$I_{DA} = I_D^0 \exp\left[-\frac{t}{\tau_D} - 2\gamma\left(\frac{t}{\tau_D}\right)^{d/6} \right] \quad (1.14)$$

where d= 3, 2 and 1 for tri-, two- and uni-dimensional distribution, I_D is donor decay time in the absence of acceptors and γ is a function related to the concentration of the acceptor and the dimensionality of the system.

The extent of energy transfer (equation 1.14) for the same concentration of acceptor molecules is higher in uni-dimensional than in three-dimensional system. As described in this thesis, this characteristic of energy transfer results in improved sensitivity of FRET based sensors compared to FRET measurements in solution. Although the theory of FRET for multiple acceptors, restricted geometries and diffusion of donor – acceptor is quite complex, FRET is one of few reliable methods for studying the proximity and geometric distribution of fluorescent molecules in biological systems. However, often unavoidable interfering processes could take place when donor and acceptor molecules are present in the same system. Such processes are named inner filter effects (IFE). They involve transfer of energy as well.

1.2.1.2.2. Inner Filter Effects (IFE)

The inner filter effect is a decrease in the fluorescence intensity due to absorption of the excitation/ emission light by an absorbing molecule. Inner filter effects are classified as a primary inner filter effect when the fluorophore excitation light is absorbed and a secondary inner filter effect when the emission of the fluorophore is absorbed by a molecule present in the solution. The theory of inner filter effects in macroscopic

samples is well established [67]. Several studies on the theory of IFE in microscopic droplet domains were published [68]. The fluorescence intensity ratio of the fluorophore prior and following the addition of an absorbing species is expressed as:

$$\frac{F}{F_0} = \frac{1-10^{-\varepsilon_{ex}|Q|b}}{2.303\varepsilon_{ex}|Q|b} \tag{1.15}$$

for primary IFE and as :

$$\frac{F}{F_0} = \frac{1-10^{-\varepsilon_{em}|Q|b}}{2.303\varepsilon_{em}|Q|b} \tag{1.16}$$

for secondary IFE.

Where ε_{ex} and ε_{em} are the molar absorption coefficients for absorption and emission of the absorber, b is the effective pathlength of light and |Q| is the concentration of the absorber/quencher. The fluorescence intensity of the sample in the presence of absorber depends not only on the absorber concentration,but|Q| , also on the light harvesting conditions of the instrumental set-up (slit-width, volume and pathlength of the cuvette and wavelength of excitation). IFE based sensors were previously employed for the detection of different ions of clinical importance [69, 70]. Unlike FRET based sensors, IFE based sensors do not provide site specific information and cannot be used to determine donor-acceptor interactions.

1.3. Measurements of FRET Efficiency Using Fluorescence Microscopy

Fluorescence microscopy has enabled the investigations of structure–function relationships in living cells. However, conventional microscopy techniques are limited by the light diffraction limit (λ/2), which is about 250 nm. In contrast, FRET microscopy could be used to overcome the diffraction limit and to provide information about cellular interactions in the nanometer scale [71, 72]. This chapter is reviewing the methods used in FRET microscopy for the measurement of energy transfer in solution and cells. The theory is adapted mostly from references 73 and 74.

Donor Quenching and Acceptor Sensitized Emission

Generally, three images are necessary for calculating the efficiency of energy transfer between donor and acceptor molecules. I(d/d) is acquired using donor excitation and emission filters. I(d,a) is acquired using donor excitation and acceptor emission filters, and I(a/a) is acquired using acceptor excitation and emission filters. These images are processed for camera bias, dark current, and inhomogeneities [75, 111]. The inhomogeneity conditions result from deviations in the image position introduced by differences between dichroic mirrors and emission/excitation filters used to acquire the images. It could be corrected by X-Y translations, which are generally less than 10 pixels. Then, these images are corrected for overlaps between the donor and acceptor excitation and emission spectra. The bleed-trough factors could be calculated from images of the samples labeled only with donor or acceptor molecules.

The corrected donor and acceptor emissions can be expressed as [73]:

I(d,r) = donor emission, I(d,d), after image corrections (1.17)

I(a,s) = sensitized acceptor emission= $I(d,a)-b_1I(d,d)-b_2 I(a,a)$ (1.18)

In equation (1.18), the first bleed-through factor, b_1, describes the donor emission in the acceptor channel and the second factor, b_2, reflects the direct excitation of the acceptor at the donor wavelength used. The final step is to correct I(a,s) with a factor, ξ, that depends on the microscope used for FRET measurements. This factor accounts for the differences in absorption, cross-sections, and excitation intensities and detectors efficiency. The energy transfer efficiency is calculated for each pixel after the evaluation of the bleed-though factor: $E=I(d,t)/I(d,tot)$ (1.19)

where $I(d,t)= I(a,s)\ \xi$ and $I(d,tot)=I(d,r)+I(d,t)$. I(d,t) is the fluorescence resonance energy transferred from the donor to the acceptor. This method is fairly practical but is subjected to cumulative errors associated with the correction factors. Nearly equals values are subtracted and divided thus making this method sensitive to small errors in the experimental data.

Our Practical Approach for FRET microscopy

As previously mentioned the analysis of FRET experimental results is prone to artifacts and errors. We preferred to evaluate FRET efficiency either from the acceptor sensitized emission or from the quenching the donor emission. When acceptor sensitized emission was used, the FRET ratio between the fluorescence intensities of the acceptor and donor was calculated. The FRET ratio takes advantage of the sensitized acceptor emission and the quenching of the donor fluorescence. The two effects cause the numerator to increase and the denominator to decrease; therefore the

FRET ratio increases as the energy transfer efficiency increases. Unfortunately, sometimes the measurement of the acceptor sensitized fluorescence can introduce large errors, for example when the signal to noise in the FRET channel is low or geometric errors given by the displacement of the filters from different filter combinations occur. In the case of the carbohydrate/glycoprotein screening project, the augment of the acceptor fluorescence ranged from signal to noise values of 1 to 10. The use of FRET ratio could only degrade the quality of the results. Therefore, we used the donor quenching method to calculate the FRET efficiency. The excitation wavelength was set at the donor absorption and the emission wavelength at the donor emission. The donor emission wavelength was selected such that no contribution from the acceptor fluorescence was observed.

1.4. Carbohydrate Binding Proteins: Lectins.

Lectins are carbohydrate-binding proteins that bind specifically and reversibly to sugar molecules [76-81]. On the basis of their specificity they can be classified into five groups according to the monosaccharide, which provides the highest specificity: mannose, galactose/ N-acetylgalactosamine, N-acetylneuraminic acid, N-acetylglucosamine and fucose (sugars are in D configuration, except for fucose that appears as L configuration). The interaction of lectins with monosaccharides is usually weak with association constants in the range of millimolars [77,80]. Lectins exhibit higher specificity for di, tri, and tetrasaccharides with 1000-fold greater association constants compared to monosaccharides. Molecular modeling and high resolution NMR

measurements have shown that the affinity of lectins to oligosaccharides is affected by the shape of the oligosaccharides. Oligosaccharides are flexible molecules due to the rotation around the glycosidic bonds that connect the constituent monomers [83-87]. The amino-acid sequence and three-dimensional structures of lectins have been investigated and elucidated [88-93]. The elucidation of lectin structures enabled the classification of lectins based on their common characteristics. The majority of lectins are simple, mosaic and organized in macromolecular assemblies.

Lectins from plants, such as Concanavalin A or wheat hemmaglutinin, are the most studied carbohydrate binding proteins. They have been used as models for understanding the complexity of animal lectins [94,95]. Typically, plant lectins consist of two or four identical or almost identical subunits of 25-30kDa, each with a small specific binding site for a carbohydrate. Divalent ions, especially Ca^{2+} and Mg^{2+}, are required for saccharide binding [96]. The plant lectin subunits are mainly composed of two antiparallel β sheets, one of six strands and the other of seven strands. The six-stranded sheet is almost flat and the other is concave. The concavity of the face provides the carbohydrate-binding site, which is easily accessible to monomeric and polymeric carbohydrates. The metal ions Ca^{2+} and Mg^{2+} are in close proximity (9-10 Å) to the carbohydrate-binding site. They play a role in positioning the amino acids responsible for carbohydrate binding. A correlation between the size of binding loops and monosaccharide specificity has been shown [97].

Many lectins participate in multivalent interactions with oligosaccharides and carbohydrate polymers. The apparent affinity binding constants of oligosaccharides to

lectins are higher than the binding constants calculated as the oligosaccharides bind to a single receptor. Several mechanisms could explain these multivalent interactions: chelate effect, subsite binding, steric stabilization, statistical rebinding, and receptor clustering [184,186].

The recognition sites of lectins are shallow depressions on the surface of the proteins [98]. It seems that the recognition sites are preformed since few noticeable conformational changes occur due to carbohydrate binding. The main chain positions of the amino acids forming the carbohydrate-binding site remain almost rigid prior and following sugar complexation. However, the side chains undergo drastic conformational changes upon binding [104,105]. The binding sites of the lectins are similar but quite different for various lectin families, even if the lectins specificity is the same [103-105]. In general, carbohydrate ligands bind only to one of the protein faces [102,105].

The interactions between carbohydrates and lectins are based on hydrogen bonds and hydrophobic effects. The hydrogen bonds are formed between carbohydrate hydroxyl groups and amino, hydroxyl and carboxylic groups of the lectins. The metal ion coordinations seem to play a role in the saccharide-lectin interactions [101,102]. It is also possible that hydrophobic effects exist due to hydrophobic regions of carbohydrates and proteins even if the saccharides are highly polar. Water molecules sometimes mediate the interaction between the sugar and the protein by water bridges. Calorimetric studies of the carbohydrate-protein binding showed that the interactions between lectins and carbohydrates are enthalpy driven. The unfavorable loss of entropy is compensated by enthalpy gained due to the removal of water molecules bound to lectins [103].

CHAPTER 2

EXPERIMENTAL

This chapter describes the experimental methods and instruments used to complete the studies performed in this dissertation. Specific technical and experimental details are given in the results sections.

2.1. Materials and Reagents

Microscope glass cover slips used for microscopy and Lab-Tek II chambered coverglass were purchased from VWR Corporation. 1,2-Dimyristoyl-sn-glycero-3-phosphocholine(DMPC),1,2-dimyristoyl-sn-glycero-3-phosphate,1,2dioleoyl-sn-glycero-3-phosphocholine(DOPC), dioleoyl-sn-phophoethanolanime-N-succinyl(N-succinyl-DOPE), 1,2-dihexadecanoyl-*sn*-glycero-3-phosphoethanolamine(PE), and 1,2-dimyristoyl-sn-glycero-3-phosphate monosodium salt (DMPA) were purchaesd from Avanti Polar Lipids. Cholesterol and dihexadecyl phosphate (DP) were purchased from Aldrich. *N*-(Fluorescein-5-thiocarbomyl)-1,2-dihexadecanoyl-*sn*-glycero-3-phosphoethanolamine(Fl-DHPE), carboxyfluorescein, sulforhodamine, dextran-Texas Red (dextran-TR, 10000 MW, neutral), Fluorescein diacetate (FDA), Calcein Am (Cal Am) and Cell Tracker Orange were obtained from Molecular Probes. Polystyrene particles (mean diameter: 1.6 μm, -/+ 0.5%) were purchased from Bangs Laboratories

, Inc. and Polyscience Inc. Chloroform, methanol, hexane, cholesterol (CH), FITC conjugate of concanavalin A (FITC-ConA), concanavalin A type IV, D(+) mannose, Ovalbumin (grade V), Glucose-oxidase (245.9 units/g solid), Avidin (10.8 units/mg solid), Galactose, Mannose, HEPES buffer, Bovine Serum Albumin (BSA), poly -L-lysine, NaCl, $CaCl_2$ and $MnCl_2$ were purchased from Sigma. Sodium hydroxide and hexane were purchased from EM Sciences. Spectroscopic grade ethanol was purchased from Aldrich. Phosphate buffer (PBS, 100mM, pH=7.4) were obtained from Amresco. All aqueous solutions were prepared with 18 MΩ deionized water purification system (Barnstead Thermolyne Nanopure). Dulbecco's modified Eagle's medium, L-glutamine, sodium pyruvate, and fetal bovine serum for the cell culture were purchased from Invitrogen.

2.2. Instrumental Methods

2.2.1. Spectrofluorometry Measurements

A spectrofluoremeter generates the wavelength of light required to excite the sample of interest, selects the emitted wavelengths and then measures the intensity of the emitted light. A fluorescence spectrum depicting the intensity of emission versus wavelength is obtained. The excitation and emission spectra of free dyes, as well as the response of fluorescence probes and sensors in solution were acquired using a Photon Technology International spectrofluoremeter (QM-1 model, PTI, Ontario, Canada). Each spectrum presented in this dissertation is an average of three replicate spectra unless otherwise noted.

Generally, the excitation wavelength is selected with a narrow bandwidth by the excitation monochromator from the light source. Additionally, filters could be used to narrow down the excitation light wavelength range. Then, the emitted light reaches the sample and excites it. The sample emission is collected and passed through the emission monochromator, which separates the wavelength in order to obtain a spectrum. The general characteristics of spectrofluoremeter individual components are described below. The instrument used in our experiments was equipped with a xenon lamp as an excitation light source, two monochromators and a photomultiplier tube detector.

2.2.1.2. Light Source

The PTI spectrofluoremeter is equipped with a 75 W high-pressure xenon (Xe) lamp, which is used as the excitation light source. A continuous and homogeneous, intensity light output is obtained from 250 nm to 750 nm. Two electrodes are sealed in a glass bulb containing Xe under high pressure. When the lamp power is turned on, a high voltage discharge occurs between the electrodes and Xe ions are formed. The arc lamps emit light continuously as a result of the recombination of electrons with ionized Xe atoms. The lamp housing helps to collect the lamp output, which is then focused into the entrance slit of the monochromator. The housing also serves to remove excess heat and ozone by directing cooled air directly over the lamp.

2.2.1.2. Monochromator

A monochromator is the wavelength selector part of a spectrophotometer. Monochromators contain: an entrance slit, a collimating lens, a dispersing device, a focusing lens and an exit slit. The dispersing element can be a prism or a grating. The polychromatic radiation emitted by the source is directed through the entrance slit and collimated by the collimating lens. Then, the light strikes the dispersing element at a certain angle and the polychromatic radiation is divided into its component wavelengths by dispersion through the prism or the grating. Radiation of only a particular wavelength is selected moving the dispersing element in front of the exist slit. The fluoremeter used in our studies was equipped with two monochromators; one for excitation and one for emission. The monochromators were autocalibrated and under computer control for scanning and positioning.

2.2.1.3. Photomultiplier Tube (PMT) Detector

Photomultiplier tubes (PMTs) are light detectors that convert photons into an electrical signal. They have a high internal gain. Photomultiplier tubes are very sensitive light detectors for low intensity applications. A photocathode, a series of dynodes, and an anode are placed in evacuated glass tube. The photocathode is made out of an alkali metal mixture, which makes the PMTs sensitive to photons in the UV-VIS region of the electromagnetic spectrum. The photocathodes operate at a high negative voltage in the range of –500 to –2000 volts. When a photon enters through the glass surface, it hits the photocathode which is located on the inner surface of the glass. The photocathode hit by the photon ejects a photoelectron due to the photoelectric effect. The electron is

attracted and accelerated towards the first dynode. A high voltage charges the dynodes positively. After the electron encounters the first dynode, several other photoelectrons are emitted. These electrons are subsequently attracted and accelerated to a second dynode, which has even higher positive electric potential. The process is repeated several times and, 10^5 to 10^7 electrons are created for each photoelectron ejected by the photocathode. In this way the signal is amplified greatly. The amplification power of the PMT depends on the number of dynodes and the accelerating potential difference between them. The electrical signal given by the PMT is proportional to the light intensity. A vacuum PMT with a wavelength range of 185 to 800 nm was employed as a detector in our experiments.

2.2.2. Digital Fluorescence Imaging Microscopy System

The use of fluorescence microscopy offers many advantages, including specificity, sensitivity, quantitative power and high temporal and spatial resolution [107, 108]. Since fluorescence is affected by environmental factors, fluorescence microscopy can be used to investigate pH, viscosity, refractive index, ionic concentrations, membrane potential, and solvent polarity in cells and tissues. Fluorescence measurements of fluorescent probes in single cells and of FRET based sensors were performed using an inverted epifluorescence microscope (Olympus IX-70). The microscope was equipped with three detection ports: one coupled to a spectrograph- CCD camera system, one coupled to a CCD camera for imaging, and one coupled to a 35 mm camera.

In simple terms, a fluorescence microscope can be described as a conventional light microscope with an additional excitation source and an array of filters. The microscope is constructed to ensure that the excitation light that passes through the objective has an opposite path leading to the eyepiece or detector. The filters and the dichroic mirror separate the excitation from the emitted light. The performance of a fluorescence microscope depends on the objective and the filters used to obtain the fluorescence images. The images obtained with the fluorescence microscope are recorded via a storage device such as a camera or a CCD detector. The fluorescence microscope individual components are described below.

2.2.2.1. Microscope Objective

The microscope objective performs two functions:

- Focus properly the excitation light on the sample.
- Collect the fluorescence emitted by the sample.

A microscope in which the excitation and emission light travel through the same objective is called epifluorescence [6]. The optics used for the construction of an epifluorescence microscope with low noise must separate effectively the emission and excitation light pathways. A schematic diagram of an epifluorescence inverted fluorescence microscope image is shown in the figure 2.1. The spatial resolution of a microscope is defined as the limit for the smallest resolvable distance between two points. It is expressed as:

$$D=1.22\lambda/2(NA) \qquad (2.1)$$

where NA is the numerical aperture of the objective lens, NA= n sinα; **n** is the refractive index of the medium next to the lens (e.g. air, water, immersion oil, or glycerol); α is the half angle of the cone collected by the aperture of the lens; λ is the wavelength of the light used. The optimal resolution is 500-1000 higher than the NA of the objective.

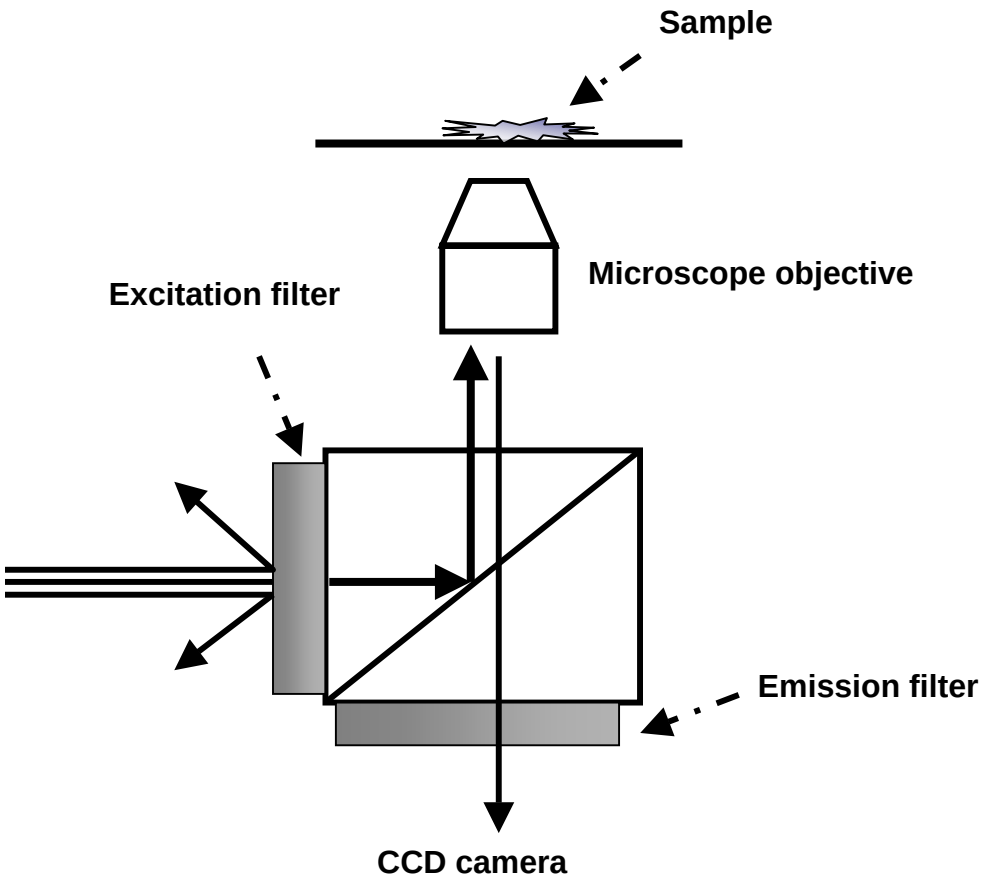

Figure 2.1. Illustration of a typical light path in an inverted epi fluorescence microscope.

Another important parameter of the microscope objective is the light gathering power that affects the image brightness. The light gathering power is proportional to the forth power of the objective numerical aperture, NA. It should be noted that high

magnification and numerical aperture increase the spatial resolution but also leads to a rapid decrease in the sample fluorescence due to photobleaching. 20X and40X objectives with a numerical aperture 0.5 or 0.7 respectively were used in our experiments.

2.2.2.2. Dichroic Mirror

The dichroic mirror is used to separate the excitation and emission light paths. In an inverted microscope, as used in our experiments, the dichroic mirror position is located below the sample. The sample placed on the microscope stage is excited and imaged from under the stage. The excitation light is reflected by the surface of the dichroic mirror into the objective and used to excite the sample located on the microscope stage. The fluorescence light emitted by the sample is collected by the objective and passes through the dichroic mirror and through the emission filter to a reflective mirror that directs the emitted light to the eyepiece or the detector. Dichroic mirrors are characterized by a transition wavelength. The dichroic mirror reflects all light of wavelengths lower than the transition value. Light at wavelengths longer than the transition value is transmitted through the dichroic mirror. The transition wavelength of the dichroic mirror must be chosen between the excitation and emission peak of the used fluorophore.

2.2.2.3. Excitation and Emission Filters

The dichroic mirror is unable to separate completely between the excitation and emission light. About 10 % of excitation light could leak into the detection channel,

which could degrade the signal to noise (S/N) ratio in the obtained images. Excitation and emission filters are placed in front and below the dichroic mirror in order to improve the separation between the excitation and emission lights. Also, the emission filter selects the emission wavelength range that reaches the detector.

2.2.2.4. The Filter Cube

The excitation/emission filters and the dichroic mirror are mounted on an optical holder commonly named a filter cube. The cube offers a convenient way to change the dichroic mirror and filters as needed for different applications.

2.2.2.5. Light Sources

Commonly, high-pressure mercury or xenon light sources are used for fluorescence microscopy. The lamps are very bright and produce abundant light for majority of applications. Sometimes, the illumination is too intense and could cause rapid photobleaching of the fluorescence probe or could harm the living organism studied. Therefore, neutral density filters are used to minimize the amount of light that the specimen encounters. A 100W mercury lamp that consists of two electrodes placed under high pressure in a quartz glass tube filled with mercury was used as the light source in our studies to evaluate fluorescence probes and the response of FRET sensing particles. The mercury lamps do not have even intensity across the electromagnetic spectrum. The emission of mercury lamps shows peaks at 313, 334, 365, 406, 435, 546, and 578 nm. At other wavelengths the emission of the mercury lamp is low. A mercury lamp has a typical lifetime of 200 hours.

2.2.2.6. Charged Coupled Device (CCD Camera)

The most commonly used detectors for fluorescence microscopy are CCD cameras that use coupled device (CCD) chip for imaging. CCD chips are silicon-based circuits, which are arrays of light sensitive pixels. Electrons are produced by the interaction of photons with the silicon atoms of the chip. These electrons accumulate in potential wells and then transported across the chip through registers (figure 2.2). The amount of charge trapped under each pixel is proportional to the amount of light that falls on it. The accumulated charge is then "read out" by changing the electrical bias of an adjacent pixel so that the charge moves out of the chip. Then it is converted into a voltage and digitized into an intensity value. A two dimensional image is formed by reading the charge at each pixel. In a silicon chip, Si atoms are covalently bound to neighboring atoms. Energies larger than 1.1 eV are required to break these bonds and create electron-hole pairs. Therefore, the shorter the wavelength of the illumination light, the shorter the photon absorption depth. There are two types of CCD camera: front and back illuminated (figure 2.3). In front-illuminated CCD cameras light enters through the CCD gates of the parallel register. The gates are made out of a very thin layer of polysilicon, which is relatively transparent at long wavelengths, but becomes opaque at wavelengths shorter than 400 nm. Using acid-etching techniques, the silicon can be transformed in a 10 μm uniform layer and used to focus an image on the backside of the CCD register (figure 2.3). Thinned back-illuminated CCDs exhibit high sensitivity to light from the soft X-ray to the near-infrared regions of the spectrum. Coating the CCD chip with proprietary phosphor improves the sensitivity of the chips in the ultraviolet region (200 nm to 400 nm).

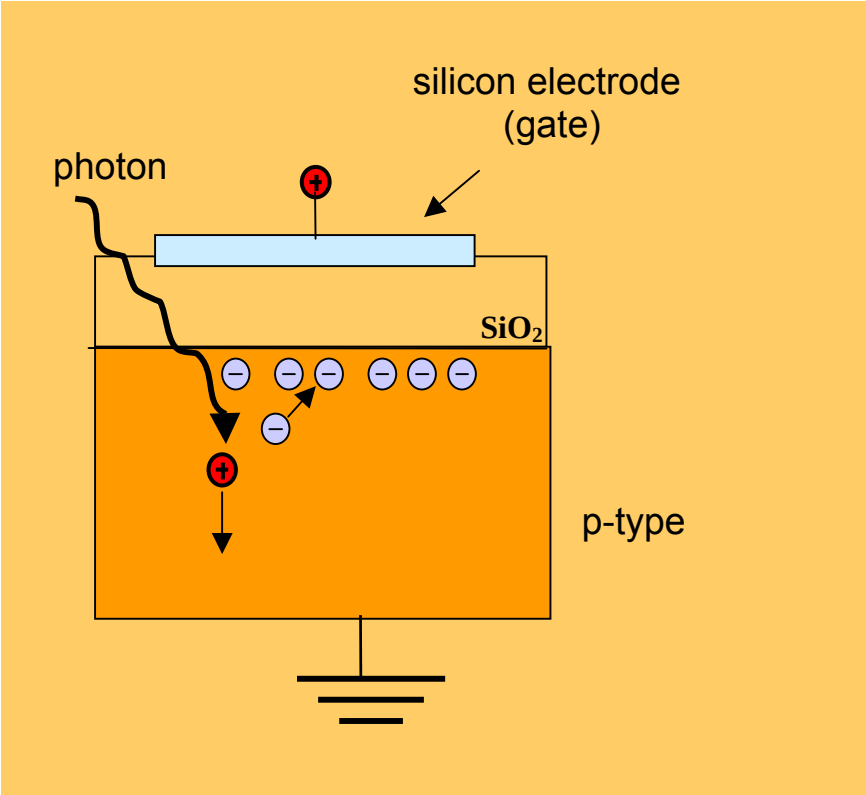

Figure. 2.2. Schematic diagram of a CCD pixel. Each pixel in a CCD is a tiny capacitor that is formed by growing a layer of silicon dioxide on top of a polysilicon substrate. A metal electrode, called gate, is deposited on this structure.

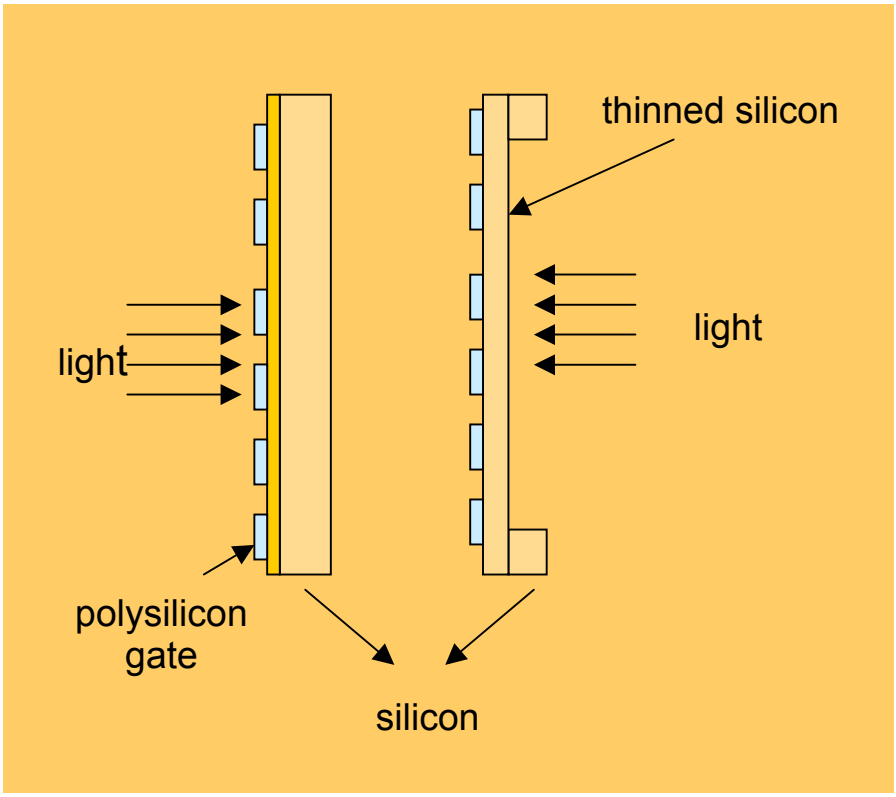

Figure 2.3. The geometry of a front and back-illuminated CCD chip.

CCD cameras are also classified as: full-frame CCD, interline transfer CCD and frame transfer CCD cameras (figure 2.4). Full-frame CCDs are used to obtain high-resolution images due to their high-density pixel arrays. The image is collected pixel by pixel. The readout is collected by shifting rows of the image in a parallel fashion, one row at a time, to a serial shift register. The serial register sends each row of image information to an output amplifier as a serial data stream. The read-out charge must be rendered to the serial register before the next row of data shifts to the horizontal array. The procedure is continued until all rows of data are sent to the output amplifier and to an analog-to-digital signal converter integrated circuit.

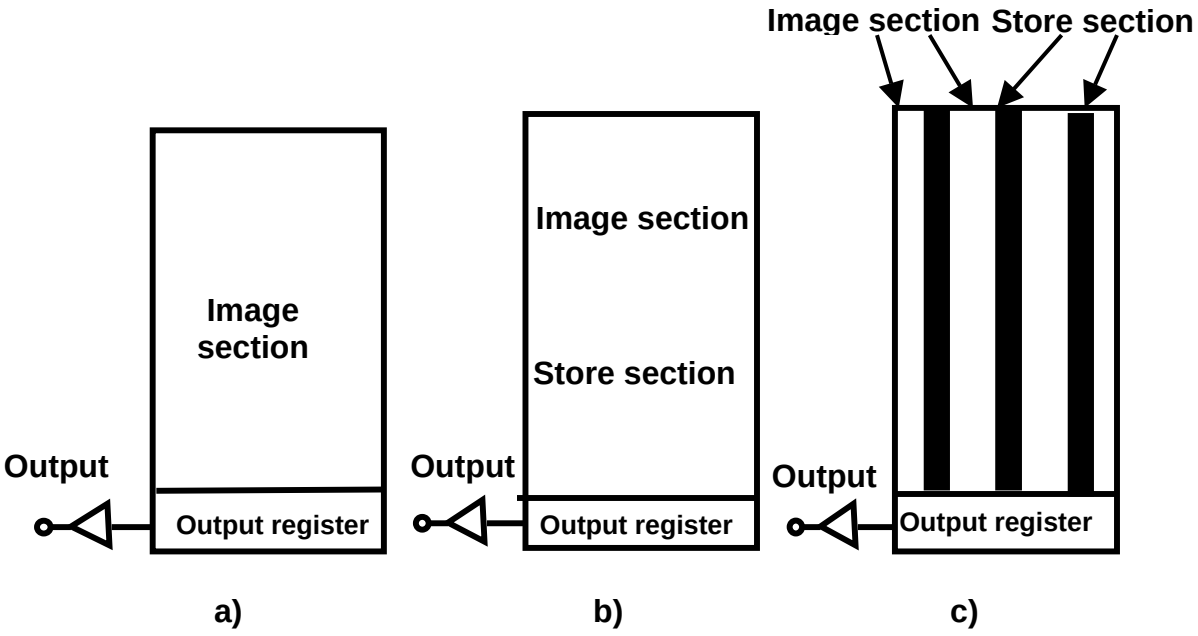

Figure 2.4. Schematic diagram of charged coupled device (CCD) cameras: (a) conventional full frame CCD with a single parallel register, (b) frame transfer and (c) inter-line transfer.

The complete pixel array of the camera is used to detect the photons emitted during exposure of the specimen. Generally, full frame CCDs has square pixel dimensions to avoid image distortions. This kind of camera is used with a shutter to prevent image smearing. Frame-transfer CCDs have a similar design to full-frame CCDs. The biggest difference is that these devices have a parallel shift register that is divided into image and storage arrays. A new image is collected while a previous one is processed. The most important advantage of this type of camera is the capability of frame-transfer devices to operate without a shutter, which increases the measurement speed. Interline-CCDs are hybrid structures incorporating a photodiode into each pixel element and an associated parallel readout CCD storage area. These two elements are isolated by a metallic mask. As in the case of frame transfer CCDs, interline transfer CCDs can function without a shutter. Several frame transfer CCD camera were used in our experiments: from Roper Scientific, model EEV with a 512 x1024 pixel array; from Andor Technology, model DV434-BV with a 1024x1024 pixel array and from Roper Scientific, model 256 HB with a 512x512 pixel array. The Roper Scientific softwares, WinSpec 1.4.3 and Winview 3.2, were used for spectral analysis when the spectrograph was coupled to the inverted microscope and for image analysis respectively. The Andor Technology camera was utilized with the Image ProPlus software, which controlled the camera and was also used for image acquisition and analysis.

2.2.2.7. Gratings

A three mirror-spectrograph (Acton Research Inc.) equipped with a 150 and 300 groves/mm gratings blazed at an optimum wavelength of 500nm was used in our experiments.

2.3. Protocols and Procedures

2.3.1. Loading of Donor or Acceptor Dyes into Macrophage Cells

- Prepare stock solutions of the cell permeable dyes in a range of 1–10 mM. Store solutions at -20 ˚C in small aliquots. Take out the medium from the chambered coverglass on which murine macrophages cells grew to 70% confluency. Wash the cells thoroughly three times with fresh PBS buffer (100mM, pH=7.4).
- Add 400 μl PBS buffer to each well.
- Pipette small aliquots of the dye stock solutions until the desired concentration is reached.
- Mix with a Pasteur pipette thoroughly.
- Incubate 30 min at room temperature or 37 ˚C using an incubator.
- Wash the cells carefully three times with PBS buffer.
- Add 400 μl PBS buffer to each well.
- Pipette small aliquots of the fluorescent and mix cautiously.

2.3.2. Preparation of pH Sensitive Sulforhodamine Encapsulating Liposomes

Prepare a stock solution with 7:1 molar ratio of 1,2 dioleoyl-sn-glycero-3-phosphocholine(DOPC) and dioleoyl-sn-phophoethanolanime-N-succinyl N-succinyl DOPE in chloroform. The overall phospholipid concentration was 250 mg/ml lipid [104].

2.3.2.1. Injection Method *[105]*

- Dry out a 40 μl aliquot of the phospholipid stock solution under nitrogen flow for two hours.
- Add 40μl dry 2-propanol with rapid vortexing.
- Inject the alcoholic solution into 1 ml of 5mM Sulforhodamine solution dissolved in PBS buffer while vortexing.

2.3.2.2. Freeze-Thaw Method for pH Sensitive Liposomes

- Dry out a 40 μl aliquot of the phospholipid stock solution under nitrogen flow for two hours
- Rehydrate the phospholipid film by adding 1ml of 5mM Sulforhodamine solution in PBS buffer to form liposomes.
- Disperse evenly the phospholipids in the working buffer by using a 47 KHz Bransonic sonicator bath for 15 minutes.
- Freeze the liposome solution by placing the vial containing the liposomes in liquid nitrogen for 15 minutes.
- Thaw the sample at room temperature for 15 minutes.
- Repeat the freeze-thaw cycle six times.

- Separate liposomes containing fluorescent dye from excess dye that is not encapsulated inside the liposomes by using a micro-column centrifuge technique described below.

2.3.2.3. Sephadex Column Preparation *[105]*

For Sephadex G50: Mix 10 g of G50 resin with 120 ml of distilled water and 0.9 g NaCl

For Sephadex G100: Mix 10 g of G100 resin with 175 ml of distilled water and 1.575 g NaCl

- Let the Sephadex solution swell overnight before preparing the Sephadex columns for separation.
- Fill a 1ml syringe with the Sephadex solution that has its tip blocked with glass wool.
- Centrifuge the syringe in a low-speed centrifuge of 2000 rpm for 5 minutes to form a dry solid Sephadex column without cracks or voids.
- Add the PBS buffer to the Sephadex containing syringe and centrifuge at the same speed as it is used for the sample (see below).

2.3.2.4. Liposome Separation by Sephadex Column

Pipette 200 μl liposome solution and centrifuge at 2000 rpm for 15 minutes.

- Collect the effluent containing the liposomes.
- The procedure should be repeated until no background from the free dye is seen using a fluorescence microscope.
- Store the liposome solution up to one week at 4˚C.

2.3.3. Delivery of Labeled Liposomes into Murine Macrophage Cells

- Prepare pH sensitive liposomes encapsulating Sulforhodamine with the initial dye: lipid ratio= 250:1 and 250 mg/ml phospholipid mixture. Remove out the medium from the chambered coverglass in which J 774 murine macrophages cells grew until 70% confluency. Wash the cells thoroughly three times with fresh PBS buffer (100mM, pH=7.2).
- Add 400 μl PBS buffer in each well.
- Pipette different aliquots of the liposome stock solution into each well.
- Mix with a Pasteur pipette thoroughly.
- Incubate cells with liposome solution for 5, 15, 30, 60 minutes.

2.3.4. Maintenance and Preparation of J 774 Murine Macrophage Culture

Murine macrophage cultures were maintained following a protocol described by Gordon et al [106]. The medium used for this culture was Dubelco's modified Eagles's medium augmented with 4mM L-glutamine, 1.5g/l sodium bicarbonate, 4.5 g/l glucose, 1 mM sodium pyruvate, and 10% fetal bovine serum. The culture was grown at 37 ^{0}C in a 5% CO_2 atmosphere. In order to prepare subcultures the cells were scraped, the medium was replaced and the cells were splitted into the new vessels. For our experiments, cells were plated onto chambered covered glasses, which had been coated with a fetal bovine serum for 2 days. Approximately 10^6 cells/ml were placed on a chambered coverglass. Then a 1 ml fresh media was added to the chambers. All chambered coverglasses were maintained at 37° C in humidified, 5% CO_2 incubator. The

macrophages were allowed to attach to the glass for 3 days. Typically, 70 % confluency was achieved in three days.

2.3.5. Phospholipid Cocktail for Lipobead Coating

50 mM lipid stock solution prepared with a 5:4:1 molar ratio of DMPC, cholesterol, and DP in chloroform, was stored at -20^0C until used.

2.3.6. Preparation of Lipobeads

- Weigh 4 mg powder polymeric microspheres and dissolve in 100 μl 1:1 (v/v) ethanol/hexane solution.
- Sonicate for 15 minutes using a 47 KHz Bransonic sonicator.
- Mix by vortexing 80 μl of phospholipid cocktail solution and 10-50 μl of 5 mM labeled phospholipid.
- Add the phospholipids to the microsphere solution and sonicate for 15 minutes using a 47 KHz Bransonic bath sonicator.
- Incubate the mixture at room temperature for 2 hours.
- Dry the mixture overnight under nitrogen gas stream.
- Add 1 ml of phosphate buffer pH 7.0 to the dried bead suspension, and sonicate for 15 minutes with a 47 KHz Bransonic sonicator.
- Stir magnetically the mixture for 2 hours to allow absorption of phospholipids onto the surface of the microspheres.

- Wash at least 3 times by slow speed centrifugation of 3000 rpm for 15 minutes to remove unbound liposomes and uncoated particles. The lipobeads were collected at the bottom of glass centrifuge while the supernatant and unbound beads or dye molecules were discarded.
- Store the lipobead suspension in a glass test tube at 4^0C up to one week.

2.3.7. HEPES Buffer for Lectin Studies

The HEPES buffer was composed of: 150 mM NaCl, 1 mM $MnCl_2$, 1 mM $CaCl_2$ and 100 mM HEPES (pH 7.2).

2.3.8. Preparation of FITC –Con A Coated Beads

- Weigh 4 mg powder polymeric microspheres.
- Add 1ml FITC-ConA 200 μg/ml dissolved in HEPES buffer and mix by vortexing.
- Stir magnetically the mixture for 2 hours to absorb the lectin on the surface of the microspheres.
- Pipette 10 μl 100 mg/ml Bovine Serum Albumine (BSA) and mix well.
- Incubate for 1 hour while stirring at room temperature.
- Wash by slow speed centrifugation of 3000 rpm for 15 minutes at least 3 times. The FITC-ConA coated lipobeads were collected at the bottom of the glass vial while the supernatant is discarded.
- Store the FITC-ConA coated beads in a glass vial at 4^0C up to 3 days.

2.3.9. Preparation of poly-L-Lysine Adhesive Slides

- Wash microscope slide cover-slips with 70% ethanol/water three times.
- Dry cover-slips at 60 ˚C for 2 minutes in the oven.
- Pipette poly-L-lysine solution (1ml/ml) on cover-slips.
- Incubate cover-slips overnight in the dark.
- Wash cover-slips with working buffer (PBS or HEPES) and incubate them with the FRET sensing bead solutions for 4 hours.

2.4. Digital Fluorescence Imaging Analysis

The softwares Winview 3.2 of Roper Scientific and Image ProPlus 4.5 of Media Cybernetics were used for image analysis. The analysis of the digital fluorescence images was carried out either by using automatic features of the software or by manually selecting the fluorescent objects. The Image ProPlus software enabled analysis of the average fluorescence intensity and size of the observed particles. The images features could be enhanced by contrast adjustment and edge emphasis and saved in TIFF or GIF standard format in order to be included in this dissertation. The contract adjustment of the fluorescence images did not affect the signal to noise ratio of the initial images.

The signal of the sample, S_{sample}, was computed as an average of the selected object intensities (figure 2.5.a and b). The average and the standard deviation were generated automatically by the software. For the background calculation 3 different areas were

chosen such that the borders of these areas were at least 3 pixels away from the bright objects. The average background signal, $S_{background}$, was calculated manually (figure 2.5c). The signal to noise of the digital fluorescence images (S/N) was determined as following:

$$S/N = (S_{sample} - S_{background}) / (3 \times \sigma_{background}) \quad (2.1.)$$

where $\sigma_{background}$ is the standard deviation of the background measurements.

2.5. Error Analysis

The error bars of our experiments were calculated from three repeated measurements of different particle samples. They represent the fluorescence average signal variation in our experiments. The results are presented as +/- standard deviation or errors bars from the average fluorescence intensity value. The standard deviation assess how broadly the measured values are dispersed from the average value, therefore it is also a measure of the reproducibility of our experiments. The standard deviation (SD) was calculated using the following standard formula:

$$SD = \sqrt{\frac{n\sum x^2 - \left(\sum x\right)^2}{n(n-1)}} \quad (2.2.)$$

where n is the number of measurements and x represents the value of each measurement.

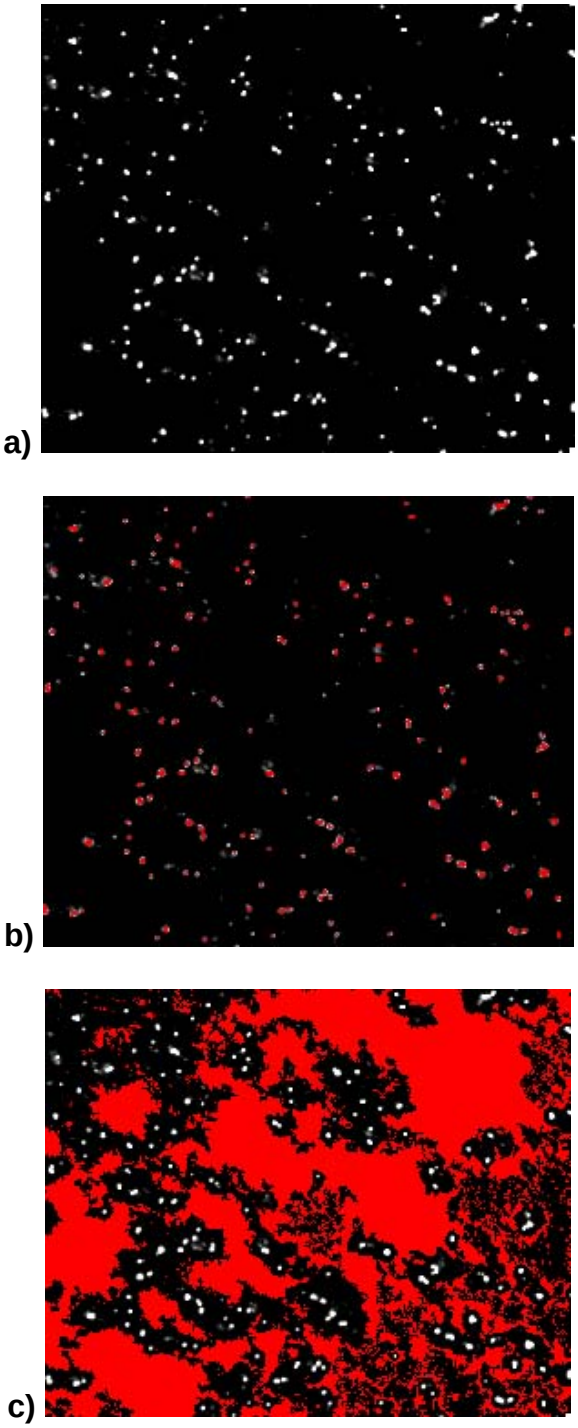

Figure 2.5. Digital fluorescence images of FRET sensing beads and their data processing: a) initial fluorescence image b) the same image after the selection of the desired beads c) and following the selection of the image background.

Rejection of Gross Errors

When a set of data contained a result that differed excessively from the average the Q test was applied to decide whether to reject or retain the deviating data point. The ratio, Q_{exp}, was calculated by dividing the absolute difference, d, between the doubtful result and the nearest data point with the spread, w, of the entire set of measurements: Q_{exp} =d/w. This ratio was compared with literature values [111]. When Q_{exp} was larger than the tabulated values, the questionable result was rejected. A 95% confidence interval was used in the rejection of the gross errors. Generally, less than 2% of data were rejected performing this test.

Sources of Errors

Every measurement was effected by many uncertainties, which combine to produce scatter results that were characterized by a standard error. For example, fluorescence microcopy measurements were affected constantly by about 5% fluctuation in the lamp energy output and heterogeneities in the excitation field. Additionally, inconsistencies in sample handling were generated by multiple washing steps required to separate particle based FRET sensors from their preparation solutions. The reproducibility of the results was improved by increasing the number of observed particles in the field of view. For our cellular studies, the inability to recognize sub-population of cells also increased the error of the measurements. The murine macrophages were a heterogeneous mixture of old and young cells, which contributed up to 30% variation in the fluorescence response of individual cells.

2.6. Methods for Evaluating the FRET Efficiency

2.6.1. Donor Quenching

The donor quenching method was often used to calculate the FRET efficiency in our experiments. The excitation wavelength is set at donor absorption and the emission wavelength at the emission peak of the donor. The donor emission wavelength is selected such that minimal contribution from the acceptor fluorescence is allowed. The energy transfer efficiency is calculated as: $E=1- F_{DA}/F_D$, where F_{DA} and F_D are the fluorescence intensities of the donor in presence and absence of acceptor molecules [14]. Both fluorescence intensities are normalized to the same donor concentration.

2.6.2. Acceptor Enhancement

This technique is used only when the acceptor molecules fluoresce and can be visualized by exciting the sample at the donor absorption wavelength. A sensitization in the fluorescence of the acceptor is recorded as the FRET efficiency increases. Since in most cases acceptor molecules display some residual absorbance at the excitation wavelength of donor, the calculation of the energy transfer efficiency based on the sensitized acceptor fluorescence is quite complicated [14]. The FRET efficiency is

calculated as: $E=1-F_A/F_{AD,}$ where F_A and F_{AD} are the fluorescence intensities of the acceptor in the absence and presence of the donor.

2.6.3. Ratio Imaging

Fluorescence microscopy often suffers from instability in light collection geometry, variations in the intensity of excitation at different wavelengths, different photobleaching rates and inconsistency in the sample background. These problems could be corrected by using ratiometric methods. Ratiometric fluorescence microscopy can be classified into several categories according to excitation or/and emission wavelengths used in the measurements [73, 109, 110]. The method used in our experiments was emission ratio. The sample was excited with a single excitation wavelength, which was the donor peak absorption. Then the fluorescence images were collected at two different wavelengths: the donor and acceptor peak emission. The ratio between the acceptor and donor intensities was calculated from the collected images or spectra. The ratiometric method was mainly used for the FRET microscopy studies in cells. The energy transfer efficiency was proportional to the ratio of the sensitized acceptor fluorescence and quenched donor emission (FA/FD). This ratio was used as a measure of the energy transfer efficiency.

2.6.4. Choice of Excitation, Emission and Dichroic Mirrors Used in FRET Microscopy

The optical filter combinations in FRET microscopy were chosen to maximize the FRET signal while minimizing the fluorescence background due to direct excitation of acceptor molecules by donor excitation light. The optimal filter combination for the donor-acceptor pair used in our experiments is shown in table 2.1. Specific combinations of filters were named as listed in the table 2.1.

Table 2.1. Optimal filter combinations for fluorescence imaging used in FRET experiments.

Channel (Ex/Em wavelength)	Excitation filter	Dichroic mirror	Emission filter
Donor/Donor (Donor)	480/30 nm (bandpass)	505 nm	535/40nm (bandpass)
Donor/Acceptor (FRET)	480/30 nm (bandpass)	505 nm	590 nm (longpass)
Donor/ Donor + Acceptor	460/50 nm (bandpass)	500 nm	515 nm BA(longpass)

CHAPTER 3

FLUORESCENCE RESONANCE ENERGY TRANSFER (FRET) - A NEW ANALYTICAL METHOD TO MONITOR DRUG DELIVERY

3.1. Introduction

In conventional therapy, drug stability and bioavailability are the major areas of concerns. Modern delivery systems are expected to increase the activity of the drugs by using localized and triggered drug delivery [112]. New drugs, including gene therapy agents, require novel technologies for their delivery. Biodegradable polymers, stimuli-sensitive polymers, kinetic- and equilibrium-modulated polymers or carriers that increase membrane permeability have been used to facilitate the delivery of drugs that are not cell permeable [113,118,121]. The most important requirements for effective drug delivery systems are [113]:

- Sustained release of drug to reduce the frequency of dosing and local side effects.
- Controlled release products, which have reliable and reproducible properties in different environments.
- Spatial targeting of drugs to a specific organ, cell, subcellular compartment or to a specific substrate.

Liposomes were used to deliver highly toxic drugs since liposomal 66

encapsulation meets the above requirements [113-115]. Recently, liposomes have also been used to deliver proteins, antibiotics, anesthetics, oligonucleotides, antifungal and anticancer into cells and tissues [104,116-117]. For effective delivery liposomes are required to meet several criteria. First, they must evade the endosome/phagosome system and release their content to the targeted site. Second, the liposomes should have long circulation times in the blood stream. The recent use of sterically stabilized liposomes increased their stability in the blood stream and improved their resistance to phagocyte uptake [118-123]. Additionally, controlled release of the internal content of liposomes under different stimuli such as temperature [124-126], pH [127], light [128] and laser light [129] was realized. Although liposomal formulations often improve performance of drugs, effective delivery of drugs into targeted cells and organelle remain a challenge. Currently used analytical techniques (HPLC, GC, MS) offer reliable quantitative information about drug delivery into specific organs and tissues. However, the cellular fate of drugs cannot be evaluated using these techniques. Moreover, poor understanding of the pharmacodynamics at the cellular level is a serious impediment to improving the design of drug delivery systems. Confirmatory images could authenticate the delivery of drugs to specific cellular organelles and support the elucidation of pharmacodynamics data associated with specific drugs.

Recently, intracellular delivery and binding affinity of newly developed drugs have been evaluated by sensitive luminescence methods. These methods are based on the interaction between a specific cellular receptor and the screened drugs. The activity of the receptor when the drug binds to it is encoded in an enzyme activity, which is quantified by measuring the conversion of a fluorogenic or luminogenic substrate

[12,13,31,32]. Unfortunately, these assays cannot offer real time information about the drug delivery or the binding affinity since the fluorescent products are allowed to accumulate to overcome the intrinsic fluorescence of the cells.

As previously mentioned, microscopy techniques have been employed for cellular studies in vitro [71, 73-75,133]. The limit of optical resolution of a microscope is about 0.2 μm, which is the limit of light diffraction. This limitation is overcome by electron microscopy that can determine the location of specific drugs in particular cellular organelles with a resolution in the range of Å. However, electron microscopy does not offer real time information since it requires multiple preparative steps to acquire images. Therefore, a real time technique is needed to characterize drug interactions with specific cells, kinetics of drug delivery and drug leakage from cells. For example, quantification of unloaded drug or drug leakage from tumor cells is essential since anticancer drugs have harsh side effects on normal cells [113, 118, 121, 130]

This chapter describes the use of FRET microcopy to measure in real time the delivery of fluorescent model-drugs into single cells. As previously mentioned the FRET efficiency depends largely on the distance between the donor and acceptor. FRET could be therefore used as a highly specific molecular ruler [131, 132]. FRET measurements were previously employed for the detection of co-localization of proteins in cellular membranes [73,133-134], hybridization of nucleic acids [135, 136], intracellular signaling [137, 138] and protein-protein interaction [139, 140]. The use of FRET imaging microscopy increased significantly following the recent discovery of the green fluorescent protein (GPF) and its mutants [141]. Fluorescence microscopic techniques have been often used to monitor the delivery of fluorescent molecules into

cells [142, 143]. However, using ordinary fluorescence microscopic techniques it was difficult to determine whether the fluorescent molecules truly permeate through the cell membrane or only adsorb to the cell surface. Although confocal microscopy indicates the localization of a fluorophore cells in a 3-dimensional space, this fluorescence microscopy technique cannot offer real time information since it is based on a lengthy laser scan across the specimen. We hypothesized that FRET measurements between fluorescent molecules preloaded into cells and permeating fluorescent molecules (donors or acceptors) would provide direct real time evidence that the fluorescent molecules truly permeate the cellular membrane. Fluorescein and Rhodamine derivatives were utilized as donor and acceptor molecules in our cellular studies. We investigated two strategies for the energy transfer in cells. The first involved the delivery of donor molecules into acceptor labeled cells. The second strategy involved the delivery of acceptor molecules into donor-labeled cells.

3.2. Specific Experimental and Technical Details

Materials and Reagents

5-(and-6)-Carboxyfluorescein and Sulforhodamine were used in our FRET studies in solution. Fluorescein diacetate and Calcein AM were utilized as donors and Sulforhodamine and Cell Tracker Orange as acceptors in our cellular studies.

Detection System

A digital florescence imaging microscopy system was employed to measure the delivery of the donor and acceptor model drugs. The excitation, emission and dichroic filter

combinations were optimized to minimize the overlap between the donor and acceptor absorption and emission peaks. Three filter cubes were used for donor, acceptor and FRET imaging (table 2.1). The fluorescence images of macrophage cells were collected using a 40X and 20X microscope objectives with NA = 0.7 and NA=0.5 respectively. Typically an exposure time of 0.3 s was used to acquire fluorescence images of the particles. A 10 % transmission neutral filter density filter was used to minimize the photo-bleaching rate of the fluorophores. The Roper Scientific software Winview 3.2 was used for image analysis. Additionally, the software Adobe PhotoShop v 3.0 and Image ProPlus v. 4.5 were utilized for image processing.

Loading of Donor or Acceptor Dyes into Cells

Stock solutions of 1–10 mM of donor and acceptor dyes in dimethylsulfoxide (DMSO) were prepared and used in our FRET experiments. Macrophage cells were grown on the chambered cover-glasses to 70% confluency. Preloading of macrophages with donor or acceptor molecules was accomplished by initially diluting the stock solution into fresh medium to final concentrations of 500 nM to 50 μM, then incubating the macrophages with the dye containing medium for 30 minutes at room temperature. Then, the excess of dye was washed out with PBS buffer (pH=7.4). The delivery of donor molecules into acceptor labeled cells was quantified and monitored after the addition of small aliquots of donor stock solution into the 400 μl PBS buffer (pH=7.4) covering the cell culture in the chambered coverglass. The buffer and the dye solutions were mixed cautiously with a disposable glass pipette. The same procedure was carried out to follow the delivery of acceptor model drugs into donor labeled macrophages.

3.3. Results and Discussion

3.3.1 Choice of Donor and Acceptor Pair

Fluorescein and Rhodamine derivatives have been utilized frequently in FRET microscopy since these dyes are characterized by high absorbance, emission quantum yield, large separation between the excitation and emission wavelengths and significant overlap between the donor emission and the acceptor absorption spectra [132c, 134]. This donor and acceptor pair is characterized by a large Forster distance (49-54 Å) that ensures large energy transfer efficiency.

3.3.2 Photostability of the Donor and Acceptor Dyes Loaded in Murine Macrophage Cells

The photostability of the donor and acceptor dyes was determined by recording the photobleaching rate after repetitive exposures to the excitation light. The Fluorescein based dyes showed a 50 % drop in their fluorescence after 10 exposures of 0.3 s. The Rhodamine based dyes had lower photobleaching rate. To minimize the photobleaching a neutral density filter with 10 % transmission was used in our experiments. Using this filter the photobleaching of fluorescence was reduced to about 5% following 30 minutes of continuous illumination. During the kinetic experiments the cells were exposed to the excitation light only during exposures of the sample to the CCD camera for an accumulative exposure time of about 1 minute. Under these conditions donor and acceptor labeled cells remain photostable throughout the experiments. Furthermore, monitoring the fluorescence intensity of the cells for one hour showed no leakage of fluorescent probes from observed cells with the exception of Fluorescein diacetate. This

dye was replaced with the Calcein AM that showed increased cellular retention and relative insensitivity of its fluorescence to pH changes in the physiological range. The cellular structure remained intact for at least 5 hours following cellular labeling with donor and acceptor molecules.

3.3.3. Delivery of Donor Fluorophores into Acceptor Labeled Macrophages

To monitor the delivery of donor molecules into acceptor labeled cells J774 murine macrophages were pre-incubated with 5 μM Sulforhodamine (acceptor). Then, the cell permeating dye Calcein-AM (donor) was added in small aliquots to the cultures. Fluorescence images of the cells were collected 15 minutes following the addition of Calcein-AM to the cultures. Digital fluorescence images of the murine macrophages loaded with Sulforhodamine prior and following the delivery of donor molecules are shown in figure 3.1.

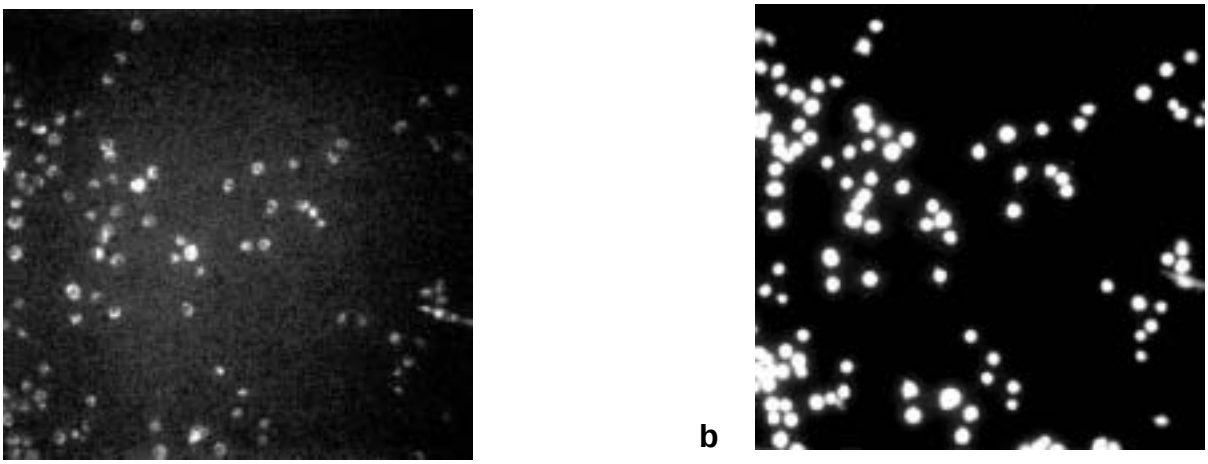

Figure 3.1. Fluorescence images of Sulforhodamine (5μM) labeled murine macrophages prior (a) and following incubation with 25nM Calcein AM for 30 minutes (b). Fluorescence images were taken through the FRET channel (λ_{ex}=480 nm, λ_{em}> 590nm).

The cells were imaged trough a 40 X objective and the FRET channel (table 2.1). The permeation of Calcein AM into the cellular cytoplasm led to a noticeable increase in the FRET signal due to energy transfer between the permeating donors and the acceptor labeled cells. To correct the donor fluorescence tail contribution into the FRET channel, ratios between the intensities of the images obtained through the FRET channel (λ_{ex}=480 nm, λ_{em}> 590nm), **Fa**, and donor channel (λ_{ex}=480 nm, 520 nm >λ_{em}> 550nm), **Fd**, were calculated. Figure 3.2 shows the dependence of **Fa/Fd** ratio on increasing donor concentrations. Curves a and b describe the dependence of **Fa/Fd** ratio on the donor concentration in the presence and absence of Sulforhodamine. It can be seen that **Fa/Fd** of acceptor labeled macrophages was 2 fold larger than **Fa/Fd** of cells in the absence of acceptor molecules (the control experiment). The error bars were obtained from 3 different experiments. Each data point was the averaged intensity of 20 cells. The increase in **Fa/Fd** ratio in the absence of acceptor molecules was attributed to the red-tail emission of donor molecules. This phenomenon is often described in the literature as “bleed-though” and should be minimized to obtain quantitative FRET measurements. The bleed-through between the FRET and donor channels was largely noticeable at Calcein AM levels higher than 25 nM when only a small difference between the **Fa/Fd** ratio in the presence and absence of acceptor was seen. The major limitation of this FRET geometry was the small dynamic range of the assay.

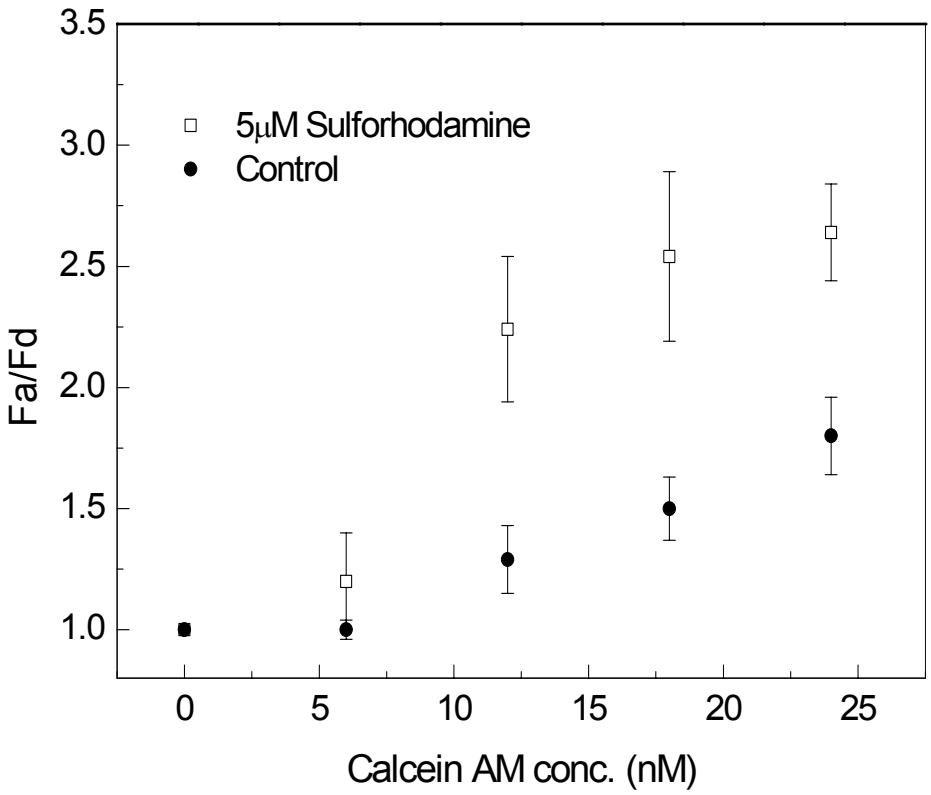

Figure 3.2 FRET efficiency between Sulforhodamine (5 μM) labeled macrophages and increasing concentrations of the donor, Calcein AM. The FRET magnitude was determined by recording the increase in the ratio between the sensitized acceptor signal, Fa, and the donor fluorescence, Fd in the presence (a) and absence (b) of Sulforhodamine.

3.3.4. Delivery of Acceptor Molecules into Donor Labeled Macrophages

The high emission quantum yield of Calcein-AM combined with the low loading efficiency of Sulforhodamine was the major shortcoming of the previous FRET sensing geometry. It resulted in a large red-tail emission of donor molecules in the FRET channel. To overcome this problem another geometry of FRET measurements was investigated. In these experiments the delivery of acceptor molecules into macrophages

preloaded with Calcein AM was monitored. The FRET efficiency was determined using the donor quenching method and was calculated as the ratio between the fluorescence intensity of the macrophages prior and following acceptor delivery ($\mathbf{F_d/F_{d0}}$).

In the initial experiments we used Sulforhodamine as an acceptor. Macrophages cells were preloaded with Calcein AM by incubating cell cultures grown in chambered cover-glasses to 70% confluency with 400 μl 5 μM Calcein AM solution for 30 minutes at room temperature. The cells were washed out of the excess donor molecules with PBS buffer and then incubated with 400 μl 500 μM Sulforhodamine for 30 minutes at room temperature. The results of these experiments are summarized in figure 3.3. The upper curve (open circles) describes the control experiment in which the donor channel signal was measured in the absence of Sulforhodamine. As expected, no quenching of the donor florescence was observed. The lower curve (the filled squares) shows the decrease in fluorescence of Calcein AM labeled cells as Sulforhodamine permeates into macrophages. The decrease in the donor fluorescence was expressed as the ratio between the fluorescence of donor labeled cells prior **($\mathbf{F_{d0}}$)** and following **($\mathbf{F_d}$)** the delivery of Sulforhodamine. Given the errors in these experiments, the decrease of about 10% in the fluorescence of donor labeled cells was deemed insignificant. Furthermore, the limited quenching of the donor labeled macrophages was not acceptor concentration dependent. Poor cellular uptake and subsequent compartmentalization of Sulforhodamine could be the reasons for the minimal FRET efficiency between the donor molecules located in the cytoplasm and the acceptor molecules that were entrapped in the cellular endosomes.

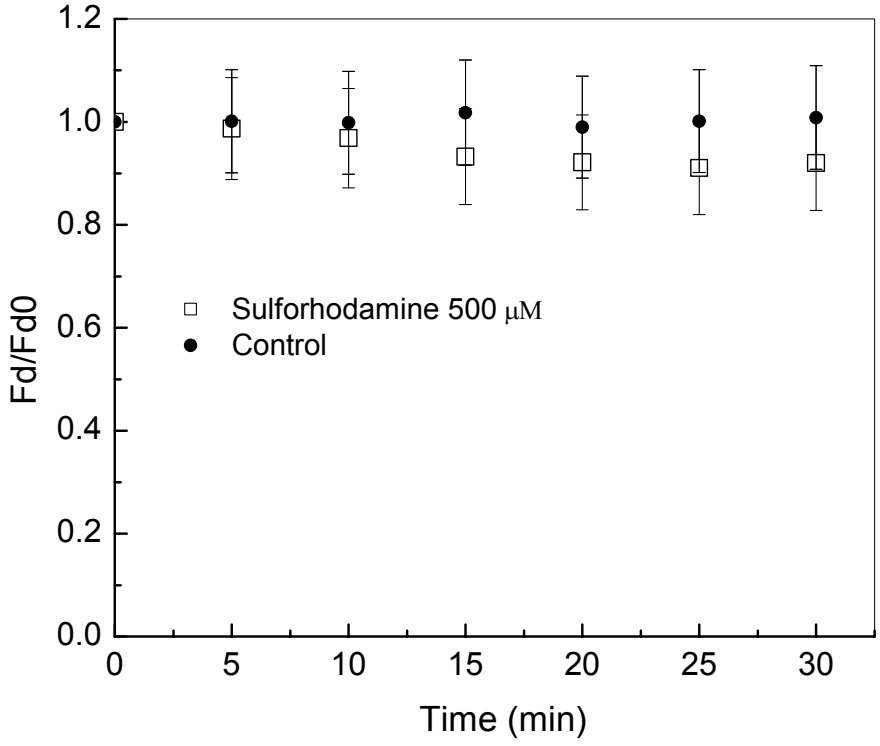

Figure 3.3. Delivery of Sulforhodamine (500 μM) into Calcein AM (5 μM) labeled macrophages. The FRET magnitude was determined by recording the decrease in the ratio between the donor signals: (a) prior (F_{d0}) and (b) following the delivery of Sulforhodamine (F_d). Fluorescence images were taken through the donor channel (λ_{ex}=480 nm, 520 nm > λ_{em}> 550nm).

To increase the cellular uptake we encapsulated Suforhodamine in liposomes and used them as cargos for intracellular delivery. Liposomes were previously used to facilitate the cellular uptake of charged large molecules like the acceptor dye, Sulforhodamine [104]. pH sensitive liposomes were prepared to overcome the entrapment of Sulforhodamine in cellular endosomes. Several experiments were performed to find the optimal encapsulation method and liposomal formulation. Different encapsulation methods were attempted including direct injection, hydration-dehydration and the

freeze-thaw method [105]. The pH sensitive liposomes were composed of phosphadityl ethanol amine which does not form bilayers at physiological pH. The phospholipid bilayer was stabilized by negatively charged phospholipids, N-succinyl DOPE to form the liposomes. The freeze-thaw method was found to be the most suitable for these fusogenic liposomes [104]. Endosomes are cell organelles characterized by an acidic environment with a pH of about 5 [34, 35]. The negatively charged liposomes were initially entrapped in the endosomes where their negative charges were neutralized by the acidic environment (pH=5). The neutralization of the N-succinyl DOPE electric charge destabilized the liposome structure and facilitated their fusion with the endosomes membrane and the subsequent release of their content into the cytoplasm.

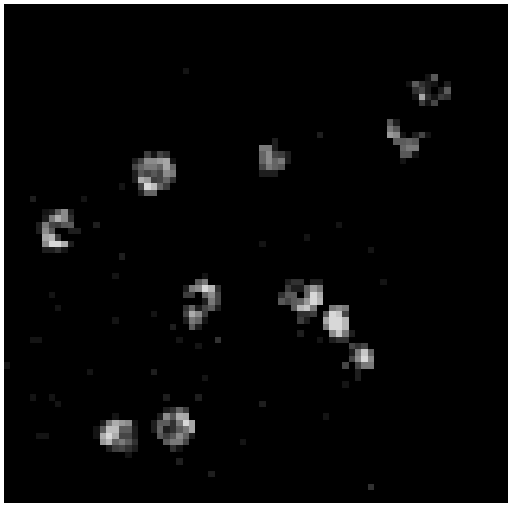

Figure 3.4. Fluorescence image of J774 murine macrophages loaded with liposomes containing Sulforhodamine. The liposomes were prepared a phospholipid cocktail containing a mixture of DOPE: N-succinyl DOPE (7:3) using freeze-thaw method. The fluorescence image was taken through the acceptor channel (λ_{ex}=546 nm, λ_{em}> 580nm).

Figure 3.4 is an image of macrophages loaded with the cell impermeable Sulforhodamine through the liposomal mediated delivery. The murine macrophages

grown at the bottom of a chambered cover-glasses to 70 % confluency were incubated with the liposomes at the final lipid concentration of 10 mg/ml for 60 minutes at 37 ^{0}C. The cells were washed with PBS at pH=7.2 and then examined by fluorescence microscopy. The delivery efficiency of Sulforhodamine from pH sensitive liposomes increased greatly compared to the delivery efficiency of the free dye experiment. However, as seen in figure 3.4 compartmentalization of Sulforhodamine in the cells was still present.

To overcome the compartmentalization of the acceptor molecules we replaced Sulforhodamine with a cell permeable dye, Cell Tracker Orange. Unlike Sulforhodamine, Cell Tracker Orange was not sequestered in endosomes. The FRET efficiency between the Calcein AM labeled cells and Cell Tracker Orange was determined based on the fluorescence decrease of Calcein AM as Cell Tracker Orange molecules permeated into the cells. It was again expressed as the ratio between the donor fluorescence in the presence and absence of acceptor molecules in the cells ($\mathbf{F_d/F_{d0}}$). In these experiments macrophages grown on the on the bottom of chambered cover-glasses to 70% confluency were first incubated with 400 μl 5 μM Calcein AM solution for 30 minutes at room temperature. The excess of Calcein AM was washed with PBS buffer at pH 7.2. Then, the cells were incubated with increasing concentrations of Cell Tracker Orange solutions ranging from 50μM to 500 μM. Fluorescence images of murine macrophages preloaded with Calcein AM (5 μM) prior (a) and following (b) the delivery of Cell Tracker Orange (500 μM) are shown in figure 3.5. The decrease in Calcein-AM fluorescence resulted from FRET between Cell

Tracker Orange molecules delivered into the observed macrophages and the Calcein AM labeled cells.

As evident in figure 3.6 the Calcein AM fluorescence decreased by about 40% when CalceinAM labeled cells were incubated with 500μM Cell Tracker Orange for 30 minutes (figure 3.6., triangle dots). Longer exposure times did not increase the donor quenching magnitude. Lower acceptor concentrations like 250μM resulted in slower donor quenching (figure 3.6., filled circles). The use of acceptor molecule permeation into donor labeled cells (strategy 2) in our FRET measurements proved to be more effective than the use of permeating donor molecules into acceptor labeled cells (strategy 1).

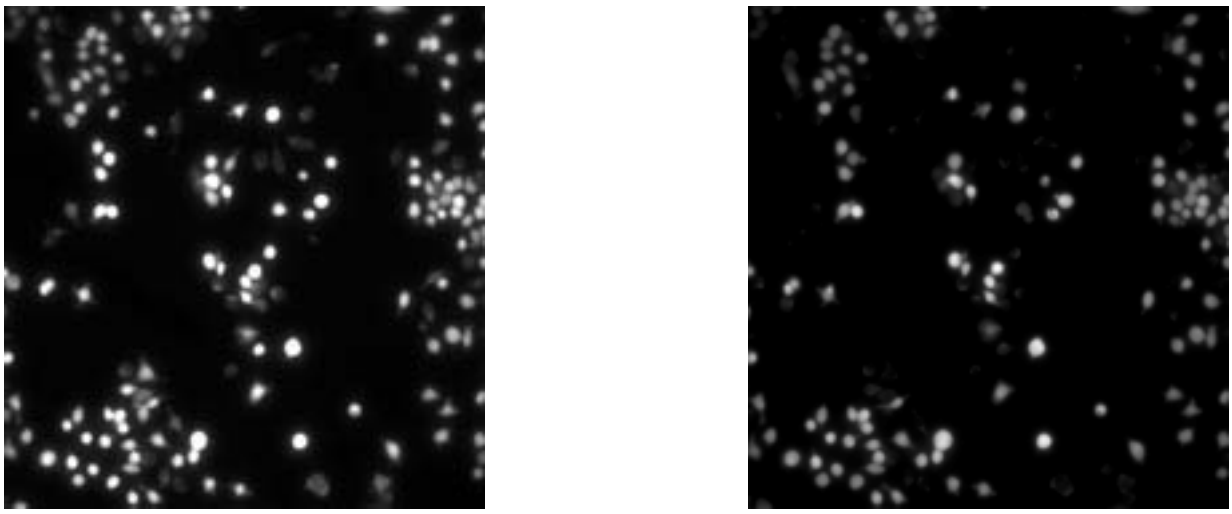

a) **b)**

Figure 3.5. Fluorescence images of the Calcein AM (5 μM) labeled murine macrophages prior (a) and following incubation with 500 μM Cell Tracker Orange for 30 minutes (b). Fluorescence images were taken through the donor channel (λ_{ex}=480 nm, 520 nm > λ_{em}> 550nm).

However, a relatively high acceptor concentration in the hundreds micromolar level was still needed to obtain measurable FRET signals in a 3-D system like the cellular milieu.

As evident in figure 3.6 the Calcein AM fluorescence decreased by about 40% when Calcein AM labeled cells were incubated with 500μM Cell Tracker Orange for 30 minutes (figure 3.6, triangle dots). Longer exposure times did not increase the donor quenching magnitude. Lower acceptor concentrations like 250μM resulted in slower donor quenching (figure 3.6., filled circles).

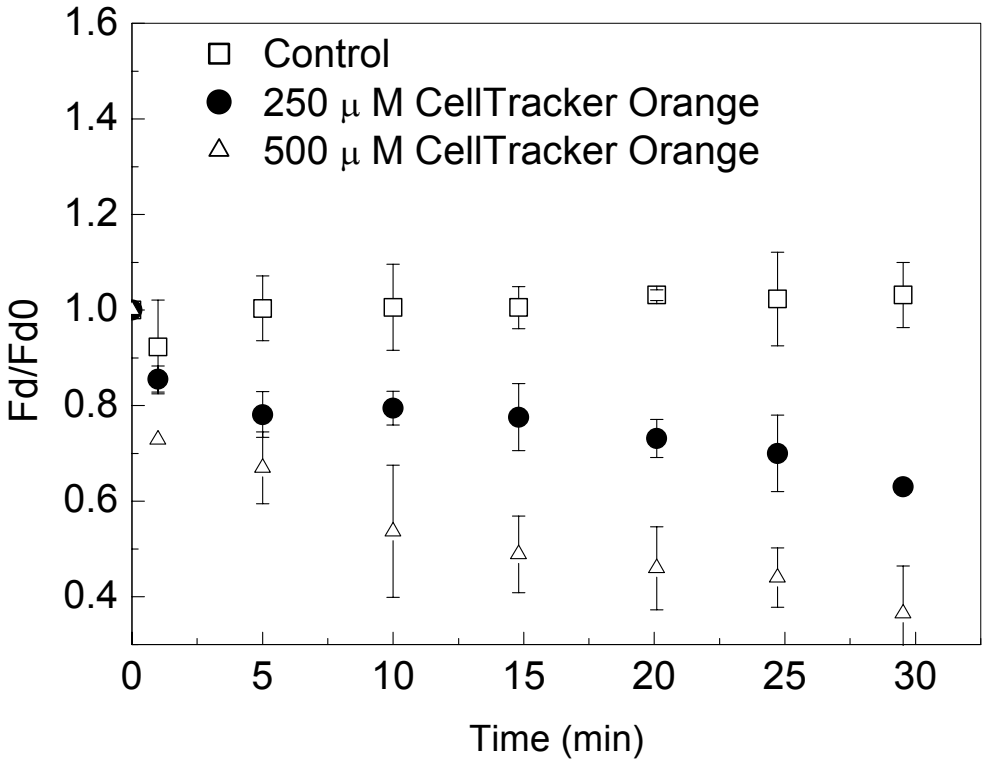

Figure 3.6. Delivery of CellTracker Orange into CalceinAm labeled macrophages monitored by FRET. Donor channel fluorescence was recorded in the absence of (square dots), the presence of 250μM (filled circle dots) and 500μM (triangle dots) CellTracker Orange.

The use of acceptor molecule permeation into donor labeled cells (strategy 2) in our FRET measurements proved to be more effective than the use of permeating donor molecules into acceptor labeled cells (strategy 1). However, a relatively high acceptor concentration in the hundreds micromolar level was still needed to obtain measurable FRET signals in a 3-D system like the cellular milieu.

3.4. Summary and Conclusions

Fluorescence resonance energy transfer (FRET) was utilized to confirm for the first time the delivery of model fluorophores into single cells. Unlike previously used analytical techniques (HPLC, GC), FRET microscopy provided valuable information about fluorophore localization in cells. Furthermore, using FRET microscopy, we were able to quantitatively monitor in real time the kinetics of the delivery of fluorescent molecules into cells. Real time measurements were not previously possible when other imaging techniques like electron microscopy and confocal microscopy were used for cellular imaging. The delivery of fluorophores was followed by FRET in two systems. First, we studied the delivery of fluorescent donors into acceptor labeled cells. Then, we studied the delivery of fluorescent acceptors into donor labeled cells.

The delivery of donors into acceptor labeled macrophages led to an increased signal in the FRET channel. The measurements of donor delivery exhibited poor dynamic range due to the large donor emission tail in the sensitized acceptor channel, often described as “bleed-through”. In spite of the bleed-through effect it was possible to conclude that FRET microscopy could be used to confirm the delivery of donor molecules into

acceptor labeled cells. Monitoring the delivery of acceptor molecules into donor labeled macrophages proved to be easier and less prone to errors since only the donor emission was monitored using a single cube. Initial attempts focused on the delivery of Sulforhodamine into cells preloaded with Calcein AM. Sulforhodamine is a cell impermeable dye. It was sequestered in endosomes, which decreased the FRET efficiency. We successfully used fusogenic liposomes to deliver Sulforhodamine into cells. However, while the loading efficiency improved significantly, compartmentalization of the delivered fluorophores was still noticeable. This precluded the use of FRET to monitor the interactions between Sulforhodamine and cells preloaded with Calcein ÅM. Sulforhodamine was then replaced with the cell permeable dye Cell Tracker Orange. Then, using donor labeled cells it was possible to determine whether the acceptor molecules were actually delivered into the cells. It was also possible to determine the localization of delivered acceptors, for example in endosomes or in cytoplasm. However, a relatively high acceptor concentration in the hundreds of micromolar level was still needed to obtain measurable FRET signals in the 3-D cellular system. The results underscored the need to reduce the dimensionality of FRET systems in order to increase FRET efficiency between donor and acceptor molecules.

CHAPTER 4

FLUORESCENCE RESONANCE TRANSFER (FRET) SENSING LIPOBEADS FOR BIOANALYSIS

4.1. Introduction

A large number of drugs with different chemical structure and broad pharmacological spectrum drugs bind strongly to phospholipid membranes. Examples include: the anticancer drug doxorubicin [144,145], the aminoglucosidic antibiotic gentamicin [146, 147], the β-adrenergic drug propanolol [148,150], local anesthetics such as lidocaine and pore forming antibiotics like gramicidin and polymyxin [151-153]. The ability of drugs to interact and permeate through cellular membranes is often correlated with drug potency. Several techniques have been used to investigate interactions of drugs with phospholipid membranes. These include fluorescence polarization [154], Brewster angle microscopy [155], NMR [156], differential scanning calorimetry [157] and FT-IR spectroscopy [158]. These approaches generally lack sufficient sensitivity, selectivity and temporal resolution. There is therefore a need for less invasive sensitive technique for real time monitoring of interactions between drugs and phospholipid membranes.

Liposomes have proved to be useful for studying interactions of drugs with phospholipid membranes [159]. The main drawback of this technique is the inherent instability of liposomes that often causes irreproducibility in the measurements. Recently developed

phospholipid supported membranes that consist of a polymer or silica matrix in which phospholipids are absorbed or covalently bound to the surface of the particles proved to be useful in the design of steadier sensors for drug discovery [160,161]. The phospholipid layers were used mainly to accommodate membranal proteins that were the biological receptors of the screened drugs. However, the majority of these sensors did not provide information regarding the kinetics of the recognition reaction between the screened drugs and their receptors. Additionally, these sensors could not be used for intracellular studies because of their large size. In our laboratory, we recently developed a new type of particle-based miniaturized sensors named lipobeads. Lipobeads are micrometric polymeric particles coated with a phospholipid membrane. Hydrophobic and hydrophilic fluorescent probes could be entrapped in their phospholipid membrane providing the possibility to assay different intracellular analytes that interact with these specific fluorophores. Intracellular pH and oxygen levels were successfully measured using lipobead based sensors [34, 35]. Lipobeads have demonstrated high physical stability and low leakage rate. Moreover, they can be used as platforms for different types of interactions since their design is very versatile.

As new formulations of drugs become available it is important to determine and quantify various effects of these drugs on membranes. Valuable information concerning the design of new therapeutics can be obtained by correlating the effect of drugs on membranes of different compositions. This chapter evaluates the use of fluorescence resonance energy transfer (FRET) sensing lipobeads to investigate interactions between fluorescent dyes and phospholipid membranes. The optical signal resulted

from FRET between donor labeled phospholipids and acceptor molecules that partition into the phospholipid membrane (figure 4.1). The cellmembrane -like phospholipid layer of FRET sensing lipobeads increases their biocompatibility and makes them suitable for future intracellular measurements.

Nakashima and colab previously showed that FRET efficiency is 100 times higher in membranes than in solution [162,163]. They used Rhodamine and Malachite Green as donor-acceptor pair. The acceptor concentration required for quantitative FRET was in the range of tens of μM compared to hundreds μM in solution. Therefore, we predicted that the sensitivity of our FRET sensing lipobeads would increase compared to FRET sensitivity in solution.

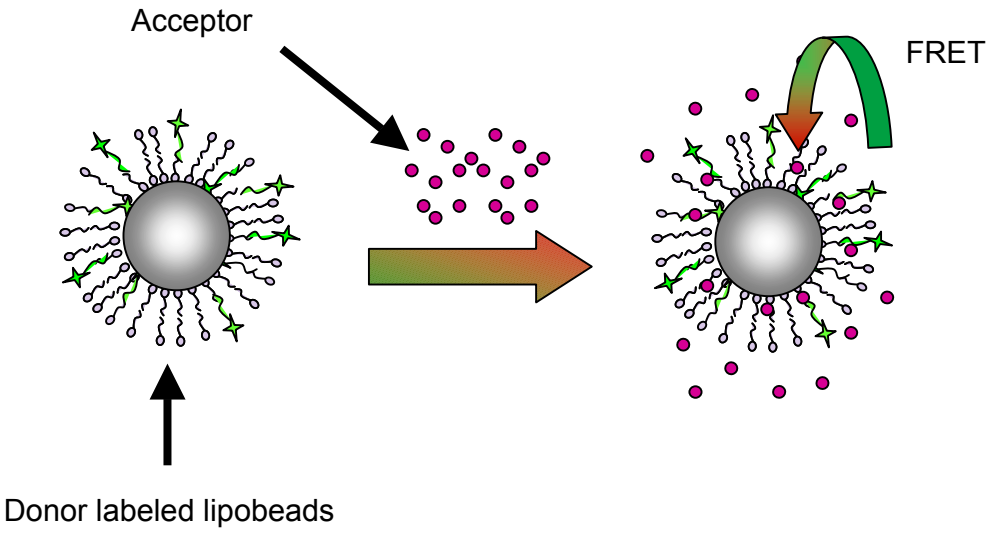

Figure 4.1. A schematic diagram illustrating the principle of FRET sensing lipobeads. Adsorption or biding of fluorescent acceptor molecules to lipobeads containing a fluorescent donor results in FRET signal enhancement.

4.2. Specific Experimental and Technical Details

Materials and Reagents

N-(Fluorescein-5-thiocarbomyl)-1,2-dihexadecanoyl-*sn*-glycero-3-phosphoethanolamine(Fluorescein-DHPE), Carboxyfluorescein and Sulforhodamine were obtained from Molecular Probes, Inc. Solid hydrophobic polystyrene microspheres with an average diameter of 1.6 μm (±1% variation) were purchased from Bangs Laboratory, Inc. Aqueous solutions were prepared with 18 MΩ deionized water produced by Barnstead Thermolyne Nanopure water purification system. Phosphate buffer (PBS, 100mM, pH=7.2) was obtained from Amresco. 1,2-Dimyristoyl-sn-glycero-3-phosphocholine (DMPC), 1,2-dihexadecanoyl-*sn*-glycero-3-phosphoethanolamine (PE), and 1,2-dimyristoyl-sn-glycero-3-phosphate monosodium salt (DMPA) were from Avanti Polar Lipids. Chloroform, methanol, cholesterol (CH) and dihexadecyl phosphate (DP) from were purchased Sigma. All reagents were used as received.

Synthesis of Fluorescent Lipobeads

Fluorescent lipobeads were synthesized based on a modified procedure originally described by Jin, J. et al [35]. The 1.6-μm polystyrene beads (4 mg/ml) were suspended in a 1:1 (v/v) ethanol/hexane solution and mixed with 80 μl 50 mM phospholipid cocktail in methanol: chloroform 1:1(v:v). The phospholipid cocktail (9:1 molar ratio) was prepared with DMPC and DMPA. To prepare donor labeled lipobeads 0.5-3% Fluorescein-DHPE (molar percentage) was added in the phospholipid cocktail. Several other phospholipid cocktails such as DMPC: PE=9: 1; DMPC: CH: DP=5:4:1 and DMPC were used to study the incorporation of Fluorescein-DHPE on different phospholipid

membranes. The beads and phospholipid suspension were incubated for 2 hours at room temperature and then dried out under nitrogen stream over night. The dried particles were resuspended in 2ml PBS buffer pH=7.4 with mild sonication. The excess phospholipid and uncoated particles were separated from lipobeads by centrifugation at 3000rpm for 15 min. The phospholipid coated particles were washed three times with the same buffer until no fluorescence background was noticed.

Energy Transfer Measurements

The excitation and emission spectra of fluorescent dye solutions were obtained using a spectrofluorimeter (PTI International, model QM-1), equipped with a 75-Watt continuous Xe arc lamp as a light source. For measuring the fluorescence of FRET sensing lipobeads, the excitation wavelength was set at 470 nm. The emission spectra were recorded at room temperature in the spectral range of the donor and acceptor dyes (Fluorescein and Rhodamine) from 490 to 700nm. The excitation and emissions slits were set at 4 nm. Three consecutive scans were averaged to obtain a single spectrum. A sample cell with 1 cm optical pathlength and 3 ml volume was used in the fluoremetric experiments. To eliminate the influence of turbidity and differences in the lipobead donor-labeling yield the ratio of the acceptor and donor fluorescence (F_A/F_D) was computed from each spectrum. The emission of peaks of the donor and acceptor were at 515 nm and 590 nm respectively. Digital fluorescence images of the FRET sensing lipobeads were acquired trough a microscope objective (40X) with a filter cube containing a 480 nm +/- 30 nm excitation filter, 505 dichroic mirror and 515nm long pass emission filter.

4.3. Results and Discussion

4.3.1. Choice of Fluorescent Indicators

Fluorescein and Rhodamine were used frequently as donor-acceptor pair in FRET applications since they are characterized by high absorbance, large emission quantum yield, sufficient separation between the excitation and emission wavelengths and significant overlap of donor emission and acceptor absorption spectra [50,167]. In this work, the Fluorescein derivative 1,2-dihexadecanoyl-*sn*-glycero-3-phosphoethanolamine(Fluorescein-DHPE) was used as a donor. The structure of the labeled phospholipid is shown in figure 4.2. Fluorescein-DHPE is a membrane surface probe that has been used for both local electrostatic potential and pH measurements [30, 31]. Since the fluorescent probe was covalently attached to the phospholipid, the leakage of dye molecules from the sensing particles was prevented. Dye leakage is one of the most common problems of fluorescence sensors that are prepared by physically entrapping fluorescent dyes in a sensor matrix. The Fluorescein label was exposed toward the aqueous solution, outside of the phospholipid layer, since the fluorescent dye was covalently bound to the phospholipid head group (figure 4.2).

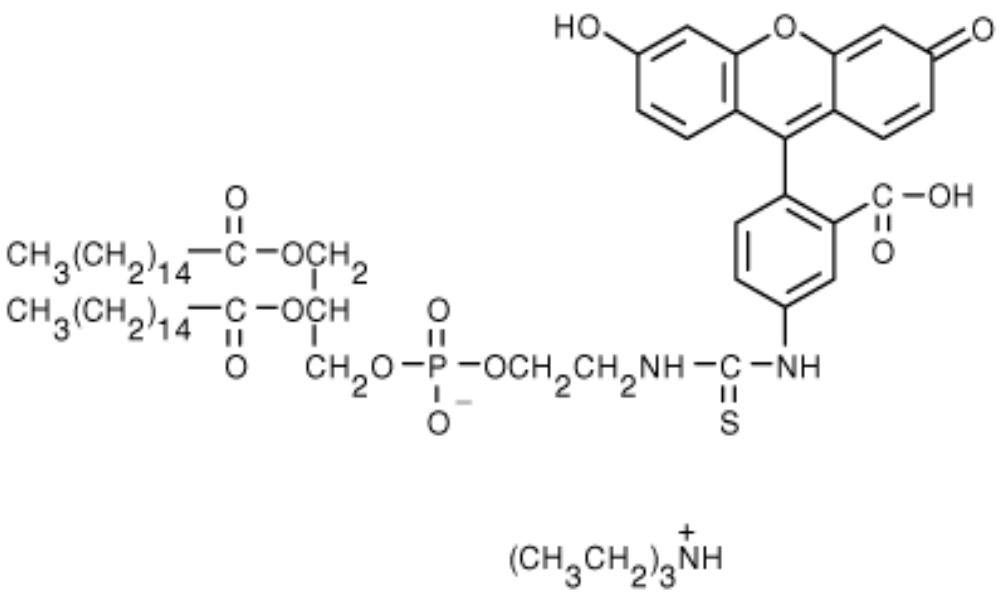

Figure 4.2. Structure of the donor labeled phospholipid used to label the FRET sensing lipobeads:*N*-(fluorescein-5-thiocarbamoyl)-1,2-dihexadecanoyl-*sn*-glycero-3-phosphoethanolamine triethylammonium salt (Fluorescein-DHPE).

4.3.2. Characterization of Donor Labeled FRET Sensing Lipobeads

A fluorescence image of FRET sensing-lipobeads averaging 1.6 μm in diameter is shown in figure 4.3. The image was taken using a 40X microscope objective and a 500 msec exposure time. Digital image analysis indicated that the ratio between the signal of the individual lipobeads and the background was approximately 250. The particles were evenly coated with fluorophores and they showed some aggregation. A 15% variation in the fluorescence intensity of the lipobeads was observed, suggesting that multilamellar films formed on some of the polystyrene particles.

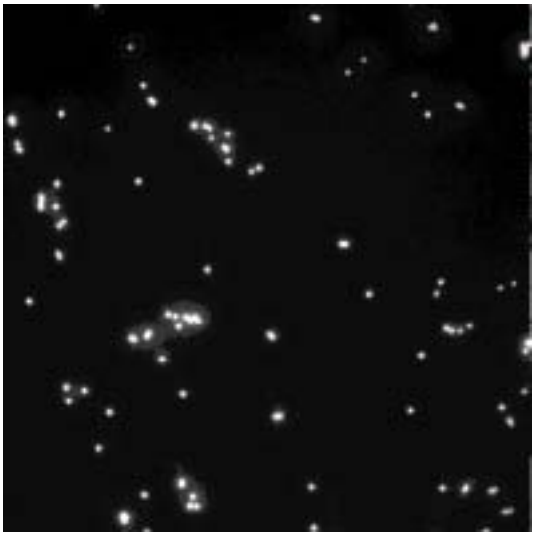

Figure 4.3. Digital fluorescence image of 1.6 μm FRET sensing lipobeads. The image was taken through an excitation filter: λ_{ex}=480 nm, a dichroic mirror: 505nm; an emission filter: λ_{em}>515 nm; objective: 40X with N.A= 0.7and a neutral density filter: 1.0 for 0.5 seconds.

4.3.2.1. Photostability of Lipobeads

The photostability of donor labeled lipobeads was tested by placing a sample of the fluorescent lipobeads on the microscope stage and continuously illuminating it at 480 nm. The fluorescence intensity of the lipobeads decreased by approximately 30% after 20 consecutive exposures. To overcome the inherent instability of Fluorescein, the lipobeads were exposed to the excitation light for only 0.3 s in each measurement. The number of exposures of the lipobeads was limited to 20. Additionally, a 0.1 OD neutral density filter was used to decrease the excitation intensity. Under these illumination conditions, all fluorophore molecules used in our experiments remained photostable throughout the experiments. No photobleaching occurred when the spectra were acquired with the fluoremeter.

4.3.2.2. Influence of the Phospholipid Composition on the Donor Absorption in the Lipobead Membrane

As described in detail in the experimental section, we labeled lipobeads with Fluorescein-DHPE. The synthesis of the fluorescent particles was first optimized to achieve maximum fluorescence intensity and FRET sensitivity**.** Several other phospholipid cocktails were used to achieve the highest Fluorescein-DHPE absorption on the beads and better lipobead dispersion in aqueous solutions. The signal to noise of the Fluorescein labeled lipobeads composed of different phospholipids is shown in figure 4.4. 1% Fluorescein-DHPE was used to label all lipobead compositions. The brightest lipobeads were obtained when a 9:1 DMPC: DMPA cocktail was used to prepare the lipobeads. Since DMPA is positively charged at pH 7.2, the FRET sensing lipobeads showed reduced aggregation compared to lipobeads prepared using other phospholipid cocktails. Consequently, a 9:1 DMPC: DMPA cocktail was used to prepare FRET sensing lipobeads.

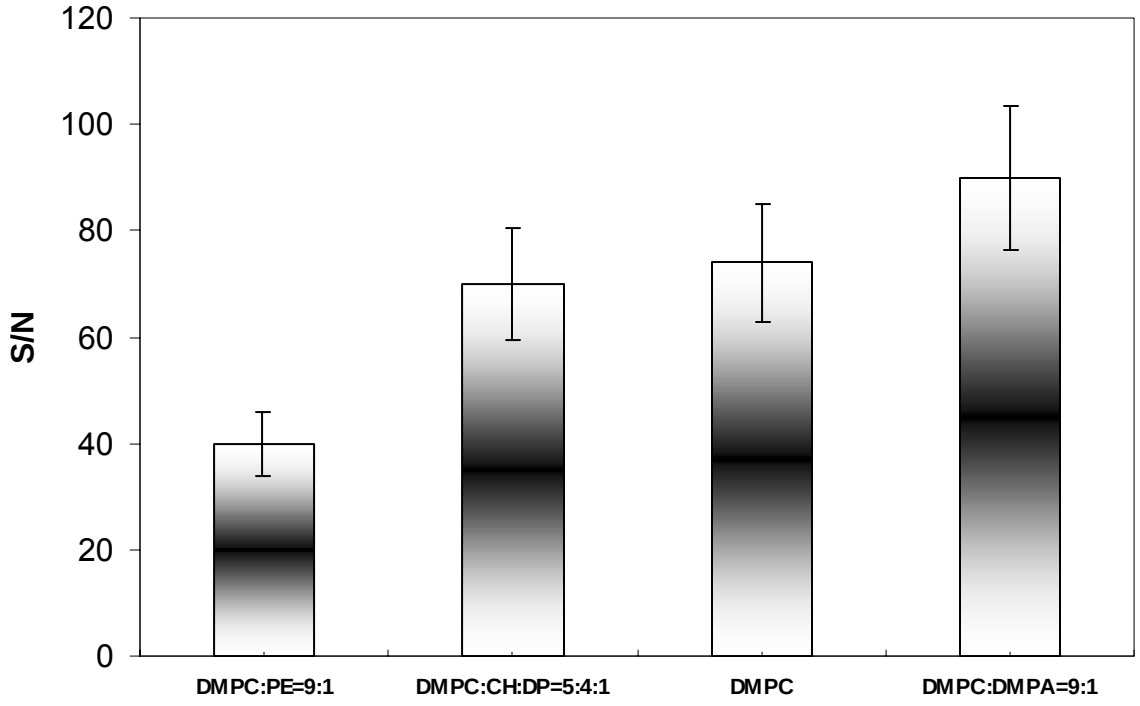

Figure 4.4. Effect of the composition of the phospholipid cocktail on the fluorescence intensity of FRET sensing lipobeads. **DMPC**=1,2-Dimyristoyl-sn-glycero-3-phosphocholine, **PE**=1,2-dihexadecanoyl-*sn*-glycero-3-phosphoethanolamine, **CH**=cholesterol, **PE=** dihexadecyl phosphate, **DMPA**=1,2-dimyristoyl-sn-glycero-3-phosphate monosodium salt.

4.3.2.3. Energy Transfer Efficiency of FRET Sensing Lipobeads

To test the FRET efficiency between donor labeled lipobeads and acceptor molecules, FRET sensing lipobeads solutions, that were adjusted to yield a fluorescence signal comparable to a solution of 500 nM Carboxyfluorescein, were mixed with Sulforhodamine. Fluorescence spectra of 1% Fluorescein-DHPE lipobeads in solution at different acceptor concentrations are shown in figure 4.5. The donor fluorescence was quenched and the acceptor fluorescence was sensitized with increasing concentrations

of Sulforhodamine. The changes and the wavelength shifts in the donor and acceptor signals resulted from FRET and inner filter effects [14, 49].

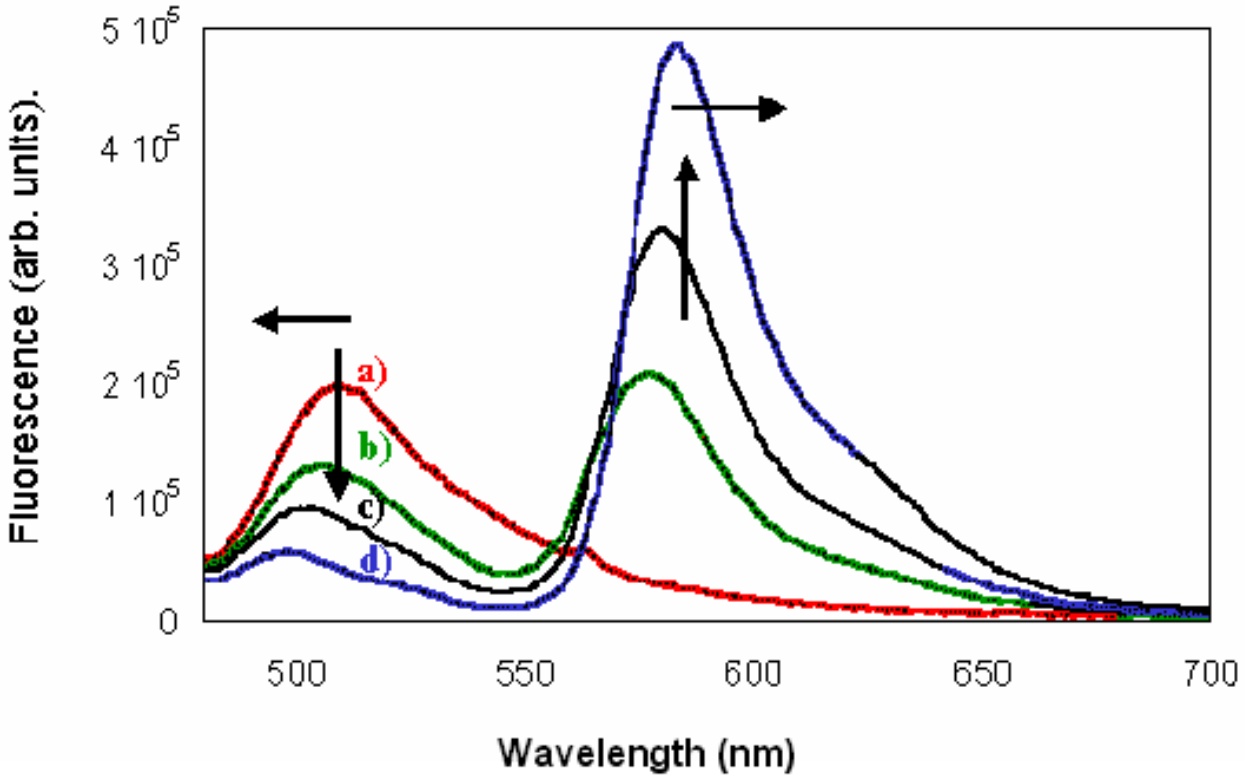

Figure 4.5. Fluorescence spectra of FRET sensing lipobeads in the presence of different Sulforhodamine concentrations: a) 0 μM, b) 10.0 μM, c) 20.0 μM, d) 40 μM. The spectra were not corrected for the inner filter effect contributions.

A comparison between the FRET efficiency of Fluorescein labeled lipobeads and free Carboxyfluorescein in solution in the presence of Sulforhodamine is shown in figure 4.6. The ratio Fa/Fd is used as a measure of FRET efficiency. It can be seen that Fa/Fd is acceptor concentration dependent. The FRET efficiency between the lipobeads and the Sulforhodamine was consistently 3-fold higher than FRET between Carboxyfluorescein and Sulforhodamine at any given acceptor concentration.

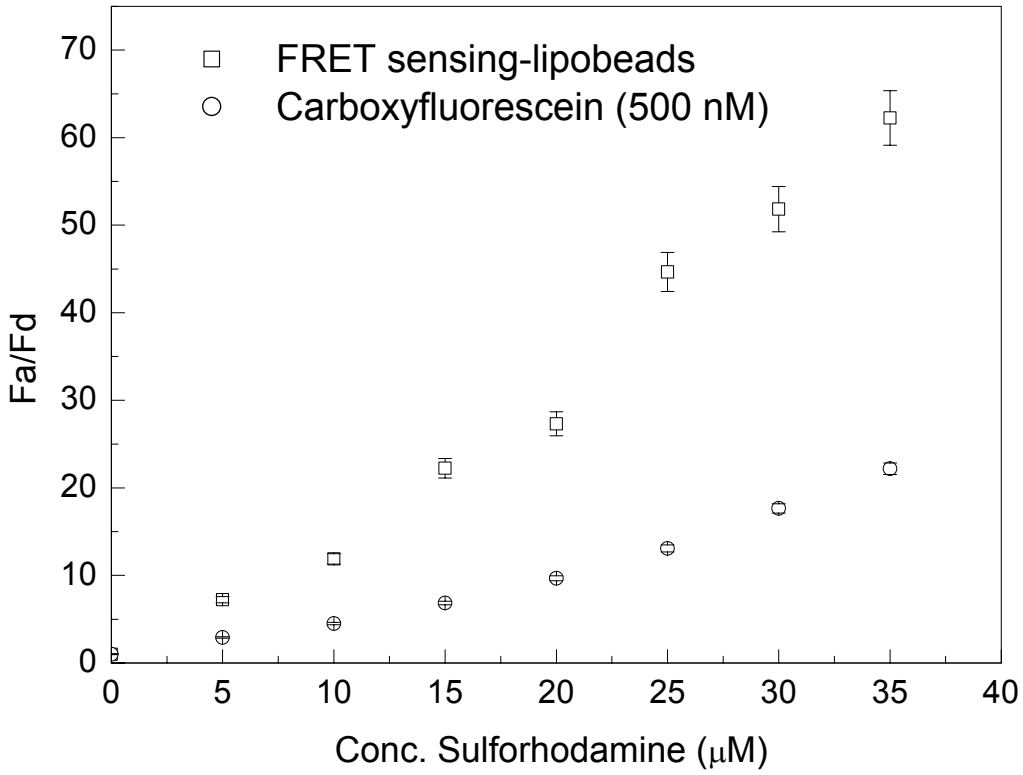

Figure 4.6. The variation of energy transfer efficiency (Fa/Fd) against increasing acceptor concentration for; a) FRET sensing lipobeads and b) Carboxyfluorescein solution (500nM).

4.4. Summary and Conclusions

A general scheme for sensitive detection of fluorescent acceptors using FRET based sensing lipobeads was developed. Using lipobeads labeled with Fluorescein we developed a method to evaluate the interaction of acceptor molecules with the phospholipid membrane of the lipobead-based sensor. The FRET efficiency between acceptor molecules that partitioned between solution and the donor labeled lipobeads was found to be approximately 3-fold larger than FRET efficiency between the donor

and acceptor molecules when dissolved in solution. The increase in energy transfer efficiency can be attributed to partition of acceptor molecules into the phospholipid layer membrane of the polymer beads, which increases the probability of FRET between the donor and acceptor molecules. As was hypothesized the change in the dimensionality of the system in which FRET occurs, improved the sensitivity of our measurements. However, the improvement in the sensitivity was lower than expected due to contributions from inner filter effects. We concluded that a biomolecular recognition component must be added to the FRET sensing lipobeads in order to decrease the acceptor concentration required for high FRET efficiency. We further hypothesized that adding a biomolecular recognition element would also decrease inner filter effects contributions and enable detection of non-fluorescent inhibitors based on their ability to compete on binding sites with acceptor molecules. These conclusions were the basis of a study, which is described in the next chapter of this dissertation. It focuses on the development of new miniaturized FRET based sensors for the detection of nonfluorescent carbohydrates and glycoproteins.

CHAPTER 5

DESIGN, SYNTHESIS AND APPLICATION OF PARTICLE-BASED FRET SENSORS FOR SCREENING CARBOHYDRATES AND GLYCOPROTEINS

5.1. Introduction

Molecular fluorescence probes have emerged in the last two decades as useful tools for the analysis of biological fluids. Recently, these probes were immobilized to particles to form particle-based fluorescence sensors. For example, Kopelman et al developed and applied particle-based nanosensors for intracellular measurements of various physiologically important ions [170-173]. In our laboratory we prepared phospholipid coated submicrometric fluorescent polymer particles and employed them to quantify the pH and molecular oxygen levels in murine macrophages and the release of zinc ions from stimulated neuron cells in culture [21,34,35,174]. Due to their miniaturized dimensions particle-based sensors are less invasive and less destructive than larger sensors. Their temporal and spatial resolution is inversely dependent on their size due to decreasing spatial dimensions and increasing surface over bulk ratio with decreasing particle size. The nanometric dimensions of these sensors enable site-specific and rapid measurements in biological samples. Furthermore, it is possible to employ digital fluorescence imaging microscopy systems for multiplexed analysis of a large number of particles simultaneously.

In particle-based fluorescence sensors the fluorescence indicator is entrapped in a polymer matrix that minimizes interactions of the fluorescent indicator with possible interfering substances. This protection increases the chemical stability of particle-based sensors in biological samples and decreases their cytotoxicity [175]. Currently used particle-based fluorescence sensors are based on a direct interaction between fluorescent indicators and their corresponding analytes. These sensors are restricted to a limited number of analytes that include pH, cations and molecular oxygen. The incorporation of enzymes and antibodies for analyte recognition has largely expanded the scope of analytes that could be determined with fluorescence sensors [176-179]. Nevertheless, there is still a need to develop new signal transduction mechanisms that could be coupled to biorecognition components like enzymes and antibodies in miniaturized sensors.

Fluorescence resonance energy transfer (FRET) is a fluorescence phenomenon during which the energy of an excited donor molecule is transferred non-radiatively to an acceptor molecule [14]. FRET spectroscopy has been used frequently in studying protein-protein interactions and protein conformational changes [180, 181]. The use of FRET microscopy practically extends the spatial resolution of optical microscopes since FRET occurs only when the donor and acceptor molecules are in close proximity (1-10nm) [182]. FRET has been previously applied in biosensors that use a change in protein or DNA oligomer conformation due to interactions with analyte molecules as a basis for molecular recognition [183]. In this study we developed particle-based FRET sensors for screening carbohydrates and glycoproteins. The detection principle was

based on selective carbohydrate-protein interactions between carbohydrates and concanavaline A (ConA), a lectinic protein.

The evaluation of protein-carbohydrate interactions is not trivial because the binding mechanism and the parameters that affect the binding affinity between carbohydrates and proteins are not fully understood [184]. The most utilized method to quantify carbohydrate-lectin interactions measures the ability of a soluble carbohydrate to inhibit the agglutination and precipitation of lectins, which are induced by a multivalent saccharide [185]. The absorption of the mixture is monitored at different carbohydrate concentrations. The carbohydrate inhibition efficiency is expressed as IC_{50}, which is the inhibitor concentration required to decrease the absorption signal by 50%. Although simple, this technique is time consuming and the results are often irreproducible. More recently, surface plasmon resonance (SPR) binding assays were used successfully to measure carbohydrate-protein interactions [186-188]. SPR methods have the ability to monitor binding events in real time and without labeling. While the assays are highly sensitive their selectivity remained a problem as SPR sensors are largely affected by non-specific interactions.

Recent literature reports have led us to hypothesize that it would be possible to employ FRET based micrometric sensors to screen carbohydrates or glycoproteins based on their selective interaction with carbohydrate binding proteins like ConA. For example, Kiessling et al [186, 187] investigated the control of multivalent interactions involving lectins and new classes of polyvalent carbohydrate ligands. The efficiency of FRET between a donor and an acceptor labeled ConA that bound to the same multivalent ligands was indicative of the lectin-carbohydrate interactions. Glucose monitoring by

the interaction of ConA with monomeric glucose was reported by Schultz and coworkers who used several experimental setups for this purpose [178]. For example, they developed a novel fluorescence hollow fiber sensor for transdermal glucose monitoring based on the competitive and reversible binding of FITC-ConA to colored sephadex beads in the presence and absence of free glucose. In this study, we used FRET as an optical signaling strategy to monitor the binding of carbohydrates and glycoproteins to polymeric particles labeled with FITC-ConA. We determined the ability of monomeric carbohydrates and glycoproteins to inhibit the binding between Texas Red-labeled dextran (dextran-TR) and the FITC-ConA labeled particles (figure 5.1). The optical signal resulted from FRET between the fluorescein labeled ConA and the Texas Red-labeled dextran molecules. In the inhibition assays the particles were pre-incubated with unlabeled carbohydrates or glycoproteins prior to adding dextran-TR to the samples. The FRET efficiency between FITC-ConA and dextran-TR decreased with increasing the concentration of binding inhibitors. The analytical properties of these newly developed particle-based FRET sensors and their potential use in carbohydrate and glycoprotein screening applications are discussed.

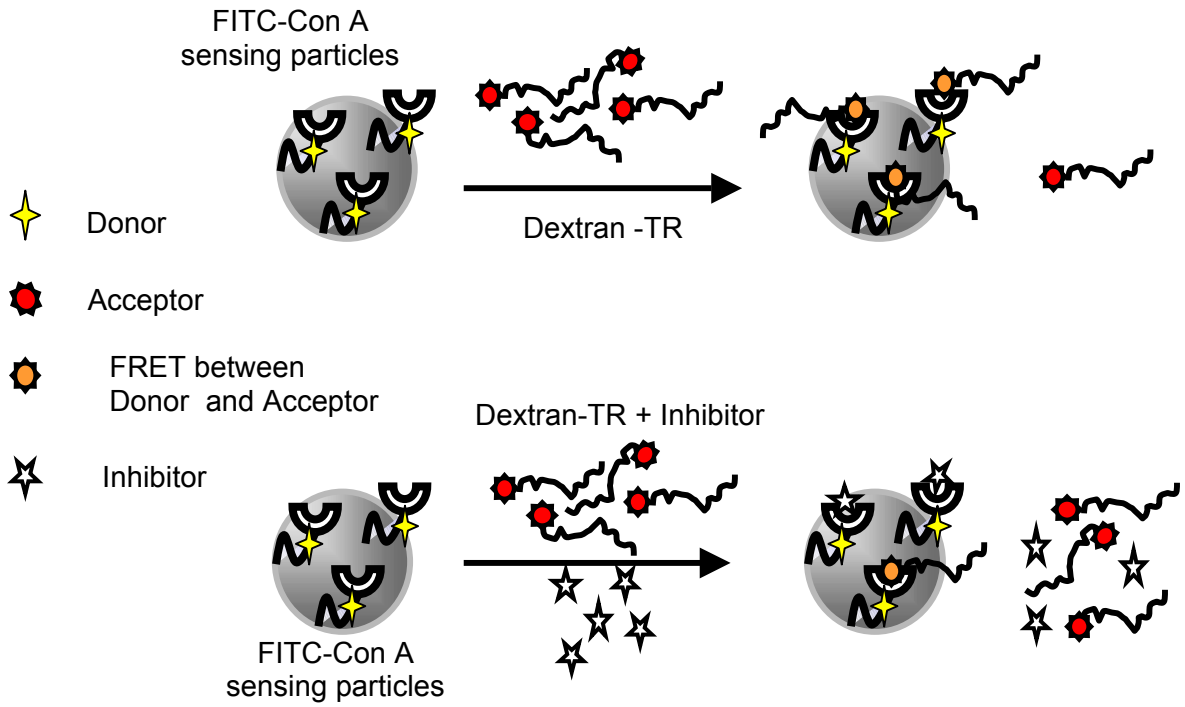

Figure 5.1. Illustration of the Particle-Based FRET Sensors for Screening Carbohydrates and Glycoproteins. FRET sensing particles in the absence (top) and presence (bottom) of glycoprotein or carbohydrate inhibitors. The FRET efficiency decreases with increasing inhibitor concentrations.

5.2. Specific Experimental and Technical Details

Synthesis of FRET Sensing Particles

FITC-ConA labeled particles were synthesized by suspending 1.6-μm polystyrene particles [16 mg/ml, 10^7 beads/ml) in a 200μg/ml FITC-ConA HEPES buffer solution at pH 7.2 for 3 hours at room temperature. The HEPES buffer solution contained 100 mM HEPES, 150 mM NaCl, and 1mM Ca^{2+} and Mn^{2+}. Lectin molecules adsorbed strongly to the hydrophobic polystyrene particles and leakage of the proteins to aqueous solution

was negligible for months. The excess protein and uncoated particles were separated from the lectin-coated particles by repeated cycles of precipitation by slow speed centrifugation (3000 rpm for 15 min) and resuspension in HEPES buffer solution at pH 7.2. The ConA-coated particles were washed until no fluorescence background from free FITC ConA molecules was noticed. The FITC-ConA particles were further incubated with 1mg/ml bovine serum albumin (BSA) for two hours. BSA was used as a blocking solution to minimize non-specific adsorption of acceptor molecules on the particles. The particles were washed of excess BSA using three cycles of precipitation by centrifugation and resuspension in HEPES buffer. The particles were finally suspended in 5 mL HEPES (100mM, 150 mM, NaCl, pH=7.2) solution and stored at 4° C until use. The density of lectin receptors on the particles was estimated to be around 10^5 molecules/particle or 10^{-12} mole/cm^2. The number of FITC-ConA molecules absorbed on the surface of the particles was calculated by measuring the absorption of the supernatant at 280 nm prior and following labeling the particles with FITC-ConA. The concentration of FITC-ConA in the supernatant was calculated by using UV absorption at 280 nm, A_{280} = 1.37 x [mg/ml ConA] [187]. The amount of lectins per particle was estimated from dividing the total concentration of FITC-ConA absorbed on the particles by the concentration of the particles in the solution. All buffers used in the experiments were autoclaved to minimize bacterial growth

Digital Fluorescence Imaging Microscopy and Spectroscopy

The fluorescence images of the FRET sensing particles were collected using a 20X microscope objective with NA = 0.5. Exposure times of 0.2 sec and 0.5 sec were used

to acquire the fluorescence spectra and images of the particles respectively. A 0.6 OD transmission neutral density filter was used to decrease the excitation light intensity of the 100-W microscope mercury lamp in order to minimize photo bleaching of the fluorophores.

Immobilization of FRET sensing particles on the surface of a multi-well chambered cover glass

A multi-well chambered cover glass [borosilicate, Nalge Nunc International) was washed with 70% ethanol/water, followed by a thorough rinse with deionized water. The cover glass was incubated overnight with 1% poly-L-lysine. The wells were then rinsed with deionized water and a working HEPES buffer at pH 7.2. A 5µl FRET sensing particles suspension was added to 200 µL HEPES buffer. The solution was added to a glass well and incubated for 4 hours at room temperature to facilitate the physical attachment of FRET sensing particles to the polylysine coated glass surface. The glass wells were washed form unbound FRET sensing particles using the HEPES buffer solution. This step was done with care to minimize contact of the micropipette used to remove the solution with the polylysine layer attached to the glass well surface.

Dextran-TR binding studies - To study the binding of dextran-TR to the FITC-ConA labeled particles we first attached the FITC-ConA labeled particles to the polylysine coated wells of the chambered cover glass. Then, a solution of 400 µL HEPES buffer at pH 7.2 with 1mM Ca^{2+} and Mn^{2+} was added to each well. Small aliquots of concentrated dextran-TR (2-4 µl) were added and the solution was mixed with a Pasteur pipette. The final concentrations of dextran-TR ranged from 0 to 15 µg/ml. The dextran-TR binding

was monitored for 15 minutes until no changes in the donor and acceptor fluorescence was observed.

FRET inhibition assays – The inhibition assays were performed in a chambered cover glass and were monitored using digital fluorescence imaging microscopy. The decrease in donor fluorescence was used to quantify the FRET inhibition efficiency. To carry out the inhibition assays the polylysine coated wells were first incubated with $5x10^4$ FITC-ConA labeled particles. Unbound particles were washed with a HEPES buffer solution at pH 7.2. Then, 200 μL HEPES buffer solution aliquots containing FRET inhibitors at various concentrations were added to the wells. The sample solutions were incubated for 1 hour at room temperature. Then, dextran-TR solution was added to each well at a final concentration of 1.2 μg/ml and the solution was mixed thoroughly with a Pasteur pipette. Digital fluorescence images from each well were taken immediately and 15 minutes following the addition of dextran-TR. Longer incubation times did not induce larger changes in the donor and acceptor fluorescence. The fluorescence intensity of the FRET particles at 15 minutes was normalized to the initial fluorescence intensity taken immediately following the addition of dextran-TR to the wells. Each assay was repeated 3 times for error analysis purposes. The digital fluorescence images were acquired using the image analysis software Image ProPlus v 4.5. The Micro Cal Origin v 7.0 software was used for data analysis.

5.3. Results and Discussion

5.3.1. Choice of Fluorescent Indicators

Fluorescein and Texas Red have been used frequently in FRET applications because of their high absorbance, emission quantum yield, large separation between the excitation and emission wavelengths and the significant overlap between the donor emission and the acceptor absorption spectra [189-191]. The absorption and emission spectra of Fluorescein and Texas Red are shown in figure 5.2. The overlap integral between the Fluorescein emission and Texas Red absorption is marked with diagonal lines. In selecting the donor-acceptor pair we also considered using Rhodamine derivatives rather than Texas Red as acceptor molecules. While the overlap integral between Fluorescein and Rhodamine was 2-fold larger than the overlap integral between Fluorescein and Texas Red, the signal to noise ratio was higher for the Fluorescein-Texas Red donor-acceptor pair. This was attributed to the minimization of leakage between the donor and acceptor channels, often described as “bleeding” [75, 192]. It results from direct excitation of acceptor molecules by the excitation light. It must be minimized to enable quantitative analysis of binding events between donor and acceptor labeled biomolecules as well as quantitative analysis of binding inhibitors.

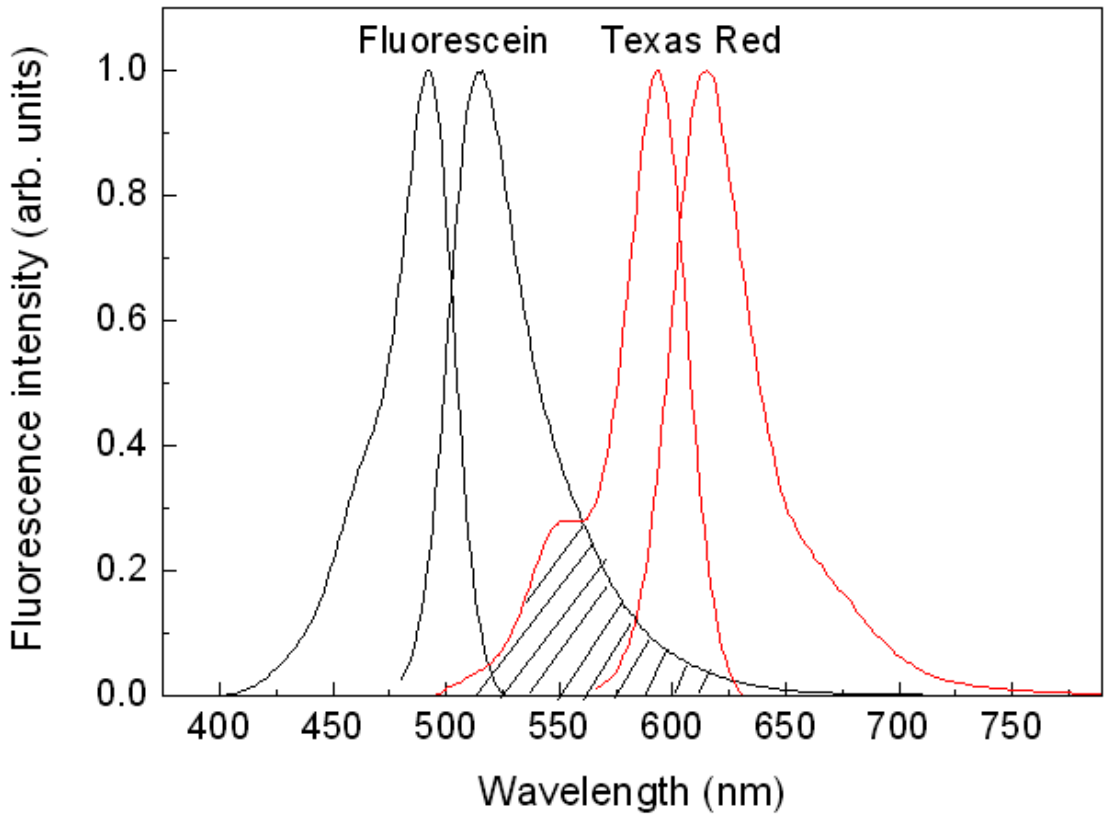

Figure 5.2. Absorption and fluorescence spectra of Fluorescein and Texas Red. The area marked with diagonal lines represents the overlap integral between the donor emission and acceptor absorption.

5.3.2. Characterization and Properties of the FRET Sensing Particles

As described in detail in the experimental section, we labeled polystyrene particles with FITC-ConA, a glucose/mannose binding protein. The synthesis of the fluorescent particles was optimized to realize maximum fluorescence intensity and sensitivity to dextran-TR binding. Further studies were performed to determine the dose response and the response time of the FRET signal to changes in dextran-TR concentration. To maximize the fluorescence intensity of the FRET sensing particles we prepared FITC-

ConA labeled particles in FITC-ConA solutions of increasing concentrations from 10 to 500 μg/ml. The fluorescence intensity of the FITC-ConA labeled particles was measured in 5 fields of view on the surface of a microscope cover slip. The fluorescence intensity of the particles increased with increasing FITC-ConA concentration in the preparation solution up to a concentration of 200 μg/ml. Then, the fluorescence intensity decreased probably due to fluorescence self-quenching between adjacent FITC molecules. The FRET sensing particles exhibited bright fluorescence with a signal-to-noise ratio (S/N) of 50. A 10% variation in their fluorescence intensity was observed, suggesting that the FITC-ConA was not distributed uniformly on the polystyrene particles or that the number of fluorescein molecules per ConA molecule varied to some degree.

5.3.3. Photostability and Leaking Stability of the FRET Particles

To test the photostability of the FITC-ConA labeled particles we attached FRET sensing particles to a multi well chambered cover glass as described in the previous section. The chambered coverglass was placed on the stage of an inverted fluorescence microscope. The FRET sensing particles were then continuously illuminated using the 100 Watt lamp of the microscope. Fluorescence images of the particles were obtained periodically. The fluorescence intensity of the FRET sensing particles decreased by about 30% during the first 5 minutes of continues illumination. To overcome the inherently poor photostability of FITC we used a 0.6 OD neutral density filter to reduce the excitation intensity. Additionally, the particles were exposed to the excitation light for only 0.5 sec in each measurement and the number of exposures was limited to 30

during a typical binding experiment. Under these illumination conditions, all fluorophore molecules used in our experiments remained photostable throughout the measurements. The FRET sensing particles were stored in a 100 mM HEPES and 150 mM NaCl buffer solution at pH 7.2 and 4°C. Under these storage conditions, the particles maintained the ConA binding activity with minimal dye leakage and no noticeable aggregation. The performance limiting factor of the FRET sensing particles was found to be their carbohydrate binding activity. When suspended in solution the FITC-ConA labeled particles retained their carbohydrate binding activity for only 4-5 days. This could be attributed to bacterial growth, which is known to affect the binding activity of lectins [193].

5.3.4. Dextran-TR Binding Studies

The stable immobilization of FRET sensing particles to the polylysine coated wells enabled real time binding measurements of dextran-TR to the FITC- binding of dextran-TR to the particles are shown in figure 5.3. Figure 5.3a shows the FRET sensing particles prior to their binding reaction with dextran-TR. When imaged through the donor+acceptor channel (λ_{ex}=470nm, λ_{em}>515 nm) the particles emitted green light.

Figure 5.3b shows a fluorescence image of the same particles following binding of the FRET sensing particles to dextran-TR. The particles emitted orange light since this channel allowed both characteristic fluorescence of Fluorescein (green) and Texas Red (red) to reach the CCD detector. Figure 5.3c shows the fluorescence of the same particles following binding to dextran-TR taken through the FRET channel (λ_{ex} =470 nm, λ_{em}>590nm). The particles emit red light, which is a clear indication that dextran-TR is

indeed bound to the particles. FRET magnitude could be determined based on the decrease of the fluorescence of FITC or based on the increase in the fluorescence of Texas Red due to FRET between FITC and Texas Red.

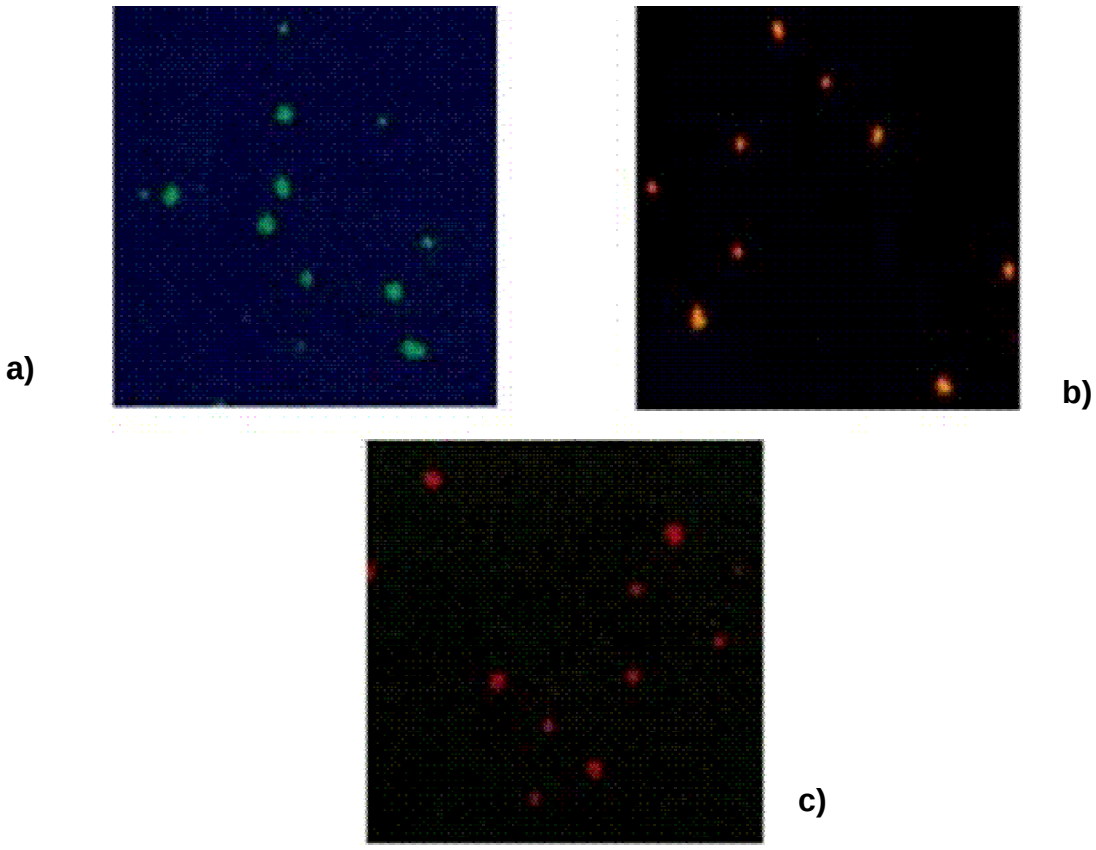

Figure 5.3. Digital fluorescence images of FRET sensing particles through the donor+acceptor channel (λex=470nm, λem>520nm) in a) the absence of dextran-TR, and b) when dextran-TR is bound to the FITC-ConA labeled particles. c) A digital fluorescence image of the particles through the FRET channel (λex=470nm, λem>590nm) when dextran-TR bound to the FRET sensing particles.

In our experiments we found that the determination of the FRET efficiency by measuring the decrease in the donor fluorescence was more reproducible than the determination of the FRET efficiency based on the increase in acceptor fluorescence. It should also be noted that under our experimental conditions the quenching of the donor fluorescence could also result from nonspecific adsorption of dextran-TR on the FRET sensing particles. To minimize non-specific adsorption we blocked the surface of the FRET sensing particles with 1mg/ml bovine serum albumin (2 hour incubation) prior to adding dextran-TR to the FRET sensing particles solution.

The dependence of the FRET efficiency between dextran-TR and FITC-ConA on the dextran-TR concentration was determined using digital imaging spectroscopy measurements. About 30 FRET sensing particles were imaged through a slit and their integrated emission spectra were used to quantify the FRET efficiency. The temporal dependence of the fluorescence spectra of the FRET sensing particles is shown in figure 5.4 for dextran-TR concentration of 0.12 μM (λ_{ex} = 470 nm). Curve a shows the fluorescence spectrum of the FRET sensing particles prior to addition of dextran-TR.

A single emission peak at 525 nm, characteristic to FITC, is seen. Curve b shows a fluorescence spectrum that was acquired immediately following adding dextran-TR to the observed sample. A slight decrease in the donor fluorescence at 525 nm and a slight increase in the acceptor fluorescence at 615 nm are seen, which are characteristics of FRET between the donor-acceptor pair. Curve c shows the fluorescence spectrum of the same sample taken 15 minutes following adding dextran-TR to the sample. A ~40% decrease in the donor fluorescence and a similar increase in

the acceptor fluorescence are seen. Longer incubation times did not increase the donor quenching or acceptor fluorescence significantly.

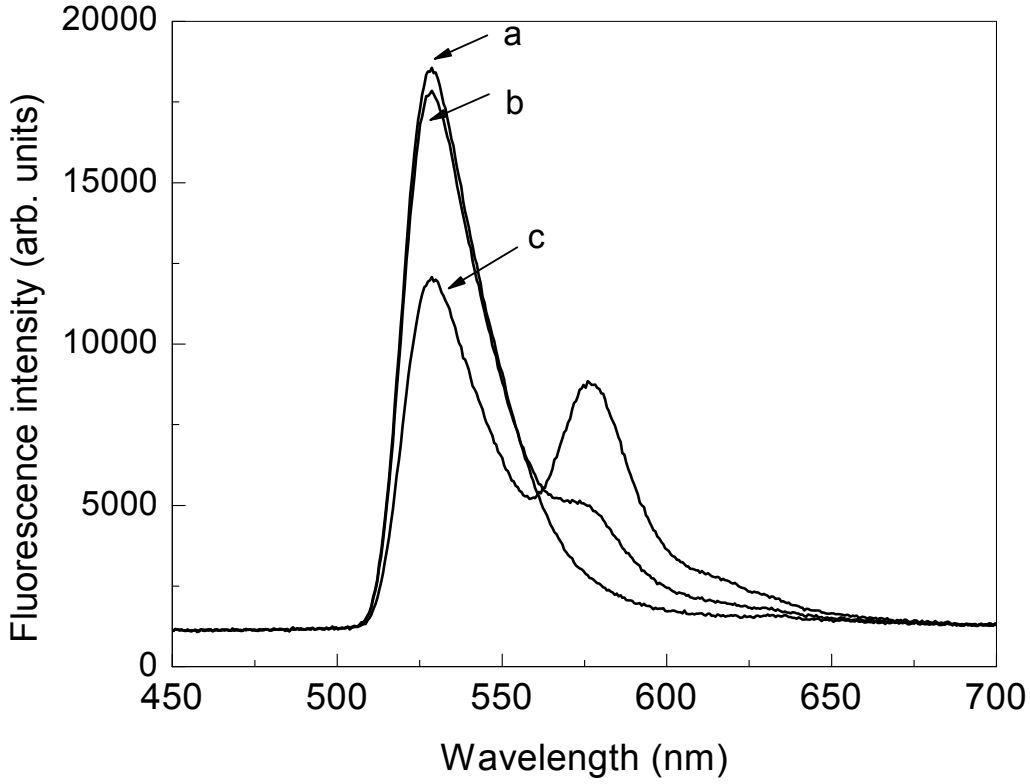

Figure 5.4. Fluorescence spectra of the FRET sensing particles: a) in the absence of dextran-TR, b) immediately following the addition of 1.2 µg/ml dextran-TR and c) when the FRET between dextran-TR and the FITC-ConA labeled particles reached equilibrium (15 min).

Figure 5.5 describes the FRET efficiency between dextran-TR and the FITC-ConA labeled particles as a function of dextran-TR concentration. The FRET efficiency was defined as F_d/F_{d0} where F_d was the donor fluorescence at a given dextran-TR concentration and F_{d0} was the donor fluorescence in the absence of dextran-TR. F_d was measured at equilibrium 15 minutes following the addition of dextran-TR to the

FRET sensing particles solution. The donor fluorescence at 520 nm decreased by about 60% at dextran-TR concentrations higher than 1 μM. The 15 minutes incubation time needed to reach equilibrium was attributed to the relatively slow permeation of dextran-TR through the poly-lysine membrane. This enabled us to conclude with high degree of confidence that the observed signal changes resulted from FRET between dextran-TR and FITC-ConA labeled particles. Other possible interfering optical effects like inner filter effects would result in instant signal changes since they would not depend on the permeation of dextran-TR through the polylysine membrane or on the chemical reaction between dextran-TR and FITC-ConA labeled particles.

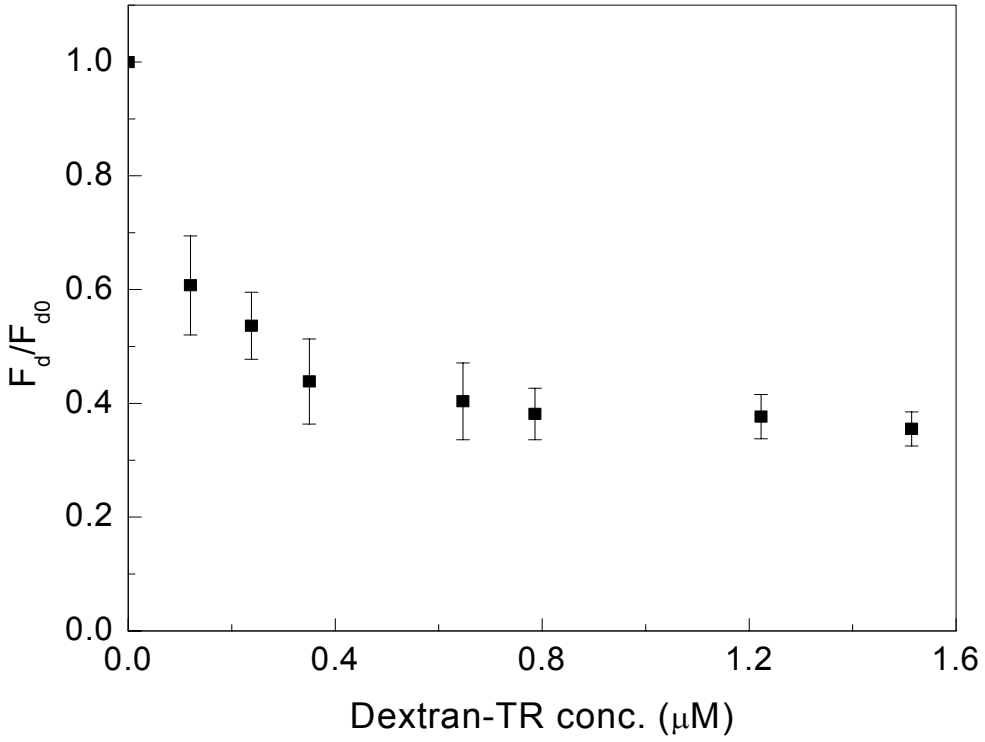

Figure 5.5. The FRET signal between dextran-TR and FITC-ConA coated particles as a function of dextran-TR concentration. The FRET magnitude was determined by following the decrease in the donor fluorescence. The fluorescence intensity of the particles (F_d) was measured through donor cube [λex=470nm, 520nm<λem<560nm) and was normalized to the initial donor fluorescence (F_{d0}).

5.3.5. Determination of Binding Constant of Dextran-TR

The binding constant of dextran-TR to the FRET sensing particles was calculated using the following expression [195]:

$$\frac{[Dextran-TR]F_0}{\Delta F} = \frac{[Dextran-TR]F_0}{\Delta F_{\max}} + \frac{F_0}{\Delta F_{\max} K_a} \qquad (5.1)$$

where F_0 is the initial intensity of the FRET sensing particles [prior to adding dextran-TR), $F_{\max}$ is the maximum donor quenching obtained at saturation, $\Delta F = F_0 - F$, F is donor fluorescence after adding dextran-TR, $\Delta F_{\max} = F_0 - F_{\max}$ and K_a is the binding constant in M^{-1}. The apparent binding constant calculated using the equation 5.1does not give any information about the cooperativity of the binding interaction between dextran-TR and the FRET sensing particles. Figure 5.6 describes the product of the concentration of dextran-TR and $F_0/\Delta F$ as a function of the product of the concentration of dextran-TR and $F_0/\Delta F_{max}$.

The binding constant K_a is calculated from the intercept of this plot to be $1.1 \times 10^7 M^{-1}$. As expected, this K_a value is an order of magnitude larger than Ka value reported earlier by Borrebaeck et al for the binding of lower molecular weight dextran to ConA-coated sepharose particles [194].

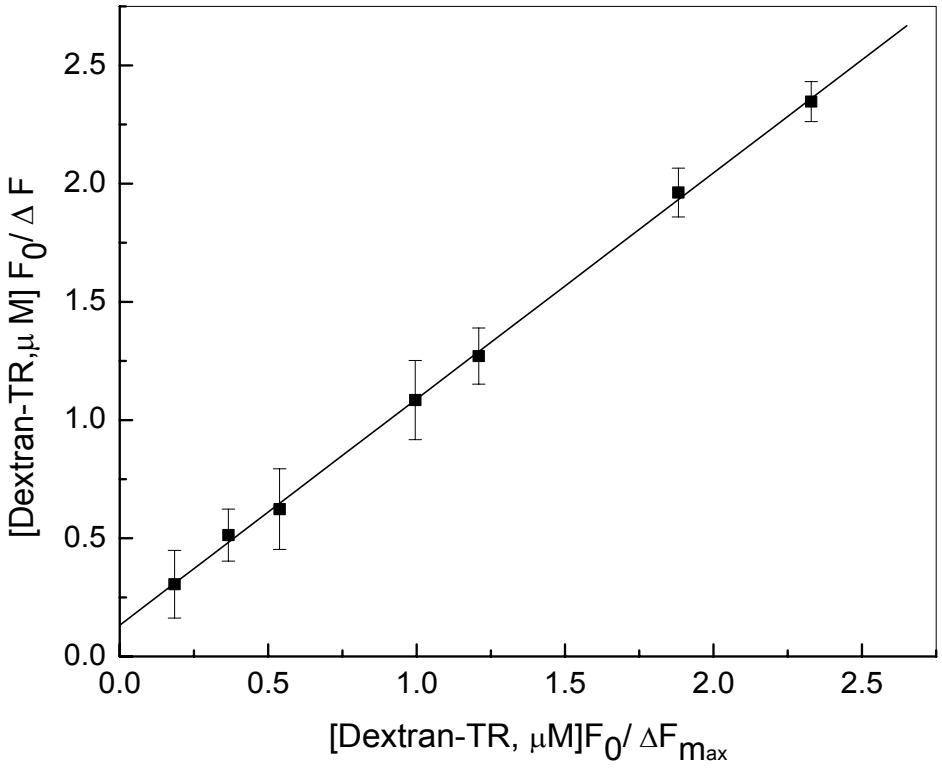

Figure 5.6. Determination of the apparent association constant between dextran-TR and FRET sensing particles based on the equation [5.1].

5.3.6. FRET Inhibition Assays

Following the dextran-TR binding studies we developed binding inhibition assays based on decreasing the binding efficiency between dextran-TR and the FITC ConA-labeled particles in the presence of carbohydrates or glycoproteins. First, a multi well chambered coverglass was coated with FRET sensing particles as previously described. Then, monomeric carbohydrate or glycoprotein solutions of various concentrations were added to the wells for a 1 hour incubation period at room temperature. Aliquots of 4µl 60 µg/ml Dextran-TR were then added to the wells.

A washing step to remove unbound inhibitor molecules was not required. It was expected that inhibitors with high affinity to ConA would cluster the lectin receptors. Dextran-TR would compete poorly on the ConA binding sites, which would result in low FRET efficiency between dextran-TR and the FRET sensing particles. In contrast, we expected that inhibitors with low affinity to ConA would be easily displaced by the dextran-TR molecules. This would result in high FRET efficiency between dextran-TR and the FITC-ConA labeled particles, which would be similar to the one obtained in the absence of inhibitor. The inhibition percentage was calculated as follows:

$$In\% = [(F_i - F_{ni}) / \Delta F] \times 100 \quad (5.2)$$

In% is the percent inhibition, F_i is the fluorescence intensity of the particles 15 minutes following the addition of dextran-TR in the presence of inhibitor, and F_{ni} is the fluorescence intensity of the particles 15 minutes following the addition of dextran-TR in the absence of inhibitor. ΔF is defined as:

$$\Delta F = F_{In100\%} - F_{ni} \quad (5.3)$$

$F_{In100\%}$ is the fluorescence intensity of the particles at 100% inhibition. It should be noted that the FRET inhibitors were quite effective with FRET inhibition larger than 90% at high inhibitor concentrations. IC_{50} values were defined as the concentrations of inhibitors required to decrease the FRET efficiency between dextran-TR and the FITC-ConA labeled particles by 50%.

Figure 5.7 summarizes the inhibition efficiency of monomeric carbohydrates and glycoproteins of the binding between dextran-TR and the FRET sensing particles. Galactose appears to be the worst performing inhibitor, which is attributed to the weak affinity between ConA and Galactose. As expected, the inhibition efficiency of Mannose is higher than that of Galactose. However, Mannose as well is characterized with a relatively high IC_{50} of 1.7 mM. It is possible that the large number of glucose residues in dextran-TR (MW =10000 Da), enhances its binding affinity to the FRET sensing particles through multivalent interactions. The mechanism of multivalent interactions between the dextran-TR and ConA is complex and still not completely understood [184, 186]. Chelate effects, subsite bindings, steric stabilization and receptor clustering could contribute to the increased affinity of dextran-TR for the FRET sensing particles [186}. As a result, high concentrations of monomeric carbohydrates like Mannose are required to effectively block the binding between dextran-TR and the FRET sensing particles.

Glycoproteins, which contain a large number of glycosylic residues, have lower IC_{50} values. For example, Glucose oxidase was found to be the most potent inhibitor with an IC_{50} value of 0.5 μM. Ovalbumine, a glycoprotein, which is not as rich in glycosylic residues showed an IC_{50} value of about 4.5 μM. Avidin, another glycoprotein, which has only four Mannose residues, had the smallest inhibition efficiency among the screened glycoproteins with an IC_{50} of 75μM.

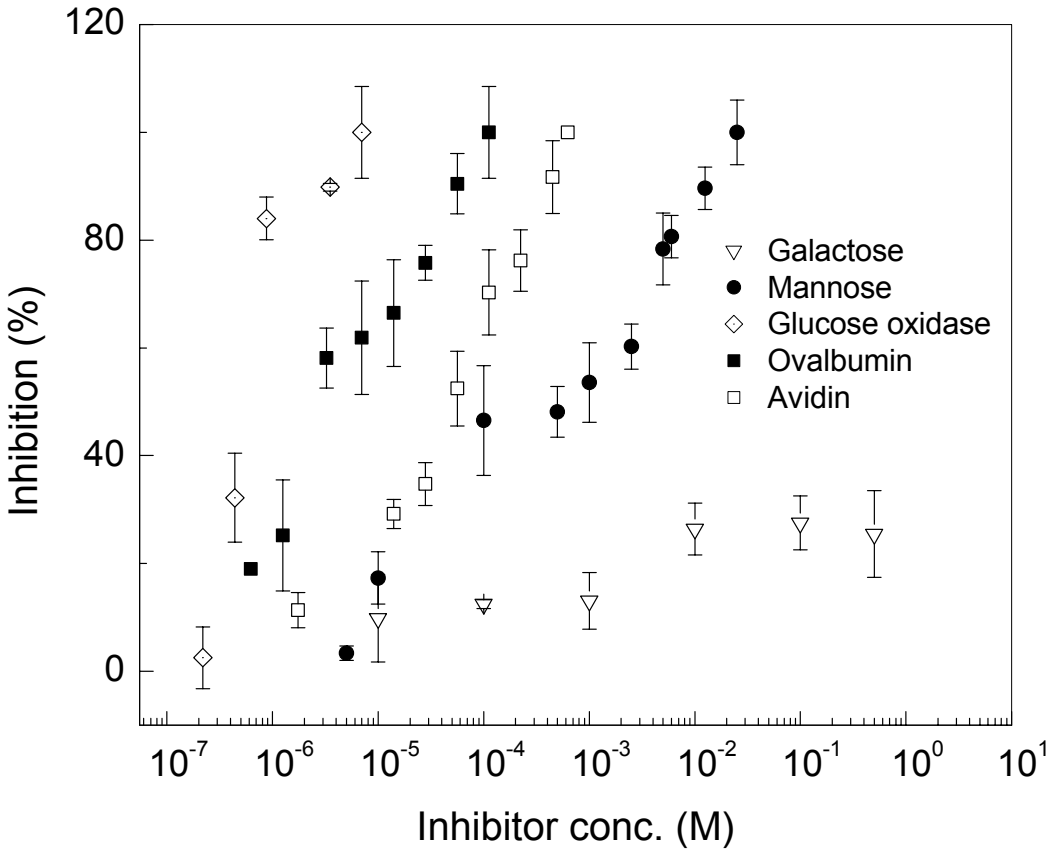

Figure 5.7 The inhibition of dextran-TR binding to FITC-ConA labeled particles by Galactose, Mannose, Avidin, Ovalbumin and Glucoseoxidase. The error bars were obtained from three analyses of fields containing about 100 particles.

5.4. Summary and Conclusions

Micrometric FRET sensing particles were prepared by labeling polystyrene particles with FITC-ConA. The particles were characterized for their fluorescence intensity, photostability and chemical stability under storage conditions. Following extensive optimization studies bright and stable FITC-ConA labeled particles were formed. The performance limiting factor of the FITC-ConA labeled was the bioactivity of ConA. In

solution the FITC-ConA labeled particles retained their carbohydrate binding activity for up to 5 days. This degradation in their binding activity was attributed to bacterial growth that is known to affect lectin activity [76,184]. Dextran-TR molecules bound selectively to the FITC-ConA labeled particles and under our experimental conditions the reaction took about 15 minutes to reach equilibrium. FRET between dextran-TR and FITC ConA-coated particles resulted in a fluorescence decrease of FITC by about 50% and a similar increase in the fluorescence of Texas Red. The FRET sensing particles were applied to evaluate the inhibition efficiency of monomeric carbohydrates and glycoproteins of the binding between dextran-TR and the FITC-ConA labeled particles. The FRET sensing particles discriminated between monomeric carbohydrates like Mannose and Galactose. However, millimolar level of inhibitors was required to effectively inhibit the FRET between dextran-TR and the FITC-ConA labeled particles. This was attributed to the large number of glycosylic residues in dextran (MW 10000 Da). Glycoproteins that contain a larger number of glycosylic residues exhibited higher inhibition efficiency. For example the IC_{50} value of Glucose oxidase was as low as 0.5 μM. The FRET sensing particles technology could be used to screen other groups of carbohydrates or glycoproteins by changing ConA with other lectins. Currently we are exploring the possibility of using the FRET sensing particles as the building blocks of FRET sensing arrays that will be designed for high throughput screening of carbohydrate and glycoprotein based drugs.

CHAPTER 6

DISCUSSION

Fluorescence resonance energy transfer (FRET) is a unique phenomenon that combines the sensitivity and selectivity of fluorescence with the strong dependence of FRET on the distance between donor and acceptor molecules. Combined with a variety of novel indicators and computational methods, FRET microscopy has been widely used in studying protein-protein interactions, protein folding, membrane topology and DNA hybridization in single cells. Using FRET and a biological sensing element enabled the expansion of fluorescence sensors other analytes inaccessible to fluorescence sensors.

Chapter 3 describes a novel method based on FRET to monitor and quantify delivery of fluorophores into cells. For the first time FRET was utilized to confirm whether fluorophores truly penetrated the cellular membrane or they were only absorbed on the cell membrane. While limited in quantitative power, FRET between delivered donor molecules and acceptor labeled cells could be used to confirm the delivery of donor fluorescent molecules into cells. The use of the acceptor permeation into donor labeled macrophages was easier and less prone to errors. Using donor labeled cells it was possible to determine whether acceptor molecules were entrapped in the endosomes or

delivered to the cellular cytoplasm. However, a relatively high acceptor concentration in micromolar level was still needed to obtain measurable FRET signals in a 3-D system like the cellular milieu. These results demonstrated the necessity to reduce the dimensionality of FRET systems in order to increase FRET efficiency between donor and acceptor molecules. The next research project was directed toward the development and application of particle based FRET sensors to increase the sensitivity of the technique.

Chapter 4 describes the synthesis and analytical properties of FRET sensing lipobeads. In lipobeads, the donor fluorophores were located on the surface of the phospholipid membrane that coated the sensor surface. The interaction of fluorophores with the phospholipid membranes was evaluated by FRET measurements between donor labeled lipobeads and acceptor molecules. The FRET efficiency between acceptor molecules and the donor labeled lipobeads was found to be approximately 3-fold higher than FRET efficiency between the same donor and acceptor molecules when dissolved in solution. We concluded that the change in the dimensionality of the system in which FRET occurred improved the sensitivity of our measurements. However, the improvement was smaller than expected due to significant contributions from inner filter effects. We then decided to design FRET sensing lipobeads that contain biorecognition elements in order to increase the affinity of acceptor molecules to the lipobeads thus reducing the concentration of acceptor molecules required for efficient FRET.

Chapter 5 focuses on the development of FRET sensing beads for non-fluorescent carbohydrates and glycoproteins. Micrometric FRET sensing particles were prepared by labeling polystyrene particles with FITC-ConA (FITC- Concanavalin A). The fluorescence recovery of the donor fluorescence intensity due to competitive binding of sugar derivatives to microspheres labeled with FITC-ConA in the presence of dextran-Texas Red provided the basis for the new developed particle-based FRET sensors. The particle-based FRET sensors were stable and showed no fluorophore leakage up to five days. The performance limiting factor of the FRET sensing particles was the bioactivity of ConA. The FRET sensing particles were applied to quantitatively determine the inhibition efficiency of monomeric carbohydrates and glycoproteins of the binding between dextran-TR and the FITC-ConA labeled particles. The particle-based FRET sensors discriminated between monomeric carbohydrates like mannose and galactose. The inhibition potency was evaluated as the inhibitor concentrations needed to realize 50 % inhibition of FRET between dextran-TR and the FITC-ConA coated beads. The newly developed FRET sensing particles could be used as the building blocks of FRET sensing arrays designed for high throughput screening of carbohydrate and glycoprotein based drugs.

Several intrinsic limiting factors affected the quantitative power of the newly developed particle-based FRET sensors. First, the relation between the calibration curves obtained in solutions and an intracellular analyte levels is unclear. Fortunately, this uncertainty in our experiments did not affect the interpretation of kinetics data, which was the main interest of our studies. For our cellular studies, the inability to recognize sub-population

of cells also increased the error in the measurements. The murine macrophages were a heterogeneous mixture of old and young cells, which contributed up to 30% variation in between fluorescence response of individual cells. In future studies the selection of cell subpopulations will enhance the precision of FRET measurements in cells.

In the case of the FRET sensing lipobeads the sensitivity of FRET measurements efficiency was affected by significant contributions from inner filter effects. Future experiments with FRET sensing lipobeads should correct for these errors. Recently, the covalent attachment of the phospholipid membrane and the fluorophores to the microsphere surface carried out in our laboratory increased the stability of lipobead-based sensors. The covalent binding of the donor and acceptor molecules on this type of particles will provide the opportunity to evaluate the interaction of non-fluorescent drugs with supported phospholipid membranes while minimizing inner filter effects. It is also important to develop better data processing techniques since the large number of observed particles generate large amount of data that complicate the analysis. Another important factor that affected the precision of the developed FRET sensors has been the ~5% fluctuation of the microscope light source. Replacement of the mercury lamp with a laser source could improve the precision of FRET measurements. The overlap between the donor and acceptor emission spectra given by the low resolution of the used gratings limited the selection of other donor and acceptor pairs. A spectrograph and higher resolution gratings were recently installed in our laboratory enable the use of other donor and acceptor pairs to obtain higher FRET efficiency. The activity of FITC-ConA lectin and the number of donor molecules per protein were other important factors

that affected our measurements. A controlled synthesis of the donor labeled Concanavalin A, replacing the FITC label with a more stable fluorescent probe would be desirable. The inherent instability problems of lectins could be overcome by substituting them with boronic acids that bind selectively to saccharide. Application of the FRET based sensors in intracellular analysis is limited to macrophage cells in which the sensors are engulfed through phagocytotic events. A novel approach for the delivery of the FRET sensing beads is necessary for other type of cells. The incorporation of newly discovered cell penetrating peptides on the sensor surface could allow future FRET based sensors to measure important cellular constituents, confirm drug and gene delivery into cells and provide important insights on cellular signaling mechanisms.

References

1. Ballerstadt, R.; Schultz, J. S.; *Anal. Chem.;* **2000**; *72*(17); 4185-4192.
2. Badugu, R.; Lakowicz, J. R.; Geddes, C. D.; *Anal. Chem.;* **2004**; *76*(3); 610-618.
3. Catimel B; Weinstock J; Nerrie M; Domagala T; Nice E C , J. Chromatogr. A.; **2000**; 869(1-2), 261-73.
4. Chan, S.; Horner, S. R.; Fauchet, P. M.; Miller, B. L.; *J. Am. Chem. Soc.*; **2001**; *123*(47); 11797-11798.
5. Yoshida,T.; Sato,M.; Ozawa,T.; Umezawa,Y.; *Anal. Chem.;* **2000**; *72*(1); 6-11.
6. Svetlicic, V.; Ivosevic, N.; Kovac, S.; Zutic, V.; *Langmuir;* **2000**; *16*(21); 8217-82207.
7. Mei, S. H. J.; Liu, Z.; Brennan, J. D.; Li, Y.; *J. Am. Chem. Soc.;* **2003**; *125*(2); 412-4208. N. T. K.
8. Thanh, N. T. K.; Rosenzweig, Z.; *Anal. Chem.;* **2002**; *74*(7); 1624-1628.
9. Ho, H.-A.; Leclerc, M. *J. Am. Chem. Soc.;* **2004**; *126*(5); 1384-1387
10. Cooper, M.A.; Nat*. Rev. Drug Discov*; **2002**; 1(7), 515-528
11. Frostell-Karlsson, A.; Remaeus, A.; Roos, H.; Andersson, K.; Borg, P.; Hamalainen, M.; Karlsson, R.; *J. Med. Chem.;* **2000**; *43*(10); 1986-1992
12. Numann, R.; Negulescu, P. A.; *Trends Cardiovas. Med*; 2001, 11(2), 54-59.
13. Turner, A. P. F., *Science*; **2000**, 290(5495), 1315-1317.
14. Lakowicz, J.R., *Principles of Fluorescence Spectroscopy*, Plenum Press, New York, 1999, 367- 377
15. Guilbault, G.G., *Practical fluorescence; theory, methods, and techniques*, M. Dekker Publisher, 1973
16. Rosania, G. R.; Lee, J. W.; Ding, L.; Yoon, H.-S.; Chang, Y.-T.; *J. Am. Chem. Soc.;* **2003**;*125*(5); 1130-1131.
17. Willets, K. A.; Ostroverkhova, O.; He, M.; Twieg, R. J.; Moerner, W. E.; *J. Am. Chem. Soc.;* **2003**; *125*(5); 1174-1175.
18. Sykora, J.; Mudogo, V.; Hutterer, R.; Nepras, M.; Vanerka, J.; Kapusta, P.; Fidler, V.; Hof, M.; *Langmuir;* **2002**; *18*(24); 9276-9282.
19. Toutchkine, A.; Kraynov, V.; Hahn, K.; *J. Am. Chem. Soc.;* **2003**; *125*(14); 4132-4145.
20. Baker, G. A.; Pandey, S.; Bright, F. V.; *Anal. Chem.;* **2000**; *72*(22); 5748-5752.
21. McNamara, K. P.; Nguyen, T.; Dumitrascu, G.; Ji, J.; Rosenzweig, N.; Rosenzweig, Z.; *Anal. Chem.;* **2001**; *73*(14); 3240-3246.
22. Schenning, A. P. H. J.; Peeters, E.; Meijer, E. W.; *J. Am. Chem. Soc.;* **2000**; *122*(18); 4489-4495.
23. Babendure, J. R.; Adams, S. R.; Tsien, R. Y.; *J. Am. Chem. Soc.;* **2003**; *125*(48); 14716-14717.
24. Wong, A. P.; Groves, J. T.; *J. Am. Chem. Soc.;* **2001**; *123*(49); 12414-12415.
25. Groves, J. T.; Mahal, L. K.; Bertozzi, C. R.; *Langmuir;* **2001**; *17*(17); 5129-5133.

26. Haugland, R.P, *Handbook of Fluorescent Probes and Research Chemicals*, Ninth Edition, Molecular Probes, Eugen, Oregon, 2002
27. Barhoumi, R.; Bowen, J.A.; Stein, L.S.; Echols, J.; Burghardt, R.C.; *Cytometry*; **1993**; 14(7); 747-756.
28. Burghardt R.C.; Barhoumi, R.; Lewis, E.H.; Bailey, R.H.; Pyle, K.A.; Clement B.A.; Phillips, T.D.; *Toxicol Appl Pharmacol.;* **1992**; 112(2); 235-244.
29. Jaroszeski, M. J.; Gilbert, R.; Heller, R.; *Anal. Biochem*.; **1994** , 216 (2):271-275.
30. Jaroszeski, M.J.; Gilbert, R.; Fallon, P.G.; Heller, R.; *Biophys J.;* **1994**; 67(4); 1574-1581.
31. Cooper, M. A., *Nat. Rev. Drug Discov.,* **2002**, 1(7), 515-528.
32. Zlokarnik, G.; *Anal. Chem*., **1999**; 71, 322A-328A.
33. Beeley, N.R.A.; Sage, C.;*Targets;* **2003**, 2(1), 19-25.
34. Ji, J.; Rosenzweig, N.; Griffin, C.; Rosenzweig, Z. *Anal. Chem*. **2000**, *72*, 3497-3503.
35. Ji, J.; Rosenzweig, N.; Jones, I.; Rosenzweig, Z. *Anal. Chem*. **2001**, *73*, 3521- 3246
36. J. Liu, Q. Zhang, E.E. Remsen, K.L. Wooley, *Biomacromolecules,* **2001**; 2, 362
37. N.W. Luedtke, P. Carmichael, Y. Tor, *J. Am. Chem. Soc*., **2003**;125, 12374-12375.
38. Sekar, R.B., Periasamy, A.; *J.Cell Biol* .; **2003**; 160 (5); 629-633.
39. Wen-xu, L.; Jian, C.; *Anal. Chem.;* **2003**; *75*(6); 1458-1462.
40. Rosenzweig, Z.; Kopelman;R.; *Anal. Chem.;* **1995**; *67*(15); 2650-2654.
41. Walt, D. R.; *Acc. Chem. Res.;* **1998**; *31*(5); 267-278.
42. Bronk, K.S.; Walt;D.R.; *Anal. Chem.;* **1994**; *66*(20); 3519-3520.
43. Sutter, J. M.; Jurs, P. C.; *Anal. Chem.;* **1997**; *69*(5); 856-862.
44. Liebsch, G.; Klimant, I.; Krause, C.; Wolfbeis, O.S.; *Anal. Chem.;* **2001**; *73*(17); 4354-4363.
45. Park, E. J.; Brasuel, M.; Behrend, C.; Philbert, M. A.; Kopelman, R.; *Anal. Chem.;* **2003**; *75*(15); 3784-3791.
44. Brasuel, M.; Kopelman, R.; Miller, T. J.; Tjalkens, R.; Philbert, M. A.; *Anal. Chem.;* **2001**; *73*(10); 2221-2228.
45. Kasili, P. M.; Song, J. M.; Vo-Dinh, T.; *J. Am. Chem. Soc.;* **2004**; *126*(9); 2799-2806.
46. Clark, H. A.; Kopelman, R.; Tjalkens, R.; Philbert, M. *Anal. Chem.;* **1999**, *71*, 4837-4843
47. Hongbo Su, Patrick Williams, Michael Thompson; *Anal. Chem.;* **1995**; *67*(5); 1010-1013
48. Coon, D. R.; Ogunseitan, A. B.; Rechnitz, G. A.; *Anal. Chem.;* **1997**; *69*(20); 4120-4125.
49. Vekshin, N., Energy Transfer in Macromolecules, SPIE Press, Belligham, Washington, 1997
50. Wu, P., Brand, L.; *Anal. Biochem.;* **1994**.;218:1-13
51. Stryer, L.; Annu*. Rev. Biochem.*; 1978, 47 819-46
52. Forester, Th. *Discuss.Faraday Soc*.; **1959**; 27; 7-17.
53. Forster, Th. *Naturwissenschaften*;**1946**; 33 166-75.
54. Galanin, M.D., *JETP*.;**1955**; 28,485-495.
55. Dexter, D.L.; *J.Chem.Phys.;* **1953**; 21; 836-850.
56. Srinivas, G.; Bagchi, B.; *J. Phys. Chem. B*; **2001**; 105(38), 9370-9374.
57. Sacca, B.; Fiori, S.; Moroder, L.; *Biochemistry ;* **2003**; *42*(12); 3429-3436.

58. Domanov, Y. A.; Gorbenko, G. P.; *Biophys. Chem.;* **2002**; 99(2);143-154.
59. Selvin, P.R.; Rana, T. M.; Hearst, J. E.; *J. Am. Chem. Soc.*;**1994**; 116(13), 6029-30..; Brand, L.; *Biochem*.; **1992**, 31(34), 7939-47.
61. Eisinger, J.; Dale, R. E.; *J. Mol. Biol.*; **1974**; 84(4); 643-7.
62. dos Remedios, C. G.; Moens, P. D. J.; *J. Str. Biol*.; **1995**; 115(2), 175-85.
63. Koppel, D.E., Fleming, P.J, Strittmatter, P., *Biochem*.; **1979**, 24, 5450-5457.
64. Tamai, N., Yamazaki, T.Yamazaki, I., *J.Phys.Chem*.;**1987**; 91, 3503-3508.
65. Tweet, A. O.;Bellamy, W.D.; Gains, G.L.; *J.Chem.Phys.;* **1964**, 41, 2068-2077.
66. Kwok-Keung Fung, B., Stryer, L.; *Biochem.,* **1978**; 24; 5421-5248.
67. Yuan, P.; Walt, D.R.; *Anal.Chem.***; 1987**; 59;2391-2394.
68. Tohda, K.; Lu, H.; Umezawa, Y.; Gratzl, M.; *Anal. Chem.;* **2001**; 73(9), 2070-2077.
69. Liu, Y.; Kati, W.; Chen, C.-M.; Tripathi, R.; Molla, A.; Kohlbrenner, W.; *Anal. Biochem.;* **1999**; 267(2), 331-335.
70. He, H.; Li, H.; Mohr, G.; Kovacs, B.; Werner, T.; Wolfbeis, O. S.; *Anal.Chem*.; 1993; 65(2); 123-7.
71. Elangovan, M.; Wallrabe, H.; Chen, Y.; Day, R.N.; Barroso, M.; Periasamy, A.; *Methods;* **2003**; 29 (1): 58-73.
72. Raarup, M,K,;Chandler, D.W., Olsthoorn, R.C.L.; Schmidt, T.; *Biophys J*.; **2003**, 84 (2), 299A-300A.
73. a) Jovin, T.M.; Arndt-Jovin, D.; *in Cell stucture and function by microspectrometry,* Academic Press, **1989**, 99-117. b) Jovin, T.M., Ardnt-Jovin, D. J., *Annu. Rev. Biophys. Biopys. Chem*, **1989**, 18, 271-308.
74. Elangovan, M.; Periasamy A.; *Biophys. J*.; **2001**; 80 (1); 656.13
75. Periasamy, A.; *J Biomed Opt*.; **2001**; 6 (3); 287-291.
76. Liener, I. E., Sharon, N., Goldstein, I. J., Eds.; *The Lectins: Properties, Functions and Applications in Biology and Medicine*; Academic Press, Inc.: Orlando, **1986**; 600
77. Sharon, N.; Lis, H. *Lectins*; Chapman and Hall: London, **1989**; 127 pp.
78. Drickamer, K.; Taylor, M. E. *Annu. Rev. Cell Biol.* 1993, *9*, 237
79. Sharon, N.; Lis, H. *Essays Biochem.* **1995**, *30*, 59.
80. Kilpatrick, D. C., van Driessche, E., Big-Hansen T. C., Eds. *Lectin Reviews*; Sigma Chemical Co.: St. Louis, MO., **1991**; Vol. 1, 218 pp
81. Goldstein, I. J.; Poretz, R. D. In *The Lectins: Properties, Functions and Applications in Biology and Medicine*; Liener, I. E., Sharon, N., Goldstein, I. J., Eds.; Academic Press, Inc.: Orlando, **1986**; 35.
82. Carver, J. P. *Pure Appl. Chem.* **1993**, *65*, 763
83. Bush, A. C. *Curr. Opin. Struct. Biol.* **1992**, *2*, 655.
84. Homans, S. W. In *Molecular Glycobiology*; Fukuda, M., Hindsgaul, O., Eds.; Oxford University Press: Oxford, **1994**; p 230.
85. Homans, S. W.; Rutheford, T. *Biochem. Soc. Trans.* **1993**, *21,* 449
86. Imberty, A.; Bourne, Y.; Cambillau, C, Rouge, P.; Perez, S. *Adv. Biophys. Chem.* 1993, *3*, 61.
87. Rice, K. G.; Wu, P. Brand, L.; Lee, Y. C. *Curr. Opin. Struct. Biol.* **1993**, *3*, 669
88. Rayment, I.; Baker, T. S.; Caspar, D. L. D.; Murkami, W. T. *Nature* **1982**, *295*, 110
89. Weis, W. I.; Brown, J. H.; Cusack, S.; Paulson, J. C.; Skehel, J. J.; Wiley, D. C. *Nature* **1988**, *333*, 426
90.Stehle, T.; Yan, Y.; Benjamin, T. L.; Harrison, S. C. *Nature* **1994**, *369*, 160

91. Stehle, T.; Harrison, S. C. *Structure* 1996, *4*, 183
92. Weis, W. I.; Drickamer, K.; Hendrickson, W. A. *Nature* **1992**, *360*, 127
93. Kolatkar, A.; Weis, W. I. *J. Biol. Chem.* **1996**, *271*, 6
94. Goldstein, I. J.; Winter, H. C.; Poretz, R. D. In *Glycoproteins II*; Vliegenthart, J. F. G., Montreuil, J., Schachter, H., Eds.; Elsevier Science B.V.: Amsterdam, **1997**; 403.
95. Min, W.; Jones, D. H. *Nature Struct. Biol.* **1994**, *1*, 502
96. Emmerich, C.; Helliwell, J. R.; Redshaw, M.; Naismith, J. H.; Harrop, S. J.; Raftery, J.; Kalb (Gilboa), J. A.; Yariv, J.; Dauter, Z.; Wilson, K. S. *Acta Crystallogr.* **1994**, *D50*, 749
97. Sharma, V.; Surolia, A. *J. Mol. Biol.* **1997**, *267*, 433
98. Sharon, N.; Lis, H. *Trends Biochem. Sci.* **1987**, *12*, 488-491
99. Poget, S.F., Freund, S.M., Howard, M.J., Bycroft, M., Biochemistry, **2001**, 40, 10966-10972
100. Siebert, H.-C.; Lu, S.-Y.; Frank, M.; Kramer, J.; Wechselberger, R.; Joosten, J.; Andre, S.; Rittenhouse-Olson, K.; Roy, R.; von der Lieth, C.-W.; Kaptein, R.; Vliegenthart, J. F. G.; Heck, A. J. R.; Gabius, H.-J.;*Biochemistry*; **2002**; *41*(30); 9707-9717.
101. Cambillau, C. In *Glycoproteins I*; Montreuil, J., Schachter, H., Vliegenthart, J. F. G., Eds.; Elsevier Science B.V.: Amsterdam, **1995;** 29
102. Rini, J. M. *Annu. Rev. Biophys. Biomol. Struct.* **1995**, *24*, 551
103. Toone, E. J. *Curr. Opin. Struct. Biol.* **1994**, *4*, 719
104. Lutwyche, P, Cordeiro, C., Weisman, N.J., St Louise, M., Uh, M., Hope, M.J., Webb, B., Findlay, B. B., *Antimicrob. Agents Chemother*., **1998**, 25511-25520
105. New, R.R.C, Liposomes-A practical approach, Oxford University Press, 1997, 127-137
106. Gordon, S., *BioEssays* **1995**, 17, 11, 977-9863.
107. Brian, H., Fluorescence microscopy, Bios Scientific Publishers, 1998
108. Slavík, J., Fluorescence microscopy and fluorescent probes, Plenum Press, 1996.
109. Periamasy, A., Herman, B., *Journal of Computer Assisted Microscopy*, **1994,** 6, 1, 1-26
110. Youvan, D.C., Silva, C.M., Bylina, E.J., Coleman, W.J., Dilworth, M.R., Yang, M.M, *Biotechnology et alia*, **1997**, 3, 1-18
111. Skoog, D.A., West, D.M., Holler, F.J., Analytical Chemistry. An Introduction. Saunders College Publishing, 1994, Sixth Edition
112. Anderson, A.H., Warren, H.W., McArdle, A., *Clin. Pharmacol*, 27, 3, **1994**, 191-201
113. Park, K., Controlled Drug Delivery: Challenges and Strategies, American Chemical Society Publication, 1997,1-6
114. Pidgeon C., Markovich R. J., Liu M., Hol zer T. J., Novak R. M., Keyer K.A., .*J. Biol. Chem*, **1993**, 268, 7773-7778
115. Stevenson, M, Baille, A.J., Richards, R.M. *Antimicrob. Agents Chemother*., **1983**, 742-749
116. Lagner, M. *Pol. J. Pharmacol*., **2000**, 52, 3-14
117. Longman S.A., Cullis, P.R., Choi, L., de Jong, G.,Bally, M.B., *Cancer Chemother. Pharmacol.*, **1995**, 36, 91-101
118. Lasic, D.D., *Nature*, **1996**, 380, 561-562
119. Blume, G., Cevc, C., *Biochim. Biophys. Acta*, **1993**, 1146, 159-168

120. Woodle, M.C., Lasic, D.D., *Biochim. Biophys. Acta*, **1992**, 1113, 171-179
121. Lasic, D.D., Papahadjapoulos, D., *Science*, 1**995**, 1275-1276
122. Higashi, N., Yamanchi, M., Kumura, Y.O, M. Nakanishi, Sunamoto, J., *Biochim. Biophys. Acta*, **1996**, 1285, 183-191
123 .Anderson, A., Stevenson, B.R., Rogers, J.A., *J. Control. Release*, **1999**, 60, 189-198
124. Weinstein, J.N., R.L Magin, Yatvin, M.B., Zaharko, D.S, *Science*, **1979**, 204, 188-191
125. Kim, J. -D, Bae, K.M, Kim, J. -D., *J. Biochem*, **1997**, 121, 15-19
126. Pharthapratina C., Sen, A., Wui, S.W., *J. Control. Release*, **2001**,76, 27-37
127. Lee, R.J., Wang, S, Turk, M.J., Low, P.S., *Biosci. Rep*., **1998**, 18, 2, 69-78
128. Anderson, V.C., Thompson, D.H., *Biochim. Biophys.Acta*, **1992**, 1109, 1, 33-42
129. Babincova, M., Sourivong, Chorvat, D., Babinec, P., *J. Magn. Mag. Mat*., **1999**, 194, 163-166
130. Hanahan, D, Bergers, G., Bergsland, E., *J.Clin. Inv*., **2000**, 105,8, 1045-1047
131. Straunbinger, R.M., Duzgunes, N., Papahadjopoulos, D., *FEBS Lett*., **1985**, 179, 1, 148-154
132. Stryer,L., *Annu. Rev. Biochem*., **1978**, 47, 819 b) Stryer, L.; Thomas, D.D., Meares, C.F., *Annu. Rev. Biophys. Bio.,* **1982**, 11, 203 c) Wu, P., Brand, L., *Anal. Biochem.*, **1994**, 218, 1-13
133. Kenworthy, A.K., Edidin,M., *Methods Mol Biol*.,**1999**, 116, 37
134. Oliveria, .F., Gomez, L.L.,. Dell'Acqua, M.L., *J. Cell Biol*., **2003**, 160, 101
135. Dirks, R.W., Molenaar, C., Tanke, H.J., Histochem. *Cell Biol*., **2001**, 115, 3
136. Tsuji, A., Sato, Y., Hirano, M., Suga, T., Koshimoto, H., Taguchi, T., Ohsuka, S., *Biophys. J*., **2001**, 81, 501
137. Jobin, C.M., Chen, H., Lin, A.J., Yacono, P.W., Igarashi, J., Michel, T., Golan, D.E., *Biochem*, **2003**, 42, 11716
138. Miyakawa-Naito, A., Uhlen, P., Lal, M., Aizman, O., Mikoshiba, K., Brismar, H., Zelenin, S., Aperia, A., *J. Biol. Chem*., **2003**, 12, 278, 50355
139. Niethammer, P. **,** Bastiaens, P., Karsenti, E., *Science*, **2004**,19,303, 1862
140. Szczesna-Skorupa, E., Mallah, B., Kemper B., *J. Biol. Chem*., **2003**, 278, 31269
141. Tsien, R.Y, Bacskai, B.J , Adams, S.R., *Trends Cell Biol*., **1993**,3, 242
142. Liu, J. , Zhang, Q., Remsen, E.E., Wooley, K.L., *Biomacromolecules*, **2001**, 2, 362
143. Luedtke, N.W., Carmichael, P., Tor, Y., *J. Am. Chem. Soc*., **2003**, 125, 12374
144. Speelmans, G.; Staffhorst, W. H. M.; de Kruijff, B. *Biochemistry.* **1997**, 36(28), 8657-8662.
145. Jedrzejczak, M.; Koceva-Chyla, A.; Gwozdzinski, K.; Jozwiak, Z. *Cell Biol. Inter.* **1999**, 23(7), 497-506.
146. Al-Achi, A.; Boroujerdi, M. *Drug Dev. Ind. Pharm.* **1990**, 16(8), 1325-38.
147. a) Kadurugamuwa, J. L.; Clarke, A. J.; Beveridge, T. J. *J. Bacteriology* **1993**, 175(18), 5798-805. b). Kadurugamuwa, J. L.; Lam, J. S.; Beveridge, T. J. *Antimicrob. Agents and Chemother.* **1993**, 37(4), 715-21.
148. Kramer, S. D; Braun, A; Jakits-Deiser, C; Wunderli-Allenspach, H. *Pharm. Res.* **1998**, 15(5), 739-44.
149. Dachary-Prigent, J.; Dufourcq, J.; Lussan, C.; Boisseau, M. *Thromb. Res.* **1979**, 14(1), 15-22.

150. Davio, S. R; Low, P. S. *Biochim. Biophys. Acta* **1981**, 644(2), 157-64.
151. Krivanek, R.; Rybar, P.; Prenner, E. J.; McElhaney, R. N.; Hianik, T. *Biochim. Biophys. Acta* **2001**, 1510(1-2), 452-463.
152. Greathouse, D.V.; Koeppe, R. E., II; Providence, L.L.; Shobana, S.; Andersen, O. S. *Methods in Enzymology* **1999**, 294 (Ion Channels, Part C), 525-550.
153. Colome, C.; Alsina, M. A.; Busquets, M. A.; Haro, I.; Reig, F. *Int. J. Pharm.* **1993**, 90(1), 59-71.
154**.** Rodrigues, Catarina; Gameiro, Paula; Reis, Salette; Lima, J. L. F. C.; de Castro, Baltazar. *Langmuir* **2002**, 18(26), 10231-10236.
155**.** Hidalgo, A. A.; Caetano, W.; Tabak, M.; Oliveira, O. N. *Biophys. Chem.* **2004**, 109(1), 85-104
156. Middleton, David A.; Reid, David G.; Watts, Anthony. *J. Pharm. Sci.* **2004**,
157. Pajeva, Ilza; Todorov, Dimiter K.; Seydel, Joachim. *Eur. J. Pharm. Sci.* **2004**, 21(2-3), 243-250
158. Seydel, Joachim K. *Methods and Principles in Medicinal Chemistry* ,**2002**,15, 51-139.
159. Baird, Cheryl L.; Courtenay, Elizabeth S.; Myszka, David G, *Anal. Biochem*., **2002,** 310(1), 93-99.
160. Baksh, M. M.; Jaros, M.; Groves, J. T., *Nature*, **2004**, 427(6970), 139-141.
161. Murtomaki, L.; Barker, M. H.; Manzanares, J. A.; Kontturi, K.. *J. Electroanal. Chem.,* **2003**, 560(2), 95-103.
162. a) Nakashima, K.; Duhamel, J.; Winnik, M.A. *J. Phys. Chem.* **1993**, 97 (41), 10702-10707. b) Liu, Y.S.; Zhang, P.; Duhamel, J.; Feng, J.R.; Winnik , M.A. *Langmuir* **1993,** 9 (11), 2825-2831.
163. Li, Y.; Kuwabara, H.; Gong, Y.K.; Takaki, Y.; Nakashima, K. *Photochem. Photobiol*. **1995**, 61 (6), 592-599.
164. Day, R.N., *Molec. Endocrinol*. **1998**, 12, 9, 1410-1419.
165. Kenworthy, A.K., Edidin, M., *J.Cell Biol*., **1998**, 142, 1, 69-84.
166.a) Tsuji, A., Koshimoto, H., Sato, Y., Sei-Ida, Y., Kondo, S., Ishibashi, K, *Biophys. J.,* 78, **2000**, 3260-3274 b) Tsuji, A., Sato, Y., Suga, T., Koshimoto, H., Taguchi, T, Oshusa, S., *Biophys. J.*, **2001**, 81, 501-515.
167. Chigaev, A.; Buranda, T.; Dwyer, D. C.; Prossnitz, E. R.; Sklar, L. A. *Biophys. J.*, **2003**, 85(6), 3951-3962.
168. McNamara, Kerry P.; Rosenzweig, Nitsa; Rosenzweig, Zeev., Proceedings of SPIE-The International Society for Optical Engineering, Scanning and Force Microscopies for Biomedical Applications II, **2000**, 3922, 147-157.
169. Furuike, S.; Levadny, V. G.; Li S J; Yamazaki M., *Biophys. J*., **1999**, 77(4), 2015-23.
170.Park, E. J.; Brasuel, M.; Behrend, C.; Philbert, M. A.; Kopelman, R. *Anal. Chem.* **2003**, *75*, 3784-3791.

171. Brasuel, M.; Kopelman, R.; Miller, T. J.; Tjalkens, R.; Philbert, M. A. *Anal. Chem.* **2001**, *73*, 2221-2228.

172. Clark, H.A.; Tjalkens, R.; Philbert, M.A.; Kopelman,R. *Anal. Chem.* **1999,** *71*, 4837-4843.

173. Barker, S.L.R.; Zhao, Y.; Marletta, M.A.; Kopelman, R. *Anal.*

174. Ma, A.; Rosenzweig, Z. *Anal. Chem*. **2004**, *76*, 569-575.

175. a)Vo-Dinh, T.; Alarie, J.P.; Cullum, B.M.; Griffin, G.D. *Nature Biotechnol*. **2000**, *18*, 764 – 767. b) Ferguson, J. A.; Steemers, F. J.; Walt, D. R.. *Anal. Chem*. **2000**, *72*, 5618-5624.

176. Rowe, C.A.; Tender, L.M.; Feldstein, M.J.; Golden, J.P.; Scruggs, S.B.; MacCraith, B.D.; Cras, J.J.; Ligler, F.S. *Anal. Chem.* **1999**, *71*, 3846-3852.

177. Song, X.; Swanson, B.I. *Anal. Chem.* **1999,** *71*, 2097-2107.

178. a) Ballerstadt, R.; Schultz, J.S. *Anal. Chem.* **2000**, *72*, 4185-4192. b) Russell, R. J.; Pishko, M. V.; Gefrides, C. C.; McShane, M. J.; Cote, G. L.; *Anal. Chem.* **1999**; *71,* 3126-3132.

179. Seth, A.; Otomo, T.; Yin, H.L.; Rosen, M.K. *Biochemistry* **2003**, *42*, 3997-4008.

180. Patel, R.C.; Lange; D.C.; Patel, Y.C. *Methods*, **2002**, *27*, 340-348 .

181. VerVeer, P.J.; Wouters, F.S.; Reynolds, A.R.; Bastiaens, P.I.H. *Science*, **2000**, *290*, 1567-1570.

182. Elangovan, M.; Day, R.N.; Periasamy, A. *J. Microsc*. **2002**, *205*, 3-14.

183. a)Liu, X.; Tan,W. *Anal. Chem.* **1999***, 71*, 5054-5059. b) Tsourkas, A.; Behlke, M.A.; Xu, Y.; Bao, G. *Anal. Chem.* **2003**, *75*, 3697-3703.

184. a) Lis, H.; Sharon, N. *Chem. Rev.* **1998**, *98*, 637-674, b) Dwek, R. A. *Chem. Rev.* **1996**, *96*, 683-720. c) Mammen, M.; Choi, S.-K.; Whitesides, G. M. *Angew. Chem., Int. Ed. Engl.* **1998**, *37*, 2754-2794.

185. Goldstein, I.J.; Hollerman, C.E.; Smith, E.E. *Biochemistry* **1965**, *4*, 876-883.

186. a) Roy, R.; Page, D.; Perez, S. F.; Bencomo, V. V. *Glycoconjugate J.* **1998**, *15*, 251-263. b) Burke, S. D.; Zhao, Q.; Schuster, M. C.; Kiessling, L. L.; *J. Am. Chem. Soc.* **2000**, *122*, 4518-4519. c) Cairo, C.W.; Gestwicki, J.E.; Kanai, M.; Kiessling, L.L. ;*J. Am. Chem. Soc* **2002**, *124* (8), 1615-1619.

187. Smith, E.A.; Thomas, W.D.; Kiessling, L.L.; Corn, R.M. J*. Am. Chem. Soc* **2003**, *125*, 6140-6148.

188. Whelan, R. J.; Wohland, T.; Neumann, L.; Huang, B.; Kobilka, B. K.; Zare, R. N. *Anal. Chem.* **2002**, *74*, 4570-4576.

189. Tampe, R; Clark, B.R.; Mcconnell, H.M.. *Science* **1991**, *254*, 87-89.

190. Barnard, S.M.; Walt, D. R. *Science* **1991**, *251*, 927-929.

191. Gonzalez, J.E.; Tsien, R.Y. *Biophys J* **1995**, *69*, 1272-1280.

192. Centonze, V.E.; Sun, M.; Masuda, A.; Gerritsen, H; Herman, B. *Methods In Enzymology* **2003**, *360*, 542-560.

193. Biran, I.; Walt, D.R. *Anal. Chem.* **2002,** *74*, 3046-3054.

194. Borrebaeck, C., Mattianson, B. *Anal. Biochem*. **1980**, 107, 446-450.

195. Hasegawa, T.; Kondoh, S.; Matsuura, K.; Kobayashi, K. *Macromolecules* **1999,** *32*, 6595-6603.

VITA

The author was born in Buzau, Romania. Her inclination to physical sciences developed during her high school years when attending Liceul B.P. Hasdeu, one of the best Romanian national schools in mathematics, physics and chemistry. After obtaining a BS degree in Chemical Engineering from Politehnica University of Bucharest, she worked for five years at Biotehnos S.A., a biotechnological plant. In 1999, she moved to the United States to join the graduate program of the Department of Chemistry at the University of New Orleans. In January 2000, she became a member of Professor Zeev Rosenzweig's research group. In 2002 she obtained her M.Sc. degree in Chemistry with Prof. Zeev Rosenzweig as advisor. The title of her M.Sc. thesis was "The use of derivatized magnetoliposomes for extraction of antibodies from aqueous solutions".